MOLECULAR MECHANISM OF pH DEPENDENT ANTIBODY BINDING:

Structure/Function studies on the Neonatal Fc Receptor

Thesis by

Daniel E. Vaughn

In Partial Fulfillment of the Requirements

for the Degree of

Doctor of Philosophy

California Institute of Technology

Pasadena, California

1998

(Submitted July 7, 1997)

Acknowledgments

As this thesis is the most tangible product of my graduate school experience, I would like to take this opportunity to thank the many people who helped make the experience a productive and enjoyable one.

One of major factors that brought me to California for graduate school was the presence of my family. I would like to thank them for their unbelievable support and hospitality. I would also like to thank my brother and his growing family, their generosity has been extraordinary. To my parents, I owe you most of all.

For as long as I can remember, going to school has been mostly about friends, and in graduate school I have had some of the best. Thank you for introducing me to Bott's ball, ultimate, and Pasadena. Thank you also for the diversions of football, roto-ball, and Toe's. How will I tell the cow story without your choreography?

Of course school has also been about getting an education. I would like to thank the faculty who have had the patience to indulge my meandering path of self discovery and those who have illuminated portions of the route. Thanks also to the technicians, students and post-docs who have shown me how to do science and who have made the doing more enjoyable.

Finally, thank you Pamela. I am honored that you think the Wiley curse has been fulfilled, but the even greater honor would be for my students to have an advisor like you.

Abstract

The work described here is an investigation of the molecular mechanism of pH dependent immunoglobulin G (IgG) binding by the neonatal Fc receptor (FcRn). FcRn binds IgG at acidic, but not alkaline pHs, in two important physiological processes. These processes are the acquisition of passive immunity by the fetus or newborn and protecting IgG from a default degradative pathway.

A biosensor assay is used to characterize the interaction of a soluble form of FcRn with IgG. Immobilization of FcRn on the biosensor surface reproduces the high affinity IgG binding observed for membrane bound FcRn, whereas immobilization of IgG results in lower affinity binding similar to that of the FcRn/IgG interaction in solution. The statistical method of cross-validation is used to show that there are two classes of non-interacting binding sites. The IgG binding interaction is characterized for several mutant FcRns with designed amino acid substitutions. These mutations map the functional IgG binding site on FcRn.

The structure of FcRn at an alkaline pH is described. This structure determination reveals an extensive carbohydrate mediated interaction between the dimer related FcRn molecules. The physiological relevance of this interaction is discussed in the context of the FcRn dimerization literature. A further refined structure of FcRn at an acidic pH is described that includes additional carbohydrate structure. These structures are compared with specific attention to the pH dependence of FcRn stability and IgG affinity. Finally, a mechanism for pH dependent antibody binding to FcRn is proposed based on these structures and the body of structure/function literature concerning this interaction.

Table of Contents

Introduction:	The acquisition of maternal IgG: A review of research on the neonatal Fc receptor	1
Chapter 1:	High affinity binding of the neonatal Fc receptor to its IgG ligand requires receptor immobilization	I-1
Chapter 2:	Identification of critical IgG binding epitopes on the neonatal Fc receptor	II-1
Chapter 3:	Structural basis of pH dependent antibody binding by the neonatal Fc-receptor	III-1
Appenix A:	The (Greek) key to structures of neural adhesion molecules	A-1
Appendix B:	Expression and crystallization of a soluble form of *Drosophila* fasciclin III	B-1

THE ACQUISITION OF MATERNAL IgG: A review of research on the neonatal Fc receptor

Daniel E. Vaughn

After encountering a disease, the immune system can specifically recognize the foreign antigens that characterize it. This recognition enables specific immunity to be developed for the disease. Thus, once we have had a disease such as chicken pox, we develop resistance to it. Presumably as a result of the importance of specific immunity, vertebrates have evolved multiple recognition mechanisms. For example, there is a cell-mediated specific immunity in which specialized cells of the immune system, T-cells, recognize antigenic peptides presented by MHC molecules (Figure 1a; reviewed in Bjorkman, 1997). There is also a humoral specific immunity in which antibodies recognize specific complementary three-dimensional surfaces such as an intact protein (Figure 1b). The most prevalent of these antibodies, immunoglobulin G (IgG) molecules, have two identical copies of an antigen binding domain (F_{ab}) and a single constant domain (F_c). The genes that code for antibodies undergo a process of DNA recombination that results in the generation of billions of different IgG molecules, each cell producing an antibody with a different specificity. Under certain conditions (e.g., an infection), the capacity to make those IgG molecules that have the relevant specificities is increased.

Unfortunately, specific immunity generally requires previous exposure to some form of the disease bearing organism. One exception to the general requirement of previous exposure occurs in newborns. Mothers transfer some of their IgG molecules to their offspring. Because individual antibodies last in the bloodstream for only a few weeks, this passively acquired immunity is only temporary. It does, however, provide

powerful specific immune recognition during the critical period before the baby is fully capable of its own specific immune recognition.

The acquisition of maternal antibodies is critical to the survival of mammals in general. A recent study is particularly illustrative (Gustafsson et al., 1994). Some of the mice used in this study have a deletion in the gene coding for Ig μ chain that is necessary for antibody production (μ^-). Although μ^- mothers (mated with either wild type or μ^- fathers) were able to complete pregnancy and deliver normal litter sizes, all of their babies died[1]. In contrast, all babies born to antibody-producing mothers survived (Figure 2). Therefore, infant survival depended only on whether the mother could produce antibodies and not on the infant's ability to produce antibodies.

The offspring born to antibody-deficient mothers could be rescued by nursing from antibody-producing foster mothers. Although the young had no antibodies at birth, at days 6 and 12 their antibody levels were normal. Thus the foster mothers were able to promote infant survival presumably by transferring antibodies to the infants through their milk.

Mice born to antibody-producing mothers but nursed by antibody-deficient foster mothers, survived well initially (90% survival at day 10, more than 3 times the survival rate of babies born to and nursed by antibody-deficient mothers), but often died by day 25 (> 85% mortality rate). In this case, the antibody levels were normal at birth but decreased thereafter. In normal offspring, antibody levels increase after birth. These data indicate that in mice, mothers also transfer antibodies to their offspring prenatally, and that this too promotes infant survival.

This experiment is one clear example of the importance of maternal transfer of antibodies for infant survival. Mice that were able to acquire antibodies from the milk of

---

1 Ig μ deficient mice are bred and raised in special sterile environments, and adult Ig μ deficient mice can survive adequately in the normal laboratory conditions used in this experiment.

biological or foster mothers survived until weaning while babies that nursed from antibody deficient mothers usually died. Similarly, babies that were able to receive maternal antibodies prenatally had a survival advantage especially during their first week of life. The genetic manipulations used to construct antibody deficient mice allowed a direct test of the importance of antibody transfer. Although these manipulations can not be performed in humans or most other mammals, the importance of maternal antibody acquisition to neonatal survival has been well documented across a wide range of mammalian species beginning with the pioneering work of Paul Erlich in the late 19th century (Junghans, 1997).

Evolution of antibody transmission

In the 1950s and 1960s, Brambell and coworkers studied the transmission of immunity from mother to young (Brambell, 1970). The animals that they studied included representatives from diverse branches of amniotic evolution. For each of these species they measured the developmental time and the route of antibody transmission. Interpretation of these results requires an appreciation of the differences in embryonic structures that evolved as vertebrates adapted to terrestrial existence.

Amphibians, although capable of living on land, must return to the water to reproduce. Their offspring develop rapidly using maternal nourishment that is provided by way of the egg yolk. These embryos enclose the yolk within an embryonic membrane. This yolk sac develops an extensive network of blood vessels that connect to the developing embryos circulatory system, the vitelline network. The principle function of the yolk sac is to allow the developing embryo to make use of the nutrients that the mother deposits in the yolk.

For embryos to develop on land, certain new embryonic organs were required to provide a protected aqueous micro-environment, gas exchange, and waste disposal. The

cleidoic egg (i.e., enclosed in a shell and self sufficient except for gas exchange) characteristic of most reptiles and monotremes (egg laying mammals, e.g., duck-billed platypus) provides this environment by evolving structures derived from embryonic tissues (Figure 3, left panel). These structures, four membranous sacs, are also conserved in placental mammals (Figure 3, right panel). The yolk sac is the homolog of the fish and amphibian yolk sac, and it serves the same nutrient procurement function. The allantois forms from hindgut tissue and serves initially as an excretory reservoir, homologous to the amphibians' urinary bladder. Later in embryonic development an expanded and extensively vascularized allantois also serves a respiratory function. The amnion surrounds the embryo and provides an aqueous micro-environment. The chorion (also called serosa in reptiles) encloses all other embryonically-derived tissues.

With the evolution of mammals, two new mechanisms were developed to provide nourishment to the young. All mammals provide nourishment to their young by secreting milk from mammary glands. The viviparious mammals (bear their young live) also have placentas to provide nourishment to the young in utero. Although, marsupials (e.g., opossum and kangaroo) only have a very rudimentary placenta.

The evolution of more developed placentas are characteristic of eutherial[2] mammals. Many ungulates, including the pig and horse, have the simplest kind of placenta. These placentas are diffuse (Figure 4a) because the villi that contribute to the placenta are scattered over the entire chorion. In ruminants (e.g., cattle, goats, and sheep) the placenta is cotyledonary (Figure 4b), meaning that the villi cluster into patches that are distributed over the chorion. In all ungulates, the maternal epithelium remains intact (epithelialchorial placenta) and the nutrients must pass over several layers to reach the embryo from the maternal circulation. Carnivores have a more complicated placenta. The villi cluster in a characteristic band about the center of the chorion; this arrangement

---

2 Eutherians are traditionally described as placental mammals. This is somewhat misleading because marsupials have placentas but are not classified as eutherian.

is zonal (Figure 4c). The carnivore's uterine wall breaks down to make a more intimate placental connection, although the endothelial tissues of the blood vessels remain intact (an endothiliochorial placenta). Lagomorphs (rabbits and related species) and rodents have well-developed placentae. They are discoid (the villi localize to a single patch; Figure 4D) and heamochorial (the maternal blood circulates directly over the embryonic chorion). Humans and other primates also have a placenta classified as haemochorial and discoid , but the morphology, lacunar, is unique.

The mechanisms of antibody transmission have coevolved with reproductive strategies. Brambell and collegues characterized the developmental time and route of antibody transmission for a wide range of amniotes (Table 1).

Species	Prenatal Transmission Route	Postnatal Transmission Route	Window
Birds	Egg yolk	Egg yolk	< 5 days
Wallaby	None	Gut	180 days
Horse	None	Gut	1 day
Pig	None	Gut	1-2 days
Ruminants	None	Gut	1 day
Dog, Cat	Uncharacterized	Gut	1-2 days
Rabbit	Yolk-sac	None	
Rat, Mouse	Yolk-sac	Gut	20, 16 days
Guinneapig	Yolk-sac	None	
Hedgehog	Uncharacterized	Gut	40 days
Human, Monkey	Placenta	None	

Table 1. IgG transmission in several species. Dogs, cats and hedgehogs have significant prenatal transmission; although the route of this transmission remains uncharacterized. Ruminants tested include cattle, sheep and goats. Birds tested include chicken, pigeon, dove, sparrow, crow, and swallow. (Ref. Brambell 1970.)

The transmission of passive immunity is not limited to mammals. Birds and other reptiles have an antibody, IgY, which is the homologue of both mammalian IgG (which is transmitted from mother to young) and IgE (which is not). In these species the young develops *in ovo* with all maternal contributions present in the egg. Antibody transmission

is well characterized in the chicken. Maternal IgY is secreted by the ovarian follicle into the developing egg yolk. Endodermal cells of the yolk sac absorb the IgY and vitteline vessels transport it to the developing chick's circulation. Mammalian IgG injected into the egg yolk is not effectively transmitted (Brierley and Hemmings, 1956). IgY is also transmitted through the egg yolk in the tortoise (Maung, 1963). In Brambell's work, there is no mention of amphibians transmitting passive immunity. It is possible that the transmission of immunity from mother to young also occurs in amphibians since they have both IgY and a yolk sac. There is evidence for monomeric antibodies in teliosts (bony fish), and even elasmobranches (rays, primitive sharks, etc.), although the nature of these antibodies is more controversial (Warr, 1994).

Mammals with the most primitive placentas obtain maternal antibodies postnatally. In the wallaby, a species of kangaroo, antibody transmission occurs through the milk during the entire period when the young reside in the pouch. This is the functional route of antibody transmission (Waring, personal communication cited in Brambel, 1970). As with all viviparous mammals, marsupial embryos do not derive significant nutrients from the egg yolk. If antibody transmission occurs through the egg yolk, it is insufficient to transmit immunity, and it should be considered vestigial (Bramble, 1970). Ungulates are born much more fully developed, and they receive all of their maternal antibodies immediately after birth from the colostrum (milk that is especially high in antibody and other proteins secreted for a day or two after birth).

Postnatal antibody transmission occurs by maternal secretion of IgG into the colostrum and milk, and acquisition by the neonate through its gut. The mechanism by which antibodies are secreted into the milk is unknown, although antibodies are transferred from the mother's blood stream in an at least somewhat specific manner (Jordan and Morgan, 1967). Therefore, new antibody synthesis in the mammary glands if it occurs, can not be the only mechanism of transmission. In the newborn, endocytic cells that line portions of the nursing infants' small intestines (primarily the jejunum but also a

proximal region of the ileum) transport antibodies from the gut to their blood stream, a process called transcytosis .

With the evolution of more devolped zonary placentas, mammals also evolved prenatal antibody transmission. Carnivores such as dogs and cats, are born with partial maternally derived immunity although the route of transmission has not been characterized. Most of their passive immunity is transmitted just after birth by way of the colostrum. Lagomorphs on the other hand, receive all of their antibodies prenatally.

The route of lagomorph prenatal antibody transmission was convincingly demonstrated in the rabbit by Brambell and collegues. In the final arrangement of the rabbit embryonic membranes, the chorion only partially encloses the rest of the embryonic tissue (Figure 5a), and the yolk sac endoderm is directly exposed to the lumen of the uterus. Antibodies are secreted from the maternal circulation into the lumen of the uterus where they are absorbed by a vascularized structure of the yolk sac, the splanchnopleur, and transported by the vitteline network to the foetus (Brambell et al., 1949). The critical evidence was provided by surgically constricting the yolk sac stock containing the vitteline vein (Figure 5b). Fetuses treated in this way were not able to aquire antibodies either produced by the mother, injected into the mother's circulation, or injected into the intestinal lumen. Untreated littermates acquired both antibodies and immunity from each of the antibody sources (Brambell et al., 1949).

Some rodents also receive all of their maternally derived immunity prenatally, e.g., the guinea pig, while others, e.g., mice and rats, receive the majority of their maternal antibodies postnatally and only a fraction prenatally. Unlike carnivores, postnatal transmission, when it occurs in the rodent, continues throughout the majority of the nursing period. One difference between rodents that do and those that do not acquire maternal antibodies postnatally, is that rats and mice are born less fully developed (~3 week gestation period) than are guinea pigs (~10 week gestation period). The hedgehog

is an insectivore[3] and, like rats and mice, has a haemochorial discoid placenta, a relatively short gestation period (31 days), and receives antibodies both prenatally and for an extended postnatal period.

Humans and other primates also have a haemochorial discoid placenta, but, like rabbits and guinea pigs, they have a relatively long gestation period and only receive antibodies prenatally. The transmission of immunity in these species occurs by a different route. In contrast to rodent's, the primate chorion encircles the developing embryo, isolating it from the uterine lumen, and the yolk sac is small and rudimentary throughout development, never positioned to absorb immunoglobulins directly from the exterior (Brambell, 1970). Instead, fetal cells selectively transport IgG, present in the maternal blood that bathes the chorionic villi, to the allantoic circulatory network.

Extended postnatal antibody transmission is seen in the earliest viviparous mammals, marsupials, and (along with some prenatal transmission) in rats, mice and hedgehogs. This mechanism of transmission appears and disappears throughout mammalian evolution, and its presence coincides with offspring that are born less mature. Other than this exception, the route of maternal IgG transmission seems to have evolved sequentially. Initially this transmission was via the egg yolk, as in reptiles. The evolution of mammals introduced the process of nursing, and this advance provided a route of postnatal antibody transmission. Ungulates consolidated this transmission to the colostrum presumably because their young are born with a more developed immune system obviating the need for the extended antibody transmission required of marsupials. Carnivores evolved a prenatal mechanism of transmission; although, the route of this transmission has never been characterized, and fewer antibodies are transmitted prenatally than posnatally. The routes of prenatal transmission for rabbits, rats, and mice are well characterized and are similar. However, while rabbits use prenatal transmission

---

3 Insectivores are a class of mammals that diverged relatively early from the rodent/legomorph line.

exclusively, rats and mice transmit most of their immunity postnatally. The route of antibody transmission in humans and monkeys is different from that of rabbits and rodents. In rabbits and rodents, antibodies are secreted into the uterine lumen, and acquired *in utero* by transcytosis across endocytic cells in the yolk sac. In primates, antibodies are contained in the maternal blood that bathes the placental villi, and acquired *in utero* by trancytosis across endocytic cells in these villi.

Antibody acquisition by any of these routes is accompanied by significant antibody degradation. Labelled antibodies fed to neonatal rats are both transmitted intact to the infant's circulation and digested (Halliday, 1957; Brambell et al., 1961). Transport across the rabbit yolk sac and the human placenta also include considerable antibody degradation (Brambell 1970). A set of early *in vitro* experiments allowed accurate quantitation of this process (Bamford, 1966). The small intestine of neonatal rats is turned inside out, cut into appropriate lengths, and the ends are tied off. These tissues remained viable for several hours (many cycles of antibody transport). A large volume of fluid outside these "sausages" maintains an approximately constant antibody concentration, and at the conclusion of these experiments the intact antibodies can be completely recovered. These and subsequent experiments have consistently shown that selective IgG transcytosis is accompanied by significant IgG degradation.

The neonatal Fc receptor

Three characteristics of antibody transmission: saturation, selectivity, and inhibition, led Brambell and colleagues to hypothesize that a receptor was responsible for prenatal and neonatal antibody acquisition. Using a procedure that allowed quantitative delivery of antibodies to the newborn's stomach, Halliday demonstrated that antibody transcytosis was saturatable (Halliday, 1957). That is, for modest quantities of antibody,

the amount of antibody reaching the neonate's blood stream is proportional to the amount administered, but for doses above a certain level, the amount of antibody transferred is constant regardless of the dose. Halliday further showed that antibody transmission was specific; i.e., antibodies from different species were transferred with different efficiency[4] (Halliday, 1955). Morris demonstrated that the transfer of an antibody with any given specificity could be inhibited by whole IgG molecules with a different specificity (Morris, 1957) or the Fc portion of an antibody (Morris, 1963). It was soon recognized that these properties (saturation, selectivity, and inhibition) suggest that a specific receptor is responsible for antibody transmission (Brambell, Halliday and Morris 1958).

Indeed a receptor that recognizes IgG through its Fc region was isolated from neonatal rat intestine (Jones & Waldman, 1972), and is thus known as the neonatal Fc receptor (FcRn). The isolated receptor binds IgG under slightly acidic conditions (pH 6) but not under slightly alkaline conditions (pH 7.4; Jones & Waldman, 1972). It was later shown that this pH dependent binding of IgG, or its Fc portion, occurs in the neonatal intestine as well as the isolated receptor (Rodewald, 1976; Wallace & Rees, 1980). The DNA sequence that codes for rat FcRn was identified and was found to be homologous to class I MHC molecules whose three-dimensional structures are known (reviewed in Bjorkman and Parham, 1990). Both MHC class I molecules and FcRn are composed of a common soluble light chain, β2-microglobulin (β2m), and a homologous transmembrane heavy chain (Simister and Rees, 1985).

Transgenic mice were created that do not produce β2m which is necessary for FcRn function (Zijlstra et al., 1989). These mice lack the FcRn surface expression in the neonatal intestine that is observed in wild type mice, and do not transport maternal IgG (Zijlstra et al., 1989; Israel et al., 1995). The adult $\beta 2m^-$ mice have IgG levels that are

---

4 Halliday's work also first demonstrated that some classes of antibodies are transferred more readily than others (Halliday and Kekwick 1960). This study found that the neonate's gut was more permeable to hyperimmune sera than serum taken shortly after primary immunization. In retrospect, this is consistent with IgG being transmitted and IgM being impermeable.

1/10th those of normal mice (Israel et al., 1995). The interpretation of these results is complicated because β2m is a component not only of FcRn, but also class I MHC molecules and several other proteins with homology to class I MHC molecules. Nonetheless, the observation of low IgG levels in the adult transgenic mice coupled with observations of widespread FcRn expression in adult rats (Simister and Mostov, 1989), lead several groups to reconsider Brambell's proposal of a second FcRn function (reviewed in Junghans, 1997).

In the mid 1960s, Brambell recognized that features of the IgG catabolism in the blood stream were similar to those of maternal antibody transmission. It was discovered that the rate of degradation of IgG in healthy adult mice increases with increased concentrations of IgG (Fahey and Robinson, 1963). This effect is selective for the Fc portion of IgG. Elevated concentrations of either IgG or its Fc portion, but not of either the Fab portion of IgG or of other classes of immunoglobulins (IgM or IgA), increase the rate of catabolism of IgG. Brambell and colleagues immediately recognized that the same receptor that they hypothesized transports immunity from mother to young could also be working to specifically recognize IgG and rescue it from an otherwise degradative fate (Brambell et al., 1964; Brambell, 1966).

Indeed in the year following the initial report of $\beta 2m^-$ mice having decreased IgG levels (Israel et al., 1995), three groups independently found that the low IgG levels were due to increased catabolism resulting from impairment of the normal IgG protection mechanism (Ghetie et al., 1996; Junghans and Anderson, 1996; Israel et al., 1996). Careful quantitation of this effect shows that in normal mice, the rate of IgG catabolism is seven-fold greater than the rate of catabolism of a representative serum protein, albumin (Junghans and Anderson, 1996). In contrast, the rate of IgG degradation is the same as that of albumin in $\beta 2m^-$ mice (Junghans and Anderson, 1996). In the same study, the IgG level was measured to be eight-fold higher in wild-type mice than in the transgenic mice. Thus, within experimental error, the difference in IgG concentration and rate of

catabolism are the same in normal and β2m knockout mice (Junghans and Anderson, 1996). The FcRn heavy chain is expressed in diverse tissues of the adult, including the vascular epithelium where most serum protein degradation is believed to occur (Simister and Mostov, 1989; Story et al., 1994). In addition to the prenatal and neonatal acquisition of maternal IgG, these studies strongly implicate a second FcRn function: the protection of IgG from a default degradative pathway.

The expression of a soluble form of FcRn (Gastinel et al., 1992) has facilitated structural and mechanistic studies of the FcRn-IgG interaction (reviewed in Raghavan and Bjorkman, 1996). Soluble FcRn exhibits the same pH dependent binding of IgG seen for isolated FcRn or intact neonatal intestine (Gastinel et al., 1992). Under the slightly acidic conditions that permit tight IgG binding, soluble FcRn denatures at a higher temperature and the dissociation rate of heavy and light chains is an order of magnitude slower than under the slightly alkaline conditions for which no IgG binding is observed (Raghavan et al., 1993). A biosensor based assay was developed to characterize the interaction of IgG and FcRn (Raghavan et al., 1994). This assay was used to quantitate the pH dependent binding of IgG to FcRn immobilized on a biosensor chip (Raghavan et al., 1995a). The affinity for IgG decreases by at least two orders of magnitude from pH 6.0 to 7.0. This steep pH dependence is unusual for protein interactions. From a Hill plot of the binding constant as a function of pH, a Hill coefficient of 2.6 was derived (for mIgG2a) suggesting that at least 3 residues are titrating each with a pKa of about 6.6-6.7. Solvent exposed histidine residues generally have a pKa in this range due to the deprotonization of the imidizole side chain (Fersht, 1977). Two histidine residues on the Fc ligand (His 310 and His 433) as well as one or both of two consecutive histidines on the receptor (His 250 and/or His 251) are important in the pH dependence of FcRn-IgG binding (Raghavan et al., 1995a).

The structure of soluble FcRn was determined to 2.2 Å resolution by X-Ray crystallography (Burmeister et al., 1994a). The overall fold of FcRn is very similar to class I MHC molecules (Figure 6). The α1 and α2 domains of the heavy chain form a platform composed of an eight β-strand anti-parallel sheet and two long α-helices. The α3 domain of the heavy chain and the light chain, β2m, are Ig-like domains of the C1-set. The major structural difference relative to class I MHC molecules is that the long helix of the α2 domain is bent in FcRn with the N-terminal portion of the helix and the outer two β-strands displaced as a unit. This displacement effectively closes the peptide binding groove present in class I MHC molecules. At the position where the helix bends, there is a proline residue that is conserved among the three known FcRn sequences but is a valine in class I MHC molecules. Since proline residues are substituted on their amino group they are unable to make one of the two hydrogen bonds characteristic of residues in an α-helix. Research is underway to examine the effect of substituting the FcRn proline with the class I valine (J. Lebron, ..., PJB).

In each of three crystal forms used in the FcRn structure determination, the same dimer of FcRn molecules was observed (Figure 7; Burmeister et al. 1994a). Because the binding of FcRn and IgG occurs with a stoichiometry of 2:1 FcRn:IgG (Huber et al., 1993), it was postulated that this dimer could be functionally important for IgG binding (Burmeister et al., 1994a,b). The role of FcRn dimerization in IgG binding was directly tested by introducing cysteines at positions that either facilitated or hindered receptor dimerization when FcRn was coupled through these cysteines to a biosensor chip (Raghavan et al., 1995b). High affinity binding was observed when FcRn was coupled in the orientation facilitating dimerization. Binding affinity was reduced more than 100-fold when receptor dimerization was hindered. Thus, the high affinity IgG binding observed *in vivo* requires FcRn dimerization in order to be reconstituted *in vitro.*

A low (~6 Å) resolution crystal structure was determined for FcRn complexed with the Fc portion from a mixture of rat IgGs (Burmeister et al., 1994b). These crystals

have a stoichiometry of 2:1 FcRn:IgG, with one FcRn molecule and one half of an Fc molecule in the asymetric unit (Huber et al., 1993). In this case the FcRn dimer and the Fc monomer are related by different crystallographic symmetry operators (Figure 8). In addition to the FcRn structure described above, the structure of an Fc portion of IgG was also known from a previous crystallographic analysis (Deisenhofer, 1981). Electron density for the FcRn molecule and C3 domain of Fc allowed these known structures to be positioned accurately. Because there was little or no electron density for the C2 domain, this domain's position is less well determined (Burmeister et al., 1994b). Nonetheless, this structure was used to identify the site on Fc that interacts with FcRn as the interface of the C2 and C3 domains (Figure 8). This is the same portion of Fc that binds fragment B of protein A (Deisenhofer, 1981). It had previously been shown that a genetically engineered analog of fragment B competitively inhibits FcRn binding to Fc (Raghavan et al., 1994), and that protein A-IgG complexes have a shorter serum persistence than uncomplexed IgG (Dima et al., 1983). The principle Fc binding site on FcRn is in the $\alpha 2$ domain (amino acids 113-119 and 131-137), although the N-terminus of $\beta 2m$ and some epitopes on the $\alpha 3$ domain of the dimer related FcRn molecule could also be involved (Burmeister et al., 1994b). Mutation of FcRn residues in $\alpha 3$ domain (either residues 219-224 or the consecutive histidine residues 250 and 251) to the corresponding residues in class I MHC molecules reduces the affinity for IgG slightly (~2-fold and 6- to 7-fold respectively; Raghavan et. al., 1994). Each of these mutations are at positions that would not directly affect IgG binding to an FcRn monomer, but could effect the interaction of IgG with the dimer related FcRn molecule. Taken together the low resolution FcRn-Fc complex structure and these biochemical studies have provided the crude structural epitopes for the binding of FcRn to IgG.

Site directed mutagenesis of the Fc region has identified functionally important epitopes for inhibition of FcRn binding, neonatal and prenatal transcytosis, and protection

from a default degradative pathway. For murine IgG1 (mIgG1), mutants I253A[5] or H310A have greatly reduced interaction with FcRn (Table 2). Either of these mutations reduces fetal transmission of IgG, inhibition of neonatal transmission of IgG, inhibition

Mutation	FcRn Affinity	Neonatal Transcytosis	Fetal Transcytosis	Plasma clearance
A.	inhibition (%)	inhibition (%)	transmission (%)	$t_{1/2}$ β-phase (hr)
mIgG1-Fc	68	46	1.7	83
H285A	66	45	1.4	76
I253A	12	4	0.4	20
H310A	4	6	0.2	17
H433A	52	34	1.4	115
N434A	48	40	1.3	115
N434Q				115
H435A	5	12	0.1	17
H436A	16	25	1.5	46
B.	inhibition (%)	inhibition (%)	transmission (%)	$t_{1/2}$ β-phase (hr)
mIgG1-Fc	67	55	2.8	120
I253A	31	20	0.2	26
H310A,Q311N	26	9	0.2	18
H433A,N434Q	54	44	0.7	50
310-311/433-434(*)	22	5	0.2	16
C.	Kd (nM)			
hIgG4	22			
H435R	24			
M252G,I253G,S254G	1700			
L309G,H310G,Q311G	1900			

Table 2: Site directed Fc mutants effect on FcRn funcction. This table summarizes the results of several studies which have examined the role of specific amino acid subtitution of the Fc ligan on the various FcRn functions. These studies are Medesan et al., 1997 (part A.); Kim et al., 1994a,b and Medesan et al., 1996 (part B.); and Raghavan et al., 1995 (part C.). Parts A. and B. summarize the interaction of murine FcRn with murine Fc, while part C. * The mutant labelled as 310-311/433-434 has the H310A,Q311N and H433A,N434Q mutations.

of IgG binding to FcRn, and have an increased rate of catabolism relative to wild type Fc

---

5 Throughout this chapter site directed mutants will be abreviated by the one letter amino acid symbol of the wild-type residue, the amino acid sequence number, and the mutant residue. Thus I253A is isoleucine 253 mutated to alanine.

(Medesan et al., 1997). These results are entirely consistent with previous reports on mutations in mIgG1 (Kim et al., 1994a,b; Medesan et al., 1996) and human IgG4 (hIgG4; Raghavan et al., 1995). But mutation H435A and to a lesser extent H436A but not H433A, N434Q, nor N434A reduces the interaction of the Fc fragment of mIgG1 with FcRn (Medesan et al., 1997). These results apparently contradict previous reports from the same laboratory that the double mIgG1 mutant H433A,N434Q inhibits the interaction with FcRn (Kim et al., 1994a,b; Medesan et al., 1996) and from our laboratory that mutation H435R in hIgG4 has a negligible effect on the interaction with FcRn (Raghavan et al., 1995). Regarding the conflict with their previous results, the authors suggest that "The most plausible explanation for the observed effects of mutation of both H433 and N434 is that simultaneous mutation of these two amino acids causes a local perturbation in the orientation of the adjacent histidine (H435), which, in contrast to H433 and N434, plays a critical role in the FcRn-mIgG1 interaction" (Medesan et al., 1997). Presumably mutations H433A, N434A, and N434Q are insufficient to cause this local perturbation. Similarly, regarding the hIgG4 result, the authors say "it is conceivable that in the context of differences in the sequences of surrounding residues, the relative roles of H433 and H435 are distinct in different isotypes" (Medesan et al., 1997).

The work described in the subsequent chapters is an investigation of the molecular mechanism through which FcRn binds IgG at acidic but not alkaline pHs. In Chapter 1, I describe the method that I use to characterize the interaction of IgG with FcRn and report the finding that immobilized FcRn binds IgG with higher affinity than soluble FcRn. Chapter 2 describes amino acid substitutions to FcRn and their effect on IgG affinity. This investigation provides the most detailed experimental map of the IgG binding site on FcRn. In Chapter 3, I describe the structure of FcRn at an alkaline pH and an additionally refined structure of FcRn at an acidic pH. These structures include an

extensive carbohydrate structure that is necessary for the dimerization of FcRn. These structures provide the basis upon which I propose a mechanism for the pH dependent IgG binding to FcRn. In the final chapter, I summarize our current understanding of the FcRn-IgG molecular interaction and speculate on the cellular mechanism through which FcRn mediates the acquisition of passive immunity and the protection from degradation.

Acknowledgments

I would like to thank my father for extensive editorial work, Pamela Bjorkman for figures 1A, 6, 7, and 8, and Pamela and members of her laboratory, for critical reading of the manuscript.

References

Ahouse JJ, Hagerman CL, Mittal P, Gilbert DJ, Copeland NG, Jenkins NA, Simister NE. 1993. Mouse MHC class-I like Fc receptor encoded outside the MHC. J. Immunol. 151: 6076-6088

Arey, LB. 1954. Developmental Anatomy, 6th ed. Saunders, Philadelphia.

Balinsky, BI. 1981. An Introduction to Embryology, 5th ed. CBS College Publishing, New York.

Bamford DR. 1966. Studies *in vitro* of the passage of serum proteins across the intestinal wall of young rats. Proc. R. Soc. B. 166: 30-45.

Bjorkman PJ, Parham P. 1990. Structure, function and diversity of class I major histocompatibility complex molecules. Ann. Rev. Biochem. 90: 253-88.

Bjorkman PJ. 1997. MHC Restriction in three dimensions: A view of T cell receptor/ligand interactions. Cell. 89: 167-170.

Blumberg RS, Koss T, Story CM, Barisani D, Polischuk J, Lipin A, Pablo L, Green R, Simister NE. 1995. A major histocompatibility complex class I-related Fc receptor for IgG on rat hepatocytes. J. Clin. Invest. 95: 2397-2402.

Brambell FWR, Hemmings WA, Henderson M, Parry HJ, Rowlands WT. 1949 The route of antibodies in the stomach contents of foetal rabbits. Proc. R. Soc., B. 136: 131-144.

Brambell FWR, Halliday R, Morris IG. 1958. Interference by human and bovine serum and serum protein fractions with the absorption of antibodies by suckling rats and mice. Proc. R. Soc., B. 149: 1-11.

Brambell FWR, Halliday R, Hemmings WA. 1961. Changes in ^{132}I-labelled immune bovine γ-globulin during transmission to the circulation after oral administration to the young rat. Proc. R. Soc., B. 153: 477-489.

Brambell FWR, Hemmings WA, Morris IG. 1964. A theoretical model of g-globulin catabolism. Nature. 137: 1352-1355.

Brambell FWR. 1966. The transmission of immunity from mother to young and the catabolism of immunoglobulins. Lancet. ii: 1087-1093.

Brambell FWR. 1970. The transmission of passive immunity from mother to young. North-Holland Publishing Co., Amsterdam.

Brierley J, Hemmings WA. 1956. The selective transport of antibodies from the yolk sac to the circulation of th echick. J Embryol. exp. Morph. 4: 34-41.

Burmeister WP, Gastinel LN, Simister NE, Blum ML, Bjorkman PJ. 1994a. The 2.2 Å crystal structure of the MHC-related neonatal Fc receptor. Nature 372: 379-383

Burmeister WP, Huber AH, Bjorkman PJ. 1994b. Crystal structure of the complex between the rat neonatal Fc receptor and Fc. Nature 372: 336-343

Davies DR, Metzger H. 1983. Structural basis of antibody function. Annu. Rev. Immunol. 1: 87-117

Deisenhofer J. 1981. Crystallographic refinement and atomic models of a human Fc fragment and its complex with fragment B of protein A from *Staphylococcus aureus* at 2.9- and 2.8-Å resolution. Biochemistry 20: 2361-2370

Fahey JL, Robinson AG. 1963. Factors controlling serum γ-globulin concentration. J. Exp. Med. 118: 845-868.

Fersht A. 1977. Enzyme structure and mechanism. WH Freeman and Co., New York.

Gastinel LN, Simister NE, Bjorkman PJ. 1992. Expression and crystallization of a soluble and functional form of an Fc receptor related to class I histocompatibility molecules. Proc. Natl. Acad. Sci. USA 89: 638-642

Ghetie V. Hubbard JG, Kim JK, Ysen MF, Lee Y, Ward ES. 1996. Abnormally short serum half-lives of IgG in β2-microglobulin-deficient mice. Eur. J. Immunol. 26: 690-696.

Gustafsson E, Mattsson A, Holmdahl R, Mattsson R. 1994. Pregnancy in B-cell-deficient mice--postpartum transfer of immunoglobulins prevents neonatal runting and death. Biol Reprod. 51: 1173-1180.

Halliday R. 1955. The absorption of antibody from immune sera by the gut of the young rat. Proc. R. Soc., B. 143: 408-413.

Halliday R. 1957. The absorption of antibody from immune sera and from mixtures of sera by the gut of the young rat. Proc. R. Soc., B. 148: 92-103.

Huber AH, Kelley RF, Gastinel LN, Bjorkman PJ. 1993. Crystallization and stoichiometry of binding of a complex between a rat intestinal Fc receptor and Fc. J. Mol. Biol. 230: 1077-1083

Isreal EJ, Patel VK, Taylor SF, Marshak-Rothstein A, Simister NE. 1995. Requirement for a β2-microglobulin-associated Fc receptor for acquisition of maternal IgG by fetal and neonatal mice. J. Immunol. 154: 6246-6251.

Isreal EJ, Wilsker DF, Hayes KC, Schoenfield D, Simister NE. 1996. Increased clearance of IgG in mice that lack β2-microglobulin: possible protective role of FcRn. Immunology

Jones EA, Waldmann TA. 1972. The mechanism of intestinal uptake and transcellular transport of IgG in the neonatal rat. J. Clin. Invest. 51: 2916-2927.

Jordan SM, Morganv EH. 1967, Albumin, transferrin, and gamma-globulin metabolism during lactation in the rat. Q. Jl. exp. Physiol. 52: 422-429.

Junghans RP. 1997. Finally! The Brambell receptor (FcRB). Mediator of transmission of immunity and protection from catabolism for IgG. Immun. Res. 16: 29-57.

Junghans RP, Anderson CL. 1996. The protection receptor for IgG catabolism is the β2 microglobulin-containing intestinal transport receptor. Proc. Natl. Acad. Sci. 93: 5512-5516.

Kim J-K, Tsen M-F, Ghetie V, Ward ES. 1994. Identifying amino acid residues that influence plasma clearance of murine IgG1 fragments by site-directed mutagenesis. Eur. J. Immunol. 24: 542-548.

Kim J-K, Tsen M-F, Ghetie V, Ward ES. 1994. Localization of the site of the murine IgG1 molecule that is involved in binding to the murine intestinal Fc receptor. Eur. J. Immunol. 24: 2429-2434

Mackenzie NM, Morris B, Morris R. 1983. Protein binding to the brush borders of enterocytes from the jejunum of the neonatal rat. Biochim. Biophys. Acta 755: 204-209

Maung, R. T. 1963. Immunity in the tortoise, *Testudo ibera*. J. Path. Bact. 85: 51-66.

Medesan C, Radu C, Kim J-K, Ghetie V, Ward ES. 1996. Localization of the site of the IgG molecule that regulates maternofetal tranmission in mice. Eur. J. Immuno. 26: 2533-2536.

Medesan C, Matesoi D, Radu C, Ghetie V, Ward ES. 1997. Delineation of the amino acid residues involved in transcytosis and catabolism of mouse IgG1. J Immunol. 158:2213-2217.

Morris IG. 1957. The effects of heterologous sera on the uptake of rabbit antibody from the gut of young mice. Proc. R. Soc., B. 148: 84-91.

Morris IG. 1963. Interference with the uptake of quinea-pig agglutinins in mice due to fractions of papain hydrolyzed rabbit γ-globulin. Proc. R. Soc., B. 157: 160-169.

Popov S, Hubbard JG, Kim J-K, Ober B, Ghetie V, Ward ES. 1996. The stoichiometry and affinity of murine Fc fragments with the MHC class I-related receptor, FcRn. Mol. Immunol. 33: 521-529.

Raghavan M, Gastinel LN, Bjorkman PJ. 1993. The Class I MHC-related Fc receptor shows pH Dependent stability differences correlating with immunoglobulin binding and release. Biochemistry 32: 8654-8660

Raghavan M, Chen MY, Gastinel LN, Bjorkman PJ. 1994. Identification of interaction sites in the class I MHC-related Fc receptor/immunoglobulin G complex. Immunity 1: 303-315

Raghavan M, Bonagura VR, Morrison SL, Bjorkman PJ. 1995a. Analysis of the pH dependence of the neonatal Fc receptor/Immunoglobulin G interaction using antibody and receptor variants. Biochemistry 34: 14649-14657

Raghavan M, Wang Y, Bjorkman PJ. 1995b. Effects of receptor dimerization on the interaction between the class I MHC related Fc receptor and immunoglobulin G. Proc. Natl. Acad. Sci. USA 92: 11200-11204

Raghavan M, and Bjorkman PJ . 1996. Fc receptors and their interactions with immunoglobulins. Annu. Rev. Cell Dev. Biol. 12: 181-220.

Roberts DM, Guenthert M, Rodewald R. 1990. Isolation and characterization of the Fc receptor from fetal yolk sac of the rat. J. Cell Biol. 111: 1867-1876

Rodewald R. 1973. Intestinal transport of antibodies in the newborn rat. J. Cell Biol. 58: 189-211

Rodewald R. 1976. pH-dependent binding of immunoglobulins to intestinal cells of the neonatal rat. J. Cell Biol. 71: 666-670.

Rodewald R, Kraehenbuhl J-P. 1984. Receptor-mediated transport of IgG. J. Cell Biol. 99: 159s-164s

Simister NE, Mostov KE. 1989a. Cloning and expression of the neonatal rat intestinal Fc receptor, a major histocompatibility complex class I antigen homolog. Cold Spring Harbor Symposia on Quantitative Biol LIV: 571-580

Simister NE, Mostov KE. 1989b. An Fc receptor structurally related to MHC class I antigens. Nature 337: 184-187

Simister NE, Rees AR. 1985. Isolation and characterization of an Fc receptor from neonatal rat small intestine. Eur. J. Immunol. 15: 733-738

Simister NE, Story CM. 1996. Fcγ receptors in human placenta. In Human IgG Fc Receptors, ed. J. G. J. van de Winkel and P. J. A. Capel, 25-38. R. G. Landes Company

Story CM, Mikulska JE, Simister NE. 1994. MHC class I-like Fc receptor cloned from human placenta. J. Exp. Med. 180: 2377-2381

Wallace KH, Rees AR. 1980. Studies on the immunoglobulin G Fc fragment receptor from neonatal rat small intestine. Biochem. J 188: 9-16

Warr GW. 1994. A review of antibodies and immunoglobulin genes in vertebrates. Developmental and Comparative Immunology. 18: S39.

Williams AF, Barclay AN. 1988. The immunoglobulin superfamily - Domains for cell surface recognition. Annu. Rev. Immunol. 6: 381-405

Zijlstra M, Li E, Sajjadi F, Subramani S, Jaenisch R. 1989. Germ-line transmission of a disrupted β2-microglobulin gene produced by homologous recombination in embryonic stem cells. Nature 342: 435-438.

Zijlstra M, Bix M, Simister NE, Loring JM, Raulet DH. 1990. β2-microglobulin deficient mice lack $CD4^{-}8^{+}$ cytolitic T cells. Nature 344: 742-746.

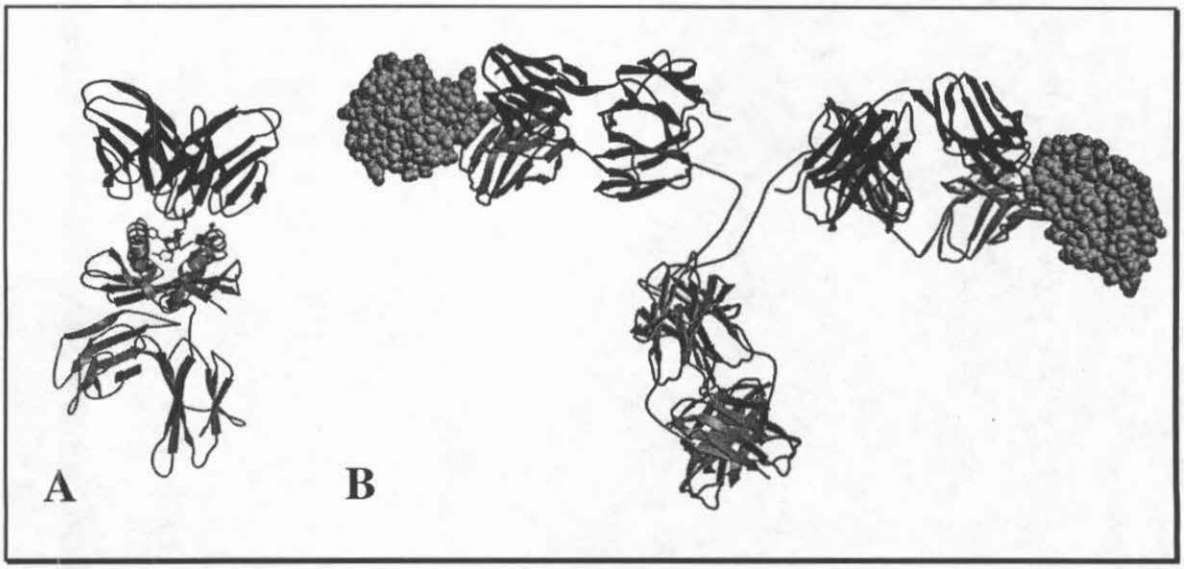

Figure1. Antigen Recognition. A) An MHC class I molecule (light grey) is shown presenting an antigenic peptide (black) to the variable portion of a T-cell receptor (dark grey). B) An antibody (with its heavy chain in light grey and it light chain in grey) is shown binding two copies of a protein antigen (light grey) through its two Fab domains. The lower domain is the Fc portion that is recognized by FcRn.

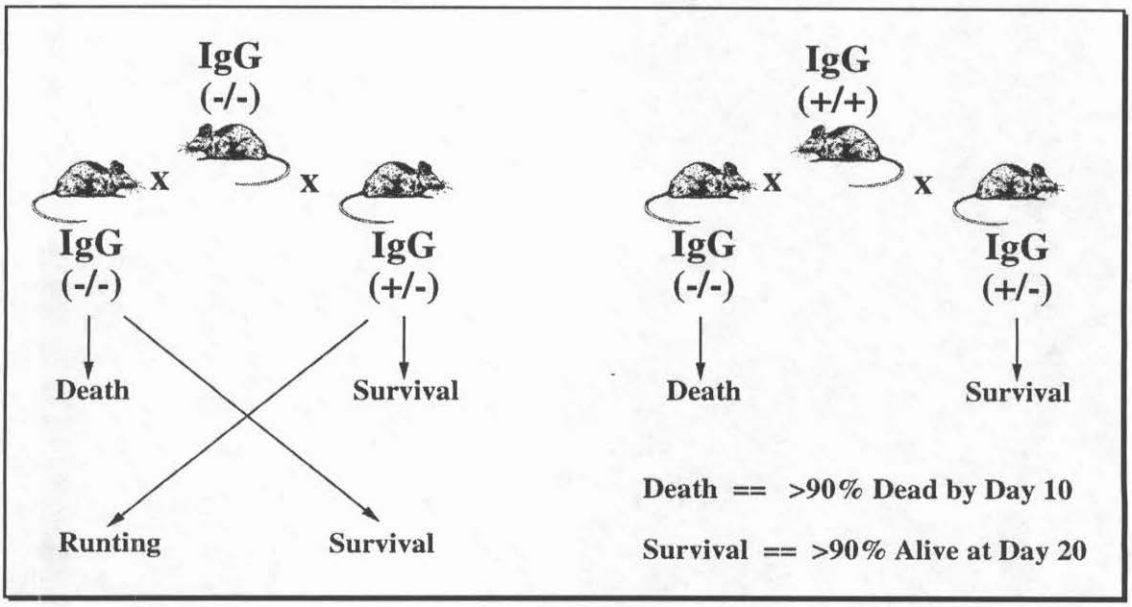

Figure 2. The importance of passive immunity--Male mice negative (left diagram) or positive (right) for IgG production were mated with female mice either negative (left mouse in each diagram) or positive (right) for IgG production. Offspring born and nursed by IgG producing mothers survived normally throughout the nursing period, whether or not the offspring themselves were able to produce IgG. Offspring born and raised by antibody deficient mothers suffered high mortality rates (> 90%) again whether or not the offspring could produce IgG. Offspring born to antibody deficient mothers, but nursed from birth by IgG producing foster mothers survived normally throughout the nursing period. Offspring born the IgG producing mothers, but nursed from birth were initially healthy, but suffered poor growth and intermediate mortality during the later stages of nursing.

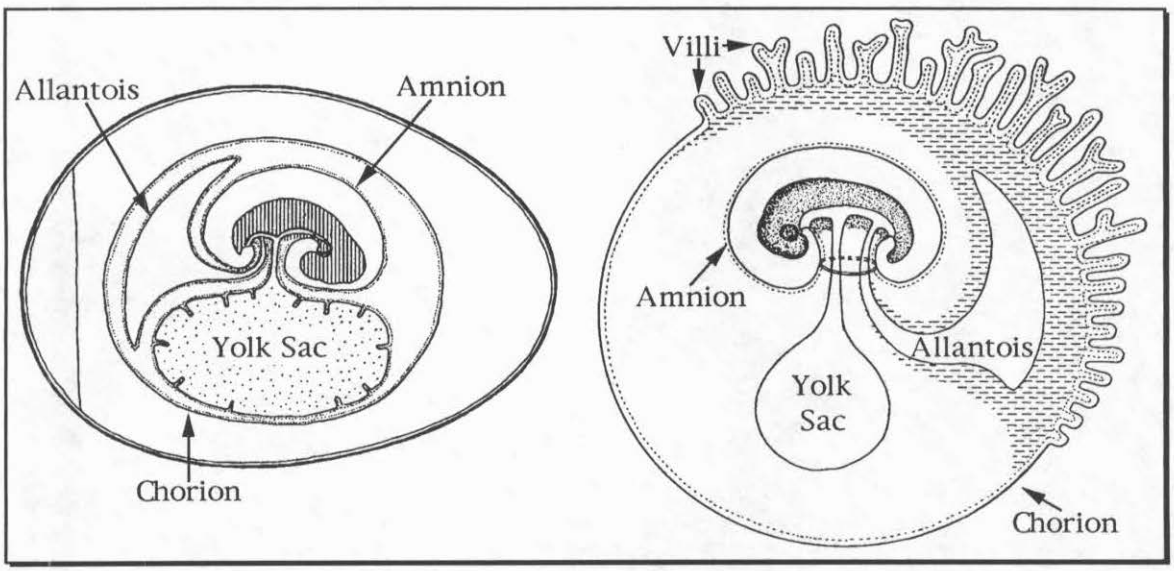

Figure 3. Embryonic Membranes--typical of a bird (left) and mammal (right). Based on similar figures in Ballinsky (1981).

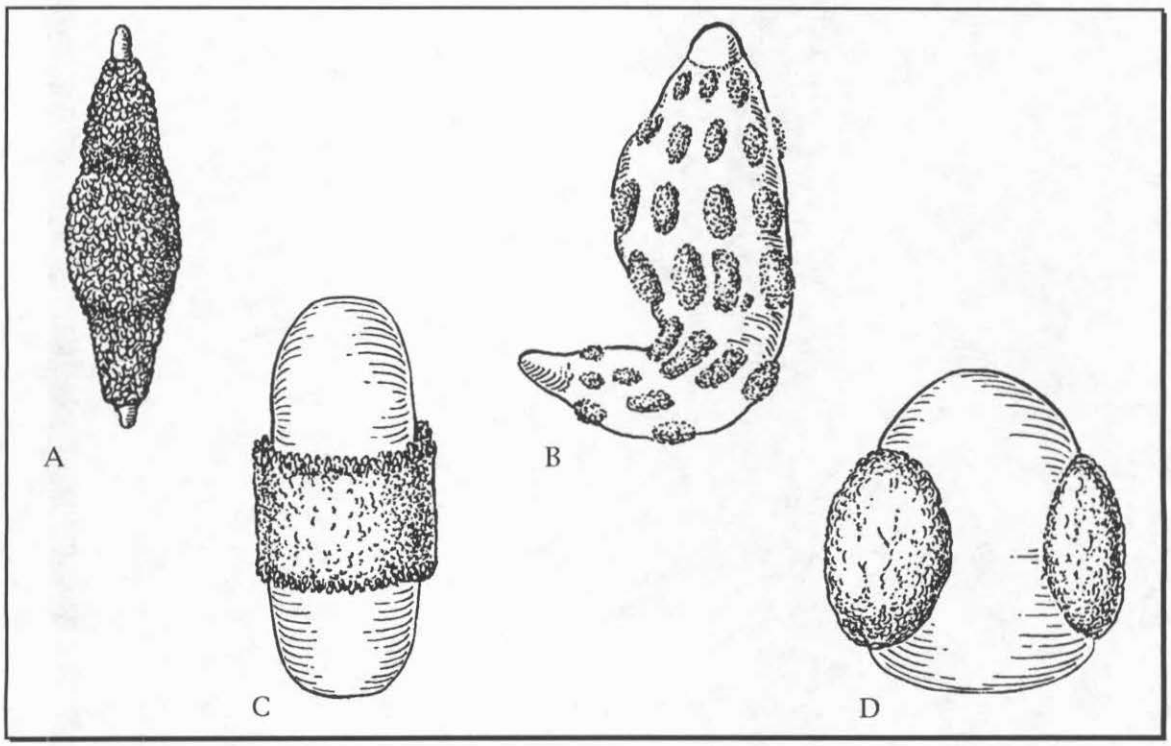

Figure 4. Placental Types--A, diffuse; B, cotyledonary; C, zonary; D, discoid. From Arey, 1954.

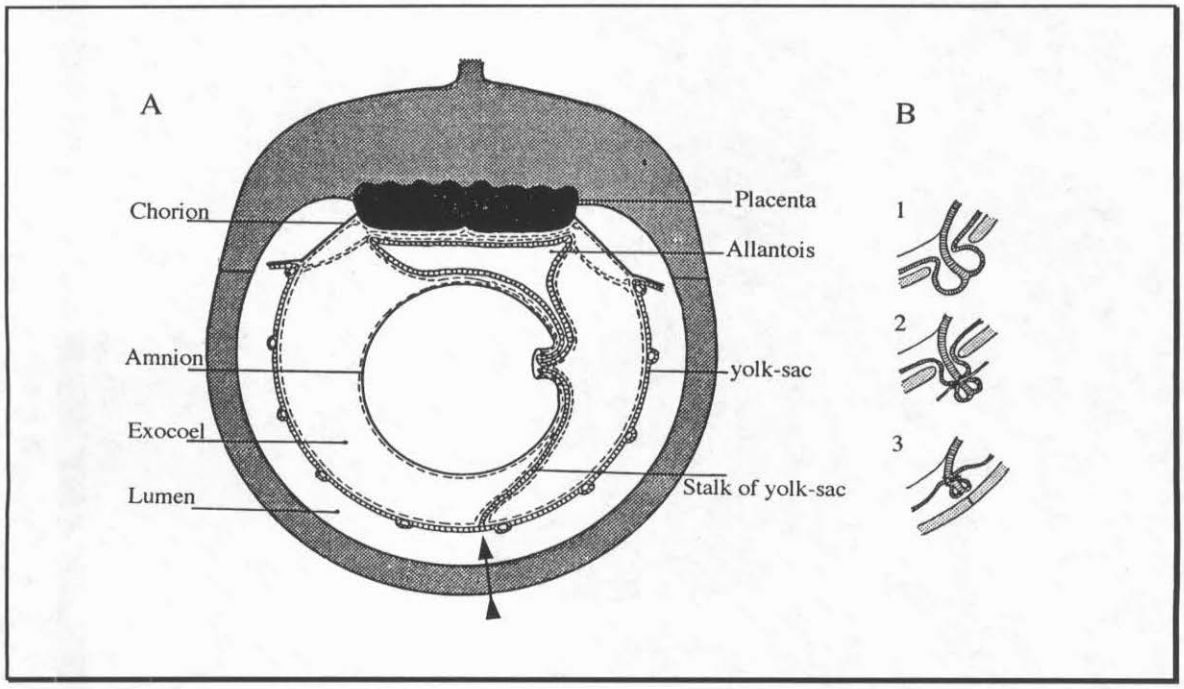

Figure 5. Ligature studies of the rabbit uterous. A) A scematic diagram showing the major embryonic membranes. The arrow points to the area that is operated on to ligate the vitrial vein. B) The stalk of the yolk sac is tied off and returned to the uterus so that the acquisition of maternal IgG by the developing fetus can be tested. Based on a similar figure by Brambell (1970).

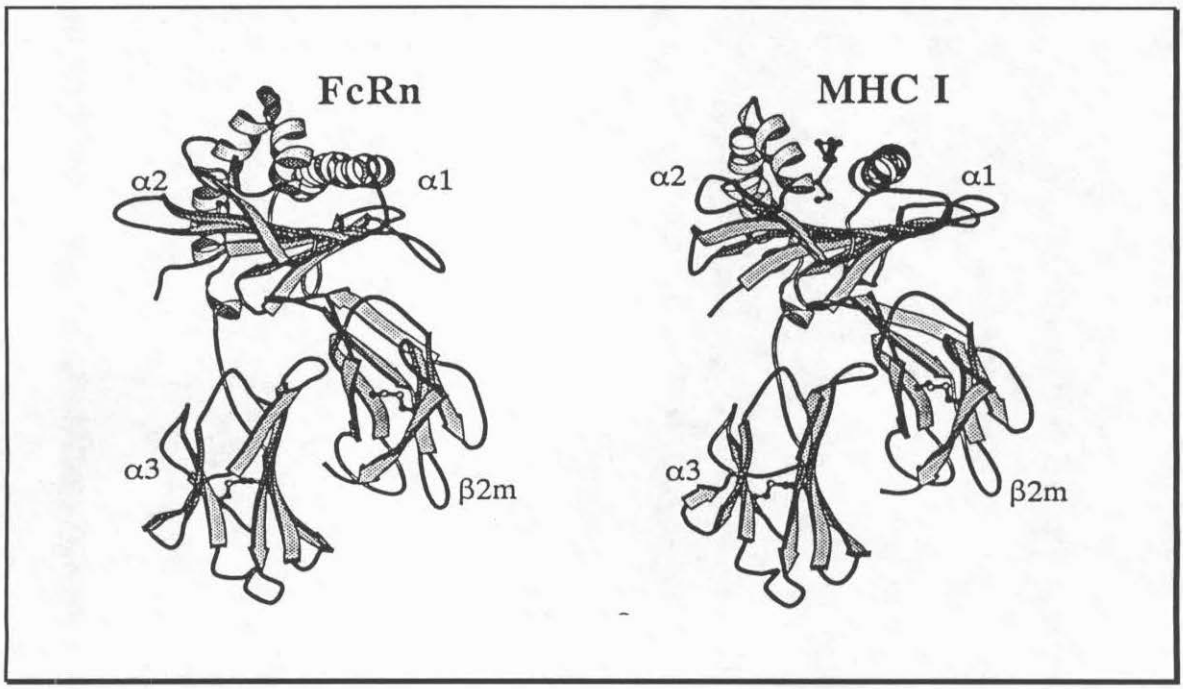

Figure 6. Ribbon diagrams of show the similar structures of FcRn and a class I MHC molecule.

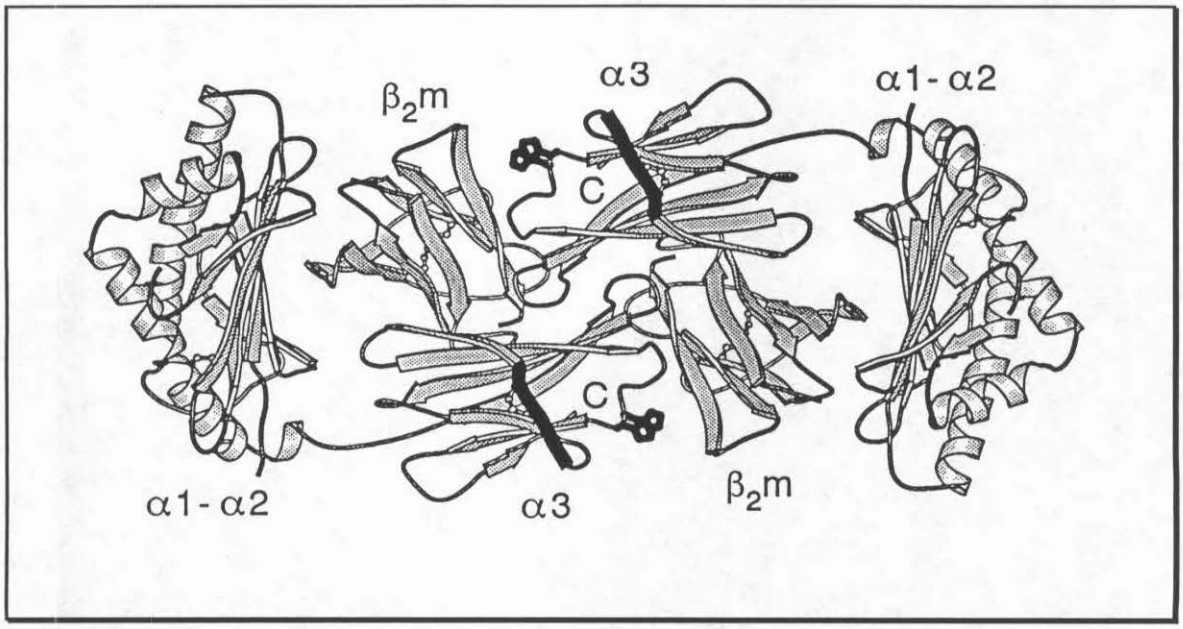

Figure 7. Two FcRn molecules pair to form a dimer observed in crystals of FcRn alone and in complex with Fc. Residues identified by site directed mutagenesis to slightly reduce the binding affinity for IgG are shown in black.

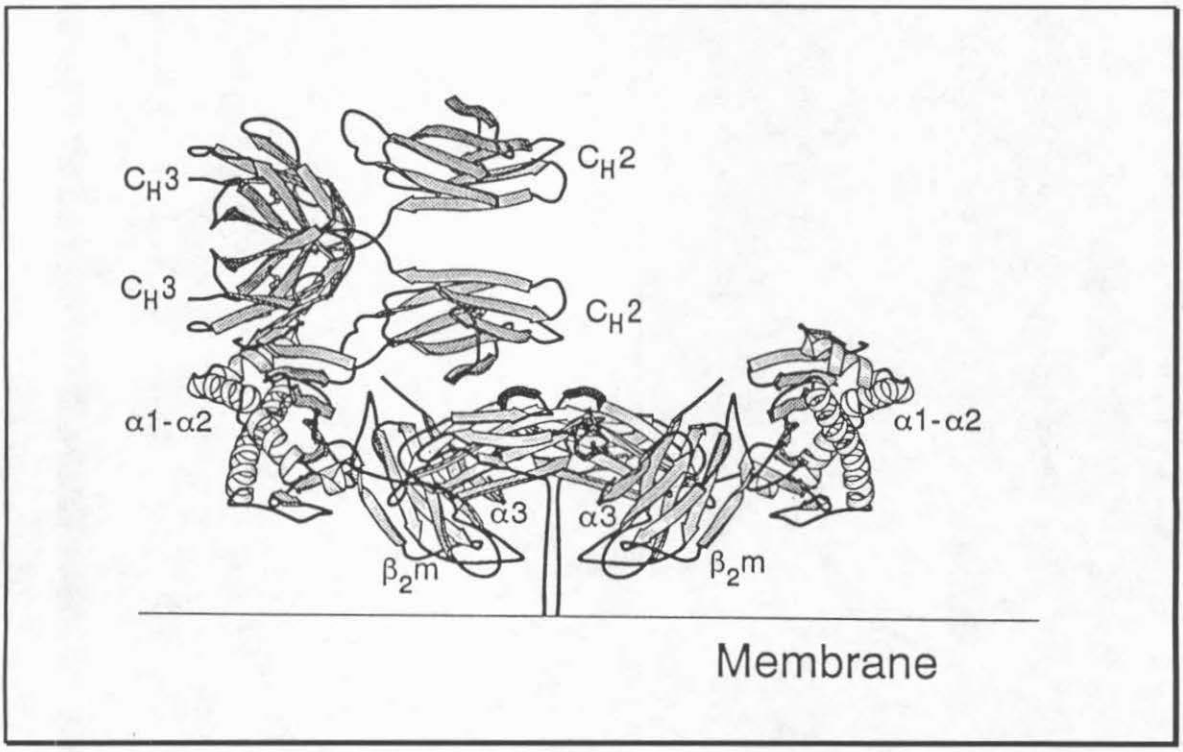

Figure 8. Complex of Fc (top) with the FcRn dimer (bottom).

9374 *Biochemistry* **1997,** *36,* 9374−9380

High-Affinity Binding of the Neonatal Fc Receptor to Its IgG Ligand Requires Receptor Immobilization†

Daniel E. Vaughn‡ and Pamela J. Bjorkman*,‡,§

Division of Biology 156-29 and Howard Hughes Medical Institute, California Institute of Technology, Pasadena, California 91125

Received April 10, 1997; Revised Manuscript Received May 20, 1997®

ABSTRACT: The neonatal Fc receptor (FcRn) binds maternal immunoglobulin G (IgG) during the acquisition of passive immunity by the fetus or newborn. In adult mammals, FcRn also binds IgG and returns it to the bloodstream, thus protecting IgG from a default degradative pathway. Biosensor assays have been used to characterize the interaction of a soluble form of FcRn with IgG. We use the statistical method of cross-validation to show that there are two classes of noninteracting binding sites, and these are sufficient to account for previously observed nonlinear Scatchard plots of FcRn/IgG binding data. We demonstrate that immobilization of FcRn on the biosensor surface reproduces the high-affinity IgG binding observed for membrane-bound FcRn, whereas immobilization of IgG results in lower affinity binding similar to that of the FcRn/IgG interaction in solution. The dependence of FcRn/IgG binding affinity on the coupled molecule provides further evidence in support of the previously hypothesized model that an FcRn dimer forms the high-affinity IgG binding site.

The neonatal Fc receptor (FcRn)[1] binds immunoglobulin G (IgG) in two important physiological processes: the transfer of IgG from mother to fetus or newborn and the protection of IgG from a default degradative pathway (reviewed in ref *1*). FcRn is structurally similar to class I MHC molecules, consisting of a homologous membrane-bound heavy chain and the class I MHC light chain, β_2-microglobulin (*2, 3*). A soluble form of FcRn, a heterodimer composed of the extracellular domains of the heavy chain complexed to β_2-microglobulin, was previously shown to be functionally active (*4*), retaining its high-affinity IgG binding at pH 6.0 with a sharp drop in affinity at pH values above 7 (*4*−*6*).

Our laboratory has used a biosensor assay to characterize the binding of soluble FcRn to IgG (*6*−*8*). Biosensors utilize a surface plasmon resonance (SPR) based assay that allows the formation of a protein−protein complex to be monitored several times per second (*9*−*11*). In this system, one molecule is immobilized at the sensor chip surface, and binding of the second molecule is monitored as it is passed over the chip. Scatchard and kinetic analyses of the binding between FcRn and IgG were used to calculate binding affinities (*6*−*8*). These characterizations were complicated by nonlinearity of the Scatchard plots, suggesting the presence of multiple classes of binding sites.

Here, we demonstrate that the interaction of IgG with immobilized FcRn can best be modeled as IgG binding to two classes of noninteracting sites on FcRn, and describe a method to derive accurate binding constants for each class. Using this method, we show that the affinities of FcRn for different IgGs are systematically higher when FcRn, rather than the IgG, is immobilized. The affinities of immobilized FcRn for IgG are comparable to those observed in binding assays using membrane-bound FcRn (*7, 12*), suggesting that immobilization of FcRn on a biosensor chip mimics the physiological situation. These results are interpreted with reference to previous work demonstrating that FcRn dimerization is required for high-affinity binding of IgG (*8*).

MATERIALS AND METHODS

Proteins and Reagents. Secreted rat FcRn (a heterodimer composed of residues 1−269 of the rat FcRn heavy chain associated with rat β2m) was purified from supernatants of transfected Chinese hamster ovary cells using pH-dependent binding to rat IgG affinity columns (*4*). 1B5 and 3F4 are murine IgG1 monoclonal antibodies against human Zn-α_2-glycoprotein (*13*). They were purified from ascites fluid by thiophillic adsorption on a T-gel column according to the manufacturer's protocol (Pierce Chemical Co.) and by FcRn affinity chromatography (*14*). Monoclonal mouse and rat antibodies of the specified subtypes were purchased from Pharmingen. Anti-CD4, a rat IgG2a, was purchased from Boehringer Mannheim. Polyclonal human IgG and Fc fragments (Hu IgG and Hu Fc; mixture of IgG1, IgG2, IgG3, and IgG4 subtypes) and polyclonal rat IgG and Fc fragments (mixture of IgG1, IgG2a, IgG2b, and IgG2c subtypes) were purchased from Jackson ImmunoResearch.

Protein concentrations were determined spectrophotometrically using extinction coefficients at 280 nm of 216 000 M^{-1} cm^{-1} [IgG; (*15*)] and 84 900 M^{-1} cm^{-1} (FcRn). The extinction coefficient for FcRn in aqueous solution was determined after measurement of the absorbance of the same

† Supported by a Camille and Henry Dreyfuss Teacher Scholar Award (P.J.B.) and a grant from the NIH (AI/GM41239 to P.J.B.).

* Corresponding author. Phone: 626 395-8350. Fax: 626 792−3683. E-mail: bjorkman@cco.caltech.edu.

‡ Division of Biology.

§ Howard Hughes Medical Institute.

® Abstract published in *Advance ACS Abstracts,* July 15, 1997.

[1] Abbreviations: β2m, β_2-microglobulin; EDC, *N*-ethyl-*N*′-[3-(diethylamino)propyl]carbodiimide; FcRn, Fc receptor, neonatal; hu IgG, human immunoglobulin G; IgG, immunoglobulin G; K_D, equilibrium dissociation constant; k_d, dissociation rate constant; mIgG, mouse immunoglobulin G; MHC, major histocompatibility complex; NHS, *N*-hydroxysuccinimide; rmsd, root mean square difference; rIgG, rat immunoglobulin G; RU, resonance units; SPR, surface plasmon resonance.

S0006-2960(97)00841-6 CCC: $14.00

concentration of protein in 6 M GuHCl and phosphate buffered saline (L. M. Sánchez and P.J.B., unpublished results). The reference solution's FcRn concentration was determined from the A_{280} in GuHCl and the theoretical extinction coefficient [valid only for denatured proteins; calculated from the amino acid sequence according to (*16*)].

Immobilization of IgG and FcRn on Biosensor Chips. A BIAcore biosensor system (Pharmacia LKB Biotechnology Incorporated) was used for real time binding experiments. This system includes a biosensor element with a dextran-coated gold surface to which FcRn or IgG was coupled using standard amine coupling chemistry as described in the BIAcore manual. Immobilization of soluble FcRn and IgG proteins using amine coupling chemistry was previously described (*6*−*8*).

Interpretation of Biosensor Data. Binding of soluble IgG or FcRn to the other molecule immobilized on the biosensor chip results in changes in the SPR signal that are directly proportional to the amount of bound protein, and read out in real time as resonance units (RU) (*9, 10*). Affinities were derived at pH 6.0 by analysis of data obtained from room temperature injections of different concentrations of injected protein in 50 mM phosphate, 150 mM NaCl. Each injection onto an FcRn- or IgG-coupled flowcell was followed by an identical injection onto a blank flowcell of the same chip in order to subtract out significant nonspecific responses.

Two methods were used to derive the equilibrium dissociation constant (K_D). In the first [a Scatchard analysis (*17*)], the slope of the plot of R_{eq}/[ligand] versus R_{eq} is equal to $-1/K_D$ (where R_{eq} is the equilibrium biosensor response and ligand refers to the injected protein). In the second, R_{eq} was plotted versus the log of the concentration of the ligand. Nonlinear regression analysis (*18*) was used to fit these data to a binding model and to derive values for the K_D and the binding response at infinite concentration of ligand (R_{max}). The fit of the data to the following binding models was examined:

(i) A single class of noninteracting binding sites. R_{eq} is represented as

$$R_{eq} = R_{max}([\text{ligand}]/K_D)/(1 + [\text{ligand}]/K_D) \quad (1)$$

(ii) A somewhat more complicated model employing a Hill constant (H) to represent the cooperativity of a class of interacting binding sites. R_{eq} is represented as

$$R_{eq} = R_{max}([\text{ligand}]/K_D)^H/[1 + ([\text{ligand}]/K_D)^H] \quad (2)$$

A Hill constant greater than 1 indicates positive cooperativity; i.e., the binding of one ligand facilitates the binding of additional ligands. A Hill constant less than 1 indicates negative cooperativity; i.e., the presence of a ligand hampers the binding of additional ligands.

(iii) Multiple classes of noninteracting binding sites. R_{eq} is represented as

$$R_{eq} = R_{max}\sum_i f_i\{([\text{ligand}]/K_{D,i})/(1 + [\text{ligand}]/K_{D,i})\} \quad (3)$$

where f_i denotes the fraction of total binding sites in each class and $\sum_i f_i = 1$. (iv) Multiple classes of interacting sites. R_{eq} is represented using eq 3 with the incorporation of Hill coefficients as in eq 2.

For comparison of the models, three statistical parameters were calculated. The correlation coefficient, r^2, is defined as $[\sum_i(x_i - \langle x\rangle)(y_i - \langle y\rangle)]^2/(\sum_i(x_i - \langle x\rangle)^2\sum_i(y_i - \langle y\rangle)^2]$. The rmsd is defined as the root mean square difference between observed and predicted responses for all concentrations tested. The free rmsd was calculated as follows: Data points were omitted one at a time, and a best fit of the model to the remaining data was calculated. For each best fit model, the difference was calculated between the predicted and observed responses for each omitted concentration. The free rmsd is the root mean square of these differences.

For calculation of kinetic constants, the BIAevaluation 2.1 software package was used to fit dissociation curves using a single-exponential dissociation rate equation ($y = R_0e^{-k_d t}$; where R_0 is the observed response at the start of the dissociation and k_d is the dissociation rate constant) or a bi-exponential dissociation rate equation [$y = R_0(f_1e^{-k_{d,1}t} + f_2e^{-k_{d,2}t}$), where $k_{d,1}$ and $k_{d,2}$ represent fast and slow dissociation rate constants and f_1 and f_2 correspond to the fraction of complexes dissociating with each rate constant]. Using the BIAevaluation 2.1 software, an F-test-based comparison between derived χ^2 values for the single-exponential or two-exponential fits yielded an estimated probability for each dissociation curve of which model produced the best fit to the data. In all cases for which two k_d values are reported, the probability that the biexponential model is valid was greater than 0.99. The possibility that the second dissociating population arises from mass transfer effects was ruled out by showing that the dissociation behavior showed no dependence on flow rate (data not shown).

RESULTS

IgG Binding to Immobilized FcRn Fits a Model for Two Noninteracting Classes of Binding Sites. We immobilized FcRn on a biosensor chip and measured the biosensor response at equilibrium (R_{eq}) for the binding of a series of concentrations of a monoclonal IgG. Since large amounts of IgG were needed for injections at high concentrations [and polyclonal rat and mouse IgG bind to rat FcRn with approximately equal affinities (*19*)], we used a mouse monoclonal IgG1 antibody available in the laboratory [1B5 (*13*)].

K_D's are typically derived from biosensor data using a Scatchard plot, in which the slope of the plot of R_{eq}/[injected protein] versus R_{eq} is equal to $-1/K_D$. Determination of binding constants by this method is straightforward for a single class of identical independent sites. However, if there are multiple classes of independent sites or cooperative interactions between sites, the resulting function is nonlinear, and the interpretation is far more complicated. The Scatchard plot for the interaction between immobilized FcRn and the 1B5 IgG shows marked nonlinearity (Figure 1A), as also observed for the FcRn interaction with other IgGs [data not shown; discussed in (*6, 8*)]. In the previous work, only the data points that correspond to the high-affinity interaction were considered for calculation of the high-affinity K_D.

An alternative method of analysis involves a plot of the equilibrium biosensor response as a function of the log of IgG concentration, and nonlinear regression fitting of these data to a binding model (Figure 1B). This method is preferred over Scatchard analysis for the derivation of binding affinities because (i) the affinity constant is derived using concentrations of protein that bracket the K_D, whereas an affinity can be extrapolated using an inappropriate concentration range in a Scatchard analysis, and (ii) less propagation of experimental error leads to more accurate calculated affinities (*20*).

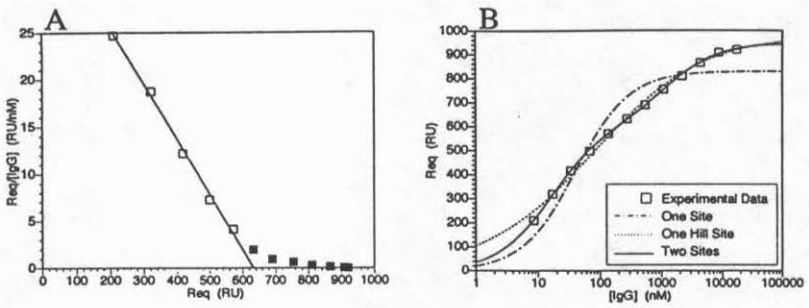

	Best Fit Parameters								Quality of Fit		
Model	$K_{D,1}$ nM	H_1	f_1 %	$K_{D,2}$ μM	H_2	f_2 %	$K_{D,3}$ μM	f_3 %	r^2	rmsd RU	Free rmsd RU
1-Site	40	----	100						0.92	59	71
1-Hill	77	0.49	100						0.994	14	20
2-Site	16	----	63	1.2	----	37			0.9997	3	4
2-Hill	15	1.01	60	1.2	0.88	40			0.9997	3	7
3-Site	15	----	60	1.6	----	30	0.25	9	0.9998	2	4

FIGURE 1: Comparison of Scatchard and nonlinear regression analyses for determining the affinity of IgG binding to immobilized FcRn. FcRn was coupled to a density of 2200 RU (for the experiment shown, and with similar results to densities from 2000 to 4000 RU, data not shown), and 1B5 IgG was injected at the concentrations indicated on the right panel. The same equilibrium binding data are plotted for Scatchard analysis (panel A) and directly as function of IgG concentration (panel B). The Scatchard plot is distinctly nonlinear. The five data points shown as open squares (which correspond to the five lowest IgG concentrations) were used to determine a best fit line from which a high-affinity K_D of 14 nM was derived. The data were also fit using nonlinear regression analysis to five potential binding models. The best fit lines for three of the models are shown; the two most complicated models superimpose closely upon the "Two Sites" model and were omitted for clarity. The best fit parameters and measures of the quality of fit for each of the models, as defined under Materials and Methods, are shown below the plots. The two-site model is the best representation because it is the simplest model that fully accounts for the data.

The binding data were fit to models assuming one, two, or three noninteracting sites and one or two interacting sites. As shown in Figure 1B, the assumption of a single class of binding sites results in a relatively poor fit to the experimental data as judged by the correlation coefficient and rmsd. Adding a Hill coefficient to account for cooperativity among a single class of binding sites improves the fit to the data, but the cooperativity model does not fit the experimental data points as well as a model assuming two classes of noninteracting binding sites. This model predicts the presence of a second lower affinity class of binding sites which are not saturated unless high concentrations of IgG are injected.

More complicated models (three classes of noninteracting binding sites and two classes of cooperative binding sites) also fit the experimental data well. Addition of parameters to a model will usually improve the best fit to the data, therefore resulting in a lower rmsd, but carries the risk of overfitting, i.e., modeling the noise. A model that accurately reproduces the experimental signal should also fit well to data which are excluded while fitting the model parameters (the statistical principle of cross-validation). Using the cross-validation method of testing statistical models (*21*), we calculated a "free rmsd" for each model. The two noninteracting sites model produced both a lower rmsd and a free rmsd than either of the one-site models, demonstrating that the two site model more fully accounts for the data. When two Hill coefficients are included in the two-site model, the rmsd stays the same, but the free rmsd increases slightly, an example of overfitting the data. Addition of a third class of sites yields a slightly lower rmsd compared to the two noninteracting sites model, but a comparable free rmsd, and thus does not significantly improve the fit of the model to the data.

The preceding analyses demonstrate that the interaction of IgG with immobilized FcRn is best represented as two independent classes of IgG binding sites. The class of receptor binding sites with high affinity for IgG is populated at lower IgG concentrations. The derived binding affinity for the high-affinity class of binding sites ($K_{D,1}$ = 16 nM) corresponds to the K_D calculated from a Scatchard analysis when only the points corresponding to the high-affinity interaction are considered [K_D = 14 nM; Figure 1A, and see ref (*6, 8*)], but the identification of these points is somewhat arbitrary. The second class of binding sites is populated at higher concentrations of IgG. An accurate estimate of the binding affinity of this class of binding sites can only be derived when the concentration range of ligand brackets the K_D, which requires large amounts of IgG (~1 mg per experiment). Under these conditions, the derived binding affinity for the lower affinity class of sites ($K_{D,2}$) is 1.2 μM (Figure 1B).

Kinetic Differences between the Classes of FcRn Binding Sites for IgG. For each concentration of IgG, we analyzed the dissociation of IgG from immobilized FcRn. After the biosensor response reached an equilibrium level, dissociation of IgG was monitored for at least 2 min, and the dissociation phase was analyzed using single and biexponential rate equations. A two-exponential dissociation rate equation fits the data better than a single-exponential rate equation. The fast and slow dissociation rates are sufficiently different to calculate the contribution of each species to the total equilibrium biosensor response for each concentration of IgG. The components of the equilibrium response corresponding to the fast and slow dissociating populations were each fit to a model of one noninteracting binding site, demonstrating that the slow dissociating species binds with a high affinity and the fast dissociating species binds with a lower affinity

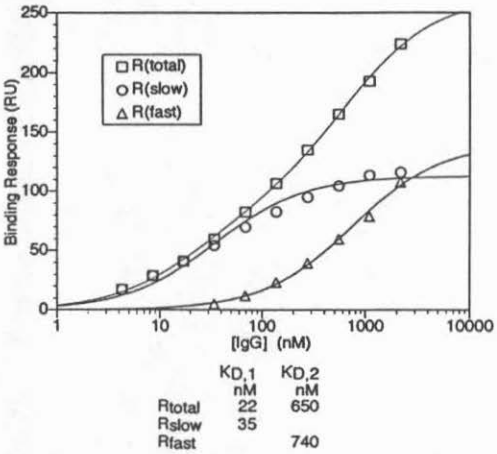

FIGURE 2: Analysis of the dissociation kinetics for the complex of IgG and immobilized FcRn. FcRn was coupled to a density of 2000 RU, and the dissociation kinetics of FcRn/IgG complexes formed at different IgG concentrations were analyzed. For IgG concentrations above 20 μM, the dissociation kinetics are best represented as a sum of two exponential decays: one with a fast rate constant and the other a slow rate constant. The contributions to the equilibrium response from the fast dissociating population (R_{fast}) and the slow dissociating population (R_{slow}) were determined and plotted as a function of IgG concentration. These data were fit to one-site binding models, and the total equilibrium response (R_{total}) was fit to a two-site model. The derived binding affinities (below panel) show that the slow dissociating population binds with high affinity, and the fast dissociating population binds with low affinity. In order to determine whether the two populations equilibrate independently or one forms from the other, we examined the dissociation behavior after various equilibration periods for a single IgG concentration (2.2 μM). A single concentration of IgG was passed over immobilized FcRn and allowed to bind for various times. The total response at the time of dissociation was measured, and the components of this response dissociating with fast and slow kinetics were calculated. The biosensor response for each population is relatively constant for each equilibration period, supporting the hypothesis that the two populations of complexes equilibrate independently (data not shown).

(Figure 2). Thus, both the equilibrium measurements and the dissociation kinetics are consistent with two populations of FcRn/IgG complexes: a high-affinity, slow dissociating species; and a low-affinity, fast dissociating species.

Since most previous determinations of FcRn binding affinities included an equilibration step followed by a washing step [e.g., (*12*, *22*, *23*)], we examined the dependence of the observed affinity on the duration of a washing step. Different concentrations of IgG were passed over immobilized FcRn, and the response was measured at equilibrium, and at 30, 60, and 600 s into the dissociation phase (Figure 3A). The equilibrium data were fit to a model of two independent binding sites. The other curves were fit assuming the values derived at equilibrium for the high- and low-affinity binding constants. Because the low-affinity complex dissociates faster, the fraction of IgG bound to the high-affinity class of binding sites increases with washing time. Indeed, after 10 min of washing, the fraction of complexes in the low-affinity class becomes negligible, and the data can be modeled as a single class of noninteracting binding sites (Figure 3B; Scatchard plots of these data become progressively more linear with increased washing time). We conclude that experiments which include room temperature washing steps of several minutes or longer would not detect either the biphasic nature of equilibrium Scatchard plots or the presence of a low-affinity class of binding sites.

High-Affinity Binding of FcRn to IgG Requires Receptor Immobilization. In previous studies of the interaction between FcRn and IgG, we noted differences in binding affinities depending on which species was immobilized on the biosensor surface (*7*, *8*). In order to characterize these differences, we immobilized the IgG used for the previous experiments (1B5) on the biosensor surface, and measured the equilibrium binding response for various concentrations of soluble FcRn (Figure 4). A best fit for each of the previously discussed five models was calculated. Using the criteria outlined above, the data are best modeled as two classes of independent FcRn binding sites on immobilized IgG. Comparing the affinities calculated for IgG immobilized to those calculated for FcRn immobilized demonstrates that, while the low-affinity binding constants are similar ($K_{D,2}$ = 2.4 μM for IgG immobilized; $K_{D,2}$ = 1.2 μM for FcRn immobilized), the high-affinity class of binding sites interacts more weakly when IgG is immobilized ($K_{D,1}$ = 210 nM for IgG immobilized; $K_{D,1}$ = 16 nM for FcRn immobilized). The dissociation kinetics for the FcRn interaction with IgG immobilized were also examined. As was the case with FcRn immobilized, the dissociation behavior is better modeled as two independently dissociating complexes than as a single species. Consistent with the comparison of the equilibrium binding results, the slow dissociating species dissociates faster when IgG rather than FcRn is immobilized ($k_{d,1} \geq 0.01$ s^{-1} for IgG immobilized; $k_{d,1}$ from 0.002 to 0.0002 s^{-1} for FcRn immobilized), while the fast dissociation rates are similar ($k_{d,2} \geq 0.01$ s^{-1} for either IgG or FcRn immobilized).

In order to examine if the difference in the affinity of the high-affinity class of binding sites generally depends on which species is immobilized, we did a systematic study of the binding interactions of nine different IgG molecules at pH 6.0, and derived K_D values corresponding to the high-affinity class of sites. For each monoclonal antibody, separate experiments were conducted with the antibody immobilized and with the receptor immobilized. For the interaction of each antibody with FcRn, the dissociation rate is slower and the affinity is higher when FcRn, rather than the IgG, is immobilized (Table 1). Because we see this effect for all of the IgG molecules tested, we conclude that these observed diffenences in affinity are a general property of the IgG/FcRn interaction.

Comparison of the Interaction of FcRn with IgG versus Fc. The binding site for FcRn is located within the Fc region of IgG, but the effects of including the F_{ab} arms of an intact antibody upon the FcRn interaction with Fc have not been systematically analyzed using biosensor technology. We therefore compared binding of several sets of IgGs and their corresponding Fc fragments to immobilized FcRn (Table 2). In each case, the binding data reveal the existence of high- and low-affinity populations of FcRn. The affinities and dissociation rates for IgG and Fc binding are similar, although high-affinity ($K_{D,1}$) FcRn/IgG complexes are slightly weaker interacting than the high-affinity FcRn/Fc complexes. This effect could be entropic (due to constraint of the IgG F_{ab} arms upon FcRn binding) and/or because the bulky F_{ab} arms interact unfavorably with FcRn. $k_{d,1}$ is faster for the Fc fragments (by a factor of ~2) than for the corresponding intact antibodies. The combination of faster dissociation rates and higher affinities for the high-affinity FcRn/Fc

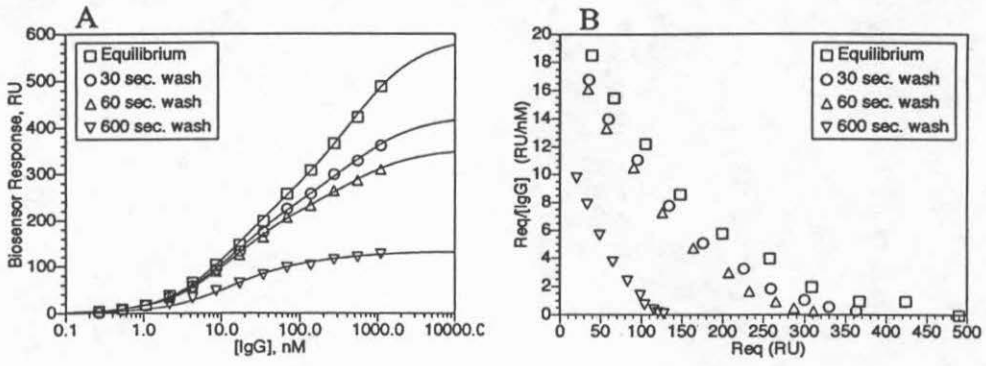

	$K_{D,1}$ nM	f_1 %	$K_{D,2}$ nM	f_2 %	R_{max} RU
R_{eq}	14	42	470	58	590
$R_{30\ sec}$	14	56	470	44	430
$R_{60\ sec}$	14	64	470	36	360
$R_{600\ sec}$	14	88	470	12	140

FIGURE 3: Effect of washing time on observed IgG affinity for immobilized FcRn. FcRn was coupled to a density of 2200 RU, and various concentrations of 1B5 IgG were injected. The biosensor response at equilibrium and after various washing durations is plotted as a function of concentration for the interaction of IgG with immobilized FcRn (panel A). The equilibrium data were best fit to a two site binding model. The curves representing experiments employing washing steps of 30, 60, or 600 s were fit to a two-site model constrained to the binding affinities determined using the equilibrium data. Because the low-affinity population dissociates with faster kinetics (Figure 2 and text), the washing step selectively depopulates the low-affinity site. Although biosensor methods allow equilibrium binding to be measured directly, many other methods employ a washing time of several minutes. For washing times of 10 min or longer, the Scatchard plots of these data (panel B) become essentially linear, and the existence of a low-affinity state would be missed.

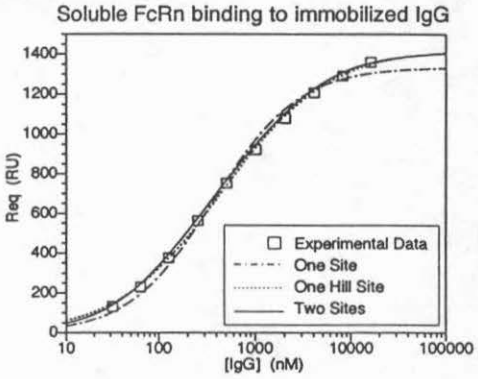

	Best Fit Parameters								Quality of Fit		
Model	$K_{D,1}$ nM	H_1	f_1 %	$K_{D,2}$ μM	H_2	f_2 %	$K_{D,3}$ μM	f_3 %	r^2	rmsd RU	Free rmsd RU
1-Site	370	—	100						0.994	36	47
1-Hill	460	0.80	100						0.9993	12	18
2-Site	210	—	66	2.4	—	34			0.99995	3	6
2-Hill	140	1.63	15	0.7	0.74	85			0.99997	2	6
3-Site	203	—	56	1.9	—	31	100*	13	0.99996	3	21

FIGURE 4: Soluble FcRn binding to immobilized IgG. 1B5 IgG was immobilized to a density of 3700 RU (for the experiment shown, and with similar results to densities from 1300 to 13000 RU, data not shown), and various concentrations of FcRn were injected. The biosensor response at equilibrium is plotted as a function of the concentration of IgG. Five binding models (see Figure 1) were fit to the data; again, the two-site model best represents the data. Asterisk: the third binding affinity in the three site model was fixed at 100 μM. Without constraint, this affinity and the corresponding R_{max} both increased toward infinity.

interaction compared to the high-affinity FcRn/IgG interaction implies that Fc fragment association rates must be faster (by a factor of ~4).

DISCUSSION

To achieve high-affinity binding comparable to that observed for cell surface FcRn, we find that the receptor, rather than its ligand, must be immobilized on the biosensor chip. Previously reported binding affinities for the interaction of IgG with rat FcRn on the surface of brush border, intestinal, or transfected cells are in the range of $K_D = 8-55$ nM (*7*, *12*). In the present study, we observe affinities ranging from 17 to 93 nM for a series of soluble IgGs binding to immobilized FcRn. For the complementary interaction, soluble FcRn interacting with the same IgGs, we consistently observed a lower affinity and faster dissociating class of

Table 1: Dependence of the High-Affinity Binding Mode on the Species Immobilized[a]

	FcRn immobilized		IgG immobilized	
	$K_{D,1}$ (nM)	$k_{d,1}$ (10^{-3} s^{-1})	$K_{D,1}$ (nM)	$k_{d,1}$ (10^{-3} s^{-1})
mIgG1	22	1.9	250	30
mIgG2a	39	0.5	370	20
mIgG2b	41	0.2	260	40
rIgG1	34	0.7	180	40
rIgG2a	15	0.3	80	10
rIgG2b	93	0.7	*	*
rIgG2c	84	1.3	740	20
anti-CD4 (rIgG2a)	24	0.5	74	30
1B5 (mIgG1)	17	1.0	210	10

[a] Equilibrium dissociation constants and dissociation rate constants are reported for the interaction of FcRn with monoclonal IgGs. For each IgG studied, either FcRn or the IgG was coupled to the biosensor surface. FcRn was coupled to a density of 2600 RU (and several concentrations between 2000 and 4000 RU for the 1B5 measurements). The same protocol was followed for coupling each IgG, resulting in densities between 500 and 7000 RU (*: rIgG2b was not coupled successfully with this protocol). Regardless of the coupling density, in each case in which IgG is immobilized, the high-affinity interaction is weaker and shows faster dissociation kinetics than the corresponding interaction when FcRn is immobilized. Only the high-affinity K_D values are reported for these experiments. The low-affinity K_D's could not be accurately determined because the quantities of most of the IgGs were limited, and we were not able to assay equilibrium binding at the high concentrations required to saturate the low-affinity binding mode. As can be seen by the close agreement of high affinity binding constants derived from three independent assays of 1B5 binding to immobilized FcRn (Figures 1−3), the high-affinity binding mode can be accurately measured in experiments in which the low-affinity mode is not saturated. The equilibrium and kinetic constants reported for 1B5 binding to immobilized FcRn are the average of the three experiments involving 1B5 presented in this paper.

Table 2: Comparison of Binding Affinities of Intact IgGs and Corresponding Fc Fragments for Immobilized FcRn[a]

	$K_{D,1}$ (nM)	$k_{d,1}$ (10^{-3} s^{-1})
3F4 IgG (mIgG1)	49	0.6
3F4 Fc	11	2.5
Hu IgG (polyclonal)	15	0.5
Hu Fc	9.7	0.9
Rat IgG (polyclonal)	4.1	0.6
Rat Fc	1.5	1.3

[a] FcRn was coupled to a biosensor chip to a density of 2600 RU. Affinities were derived for a two-site binding model by nonlinear regression analysis. Rate constants reported are an average for all concentrations of IgG injected.

binding sites (Table 1). The weaker affinities of immobilized IgGs for FcRn are comparable to the 500 nM K_D obtained by isothermal titration calorimetry for the interaction of soluble FcRn with human IgG (*14*). We conclude that FcRn must be constrained to some sort of two-dimensional surface (a membrane or a biosensor chip) to achieve high-affinity binding of IgG. In vivo, FcRn is an integral membrane protein that interacts with soluble IgGs; therefore, the interaction of immobilized FcRn with soluble IgG should be more representative of physiological conditions than the reverse situation (immobilized IgG interacting with soluble FcRn). In the study of the interaction between cholera toxin and gangliosides, it was also noted that biosensor analyses with the normally membrane-associated gangliosides immobilized reproduced whole cell assays more closely than free solution measurements, presumably because the biosensor measurements were performed on surfaces resembling the cell membrane (*24*).

Several previous studies support the hypothesis that two FcRn molecules dimerize, as observed in FcRn and FcRn/Fc crystals (*3, 25*), to form the high-affinity binding site for a single IgG. A 2:1 receptor:ligand stoichiometry was observed for rat FcRn interacting with IgG in solution and in crystals of the receptor/Fc complex (*14, 25*). Site-directed FcRn mutants with alterations that specifically affect the interaction of IgG with FcRn dimers, but not with monomers, show reduced affinities in biosensor assays and in measurements of labeled IgG binding to cell surface FcRn (*7*). Finally, the role of FcRn dimerization in its interaction with IgG was directly tested by introducing cysteines at positions that either facilitated or hindered receptor dimerization when FcRn was coupled to a biosensor chip using thiol chemistry (*8*). High-affinity binding (K_D = 22 nM) was observed when FcRn was coupled in the orientation facilitating dimerization, but the binding affinity was reduced to a $K_D > 4$ μM when receptor dimerization was hindered. In the present study, the K_D values derived for the high-affinity population of immobilized FcRn are similar to those observed for dimerization-facilitated FcRn (*8*), implying that the high-affinity population represents IgG bound to receptor dimers. When FcRn is immobilized on a biosensor chip, it is attached to a long flexible dextran moiety at concentrations $\geq\sim$100 μM (*26*). This FcRn concentration is much higher than the concentration of soluble FcRn interacting with immobilized IgG, and therefore the equilibrium between monomeric and dimeric FcRn will be shifted to include a larger fraction of dimer when FcRn is immobilized. Immobilization of FcRn also reduces the loss of entropy associated with dimerization, the major energetic hindrance to dimerization (*27*). The entropy of the monomer and of the dimer is reduced upon immobilization to the dextran molecules because some of their rotational and translational movements are restricted. Since the loss of entropy upon immobilization occurs twice for monomers but only once for a dimer, the loss of entropy upon dimerization is lower for immobilized FcRn than for soluble FcRn. Both of these effects promoting dimerization (higher local concentration and reduction in the loss of entropy) should increase the affinity for IgG for both membrane-associated FcRn and FcRn immobilized on a biosensor chip relative to the IgG affinity of soluble FcRn.

Previous biosensor analyses of the interaction of immobilized FcRn with IgG were complicated by nonlinear behavior in Scatchard analyses (*6, 8*). Here we show that two classes of noninteracting FcRn/IgG complexes are sufficient to explain this nonlinear behavior, and characterize them as a slow dissociating population with a similar affinity to the range of values calculated in studies using membrane-bound FcRn (*7, 12*), and a fast dissociating population with lower affinity. We have shown that it is the high-affinity mode that depends on which species is immobilized.

The low-affinity ($K_{D,2}$) fast dissociating ($k_{d,2}$) binding component is similar with either IgG or FcRn immobilized. This binding mode could exist under physiologically relevant conditions or could result from some specific property of the biosensor analysis. Characteristics of biosensor methodology that have been proposed to potentially alter a binding interaction include mass transfer properties of the soluble ligand and effects on the receptor due to its immobilization (*26, 28, 29*). Mass transfer considerations are important when evaluating kinetic data but irrelevant under equilibrium

conditions. Since the low-affinity populations are observed under equilibrium conditions, they cannot result from mass transfer effects. It is unlikely that the low-affinity FcRn population is an artifact of the amine coupling method because kinetic analysis revealed two classes of IgG binding sites for FcRn immobilized by thiol coupling methods (*8*). Using any coupling chemistry, steric hindrance of one immobilized FcRn molecule by another and/or occlusion of unoccupied binding sites by bound IgG molecules could introduce nonideal binding behavior. However, the excellent agreement of the equilibrium binding response to a two-site model suggests that this is not a significant effect in our case. If the low affinity-binding mode is not biosensor specific, then a population of FcRn molecules with low affinity for IgG could exist under physiological conditions. However, it would be difficult to detect on biological membranes because the techniques used to measure this interaction generally require a washing step that is long relative to the dissociation rate of the low-affinity complexes, and would therefore result in nearly complete dissociation of these complexes (Figure 3). Regardless of the origin of the low-affinity population, we can separate the contributions of the high- and low-affinity binding interactions. Therefore, our observations about the high-affinity binding mode are independent of the existence of a low-affinity mode.

Biosensor-based methods have been used to study the interaction between FcRn and IgG (*6*−*8*, *30*), and these characterizations agree well with the results from *in vivo* and cell binding studies (*7*, *12*, *31*, *32*). Some of the lessons we have learned in our studies may be relevant in other biosensor-based investigations. We have calculated binding constants using equilibrium rather than kinetic data because the latter can lead to incorrect results if the data are mass transfer limited or the reaction mechanism is unknown (*26*, *28*, *29*). In these analyses, we used a best fit procedure that optimizes the agreement between the observed and modeled equilibrium binding response equally for all concentrations of ligand. This method is preferable to Scatchard analyses which overemphasize the poorly determined weaker binding responses. The use of cross-validation, which has been widely used in the refinement of crystallographically-derived protein structures (*33*), allowed us to detect instances in which the addition of extra parameters resulted in overfitting the data by modeling noise rather than the signal. This method should be generally applicable for biosensor analyses. The significant differences in affinities we observe depending on which species is immobilized highlight the importance of characterizing a binding interaction in both orientations. Finally, for the special case of two noninteracting populations of binding sites with different dissociation rates, utilization of the dissociation phase of the measurement, either by delayed sampling or by modeling the dissociation phase and treating the components of the total response separately, could allow characterization of each population of binding sites.

ACKNOWLEDGMENT

We thank Luis Sánchez for providing purified monoclonal antibodies, Malini Raghavan and Robert Karlsson for helpful discussions, and members of the laboratory for critical reading of the manuscript.

REFERENCES

1. Junghans, R. P. (1997) *Immunol. Res. 16*, 29−57.
2. Simister, N. E., and Mostov, K. E. (1989) *Nature 337*, 184−187.
3. Burmeister, W. P., Gastinel, L. N., Simister, N. E., Blum, M. L., and Bjorkman, P. J. (1994) *Nature 372*, 336−343.
4. Gastinel, L. N., Simister, N. E., and Bjorkman, P. J. (1992) *Proc. Natl. Acad. Sci U.S.A. 89*, 638−642.
5. Rodewald, R., and Kraehenbuhl, J.-P. (1984) *J. Cell Biol. 99*, S159−S164.
6. Raghavan, M., Bonagura, V. R., Morrison, S. L., and Bjorkman, P. J. (1995) *Biochemistry 34*, 14649−14657.
7. Raghavan, M., Chen, M. Y., Gastinel, L. N., and Bjorkman, P. J. (1994) *Immunity 1*, 303−315.
8. Raghavan, M., Wang, Y., and Bjorkman, P. J. (1995) *Proc. Natl. Acad. Sci. U.S.A. 92*, 11200−11204.
9. Fägerstam, L. G., Frostell-Karlsson, A., Karlsson, R., Persson, B., and Rönnber, I. (1992) *J. Chromatogr. 597*, 397−410.
10. Malmqvist, M. (1993) *Nature 361*, 186−187.
11. Raghavan, M., and Bjorkman, P. J. (1995) *Structure 3*, 331−333.
12. Mackenzie, N. (1984) *Immunol. Today 5*, 364−366.
13. Sánchez, L. M., López-Otín, C., and Bjorkman, P. J. (1997) *Proc. Natl. Acad. Sci. U.S.A. 94*, 4626−4630.
14. Huber, A. H., Kelley, R. F., Gastinel, L. N., and Bjorkman, P. J. (1993) *J. Mol. Biol. 230*, 1077−1083.
15. Fasman, G. D. (1989) *Practical Handbook of Biochemistry and Molecular Biology*, p 265, CRC Press, Inc., Boca Raton, FL.
16. Gill, S. C., and Von Hippel, P. H. (1989) *Analy. Biochem. 182*, 319−326.
17. Scatchard, G. (1949) *Ann. N.Y. Acad. Sci. 51*, 660−672.
18. Press, W. H., Teukolsky, S. A., Vetterling, W. T., and Flannery, B. P. (1992) *Numerical recipes in Fortran. The art of scientific computing* 2nd ed., pp 678−683, Cambridge University Press, New York.
19. Huber, A. H. (1994) *A biochemical and structural characterization of Drosophila neuroglian*, Thesis, California Institute of Technology.
20. Weber, G. (1992) *Protein Interactions*, Routledge, Chapman, and Hall, Inc., New York.
21. Efron, B., and Tibshirani, R. (1991) *Science 253*, 390−395.
22. Wallace, K. H., and Rees, A. R. (1980) *Biochem. J. 188*, 9−16.
23. Rodewald, R., Lewis, D. M., and Kraehenbuhl, J. P. (1983) in *Brush Border Membranes (Ciba Found. Symp. 95)*, p 287, Pitman Books Ltd., London.
24. Kuziemko, G. M., Stroh, M., and Stevens, R. C. (1996) *Biochemistry 35*, 6375−6384.
25. Burmeister, W. P., Huber, A. H., and Bjorkman, P. J. (1994) *Nature 372*, 379−383.
26. Karlsson, R., Roos, H., Fägerstrom, L., and Persson, B. (1994) *METHODS: Compan. Methods Enzymol. 6*, 99−110.
27. Finkelstein, A. V., and Janin, J. (1989) *Protein Eng. 3*, 1−3.
28. Schuck, P., and Minton, A. P. (1996) *Trends Biochem. Sci. 21*, 458−460.
29. O'Shannessy, D. J. (1996) *Anal. Biochem. 236*, 275−283.
30. Popov, S., Hubbard, J. G., Kim, J.-K., Ober, B., Ghetie, V., and Ward, E. S. (1996) *Mol. Immunol. 33*, 521−530.
31. Kim, J.-K., Tsen, M.-F., Ghetie, V., and Ward, E. S. (1994) *Eur. J. Immunol. 24*, 2429−2434.
32. Kim, J.-K., Tsen, M.-F., Ghetie, V., and Ward, E. S. (1994) *Scand. J. Immunol. 40*, 457−465.
33. Brünger, A. T. (1992) *Nature 355*, 472−475.

BI970841R

Identification of critical IgG binding epitopes on the neonatal Fc receptor

Daniel E. Vaughn, Christina M. Milburn, David M. Penny, W. Lance Martin, Jennifer L. Johnson and Pamela J. Bjorkman

The neonatal Fc receptor (FcRn) binds maternal immunoglobulin G (IgG) during the acquisition of passive immunity by the fetus or newborn. FcRn also binds IgG and returns it to the bloodstream, thus protecting IgG from a default degradative pathway. Biosensor assays have been used to characterize the interaction of a soluble form of rat FcRn with IgG, and demonstrate that FcRn dimerization and immobilization are necessary to reproduce *in vivo* binding characteristics. Here we report the identification of several FcRn amino acid substitutions that disrupt its affinity for IgG and examine the effect of alteration of residues at the FcRn dimer interface. The role of these amino acids is discussed in the context of the previously reported structures of rat FcRn and a complex of FcRn with the Fc portion of IgG.

Introduction

The neonatal Fc receptor (FcRn) binds immunoglobulin G (IgG) in two important physiological processes (reviewed in (Junghans, 1997)). In the transmission of passive immunity from mother to offspring, FcRn mediates the transcytosis of maternal IgG across fetal and/or neonatal tissues, depending on the species involved. FcRn also binds IgG inside cells that degrade serum proteins and returns it to the bloodstream, thus rescuing it from a default degradative pathway. Each of these processes is facilitated by the pH dependence of the FcRn interaction with IgG (Rodewald, 1976; Rodewald & Kraehenbuhl,

1984). Under slightly acidic conditions (pH 6.0), FcRn binds IgG with a K_D of approximately 20 nM, while under slightly alkaline conditions (pH 7.5) there is no detectable binding for IgG concentrations of several μM (Raghavan *et al.*, 1995a).

Unlike other known Fc receptors which are composed of tandemly repeated immunoglobulin-like domains, FcRn is homologous to class I major histocompatibility complex (MHC) molecules (reviewed in Raghavan & Bjorkman, 1996). The FcRn light chain is ß2-microglobulin (ß2m) (Simister & Rees, 1985), the same light chain that associates with class I MHC heavy chains. The heavy chains of both FcRn and class I MHC molecules consist of three extracellular domains, α1, α2, and α3, followed by a transmembrane region and a short cytoplasmic sequence (Simister & Mostov, 1989; Bjorkman & Parham, 1990). The extracellular region of FcRn and class I MHC heavy chains exhibit low but significant sequence identity (22-30% for the α1 and α2 domains, 35-37% for the α3 domain) (Simister & Mostov, 1989). The 2.2 Å crystal structure of the extracellular region of rat FcRn revealed the expected structural similarity to MHC molecules and suggested the participation of a dimer of FcRn heterodimers in ligand binding (Burmeister *et al.*, 1994a). In each of three crystal forms used in the FcRn structure determination, a dimer of FcRn molecules mediated by contacts between the α3 and ß2m domains was observed. The FcRn dimer was also observed in the crystal structure of a 2:1 complex of FcRn and the Fc fragment of rat IgG which was solved to a resolution of ~6.5 Å (Burmeister *et al.*, 1994b). Although the limited resolution of this structure determination prohibited a detailed analysis of the molecular interaction, the approximate binding region on each molecule could be localized (Figure 1).

Results from studies to map the binding sites on FcRn and IgG are consistent with the binding interaction observed in the FcRn/Fc crystal structure. Three sites on the IgG ligand have been identified as important for the binding of mouse and rat FcRn: Ile253, His310, and the region including His433, His435 and His436 (Kim *et al.*, 1994a,b,c; Raghavan *et al.*, 1994; 1995a; Medesan *et al.*, 1997; Figure 2A,B). Mutation of residues

within each of these epitopes disrupts both binding to FcRn *in vitro* and FcRn mediated transport *in vivo* (Kim *et al.*, 1994a,b,c; Raghavan *et al.*, 1995a; Medesan *et al.*, 1997). There is less information available concerning the functional epitope on FcRn for binding IgG. Site directed mutagenesis was used to identify two regions on rat FcRn that exert a slight effect on its affinity for rat IgG: His250 and His251, and the α3 domain loop comprising residues 219-224 (Raghavan *et al.*, 1994). Neither of these regions is at the direct interface between the "primary" FcRn molecule that shows the majority of contacts with Fc in the 2:1 FcRn complex involving the FcRn dimer (Figure 1). His 250 and His 251 are at the FcRn dimer interface where they may exert their effect on IgG binding affinity either by modulating formation of the FcRn dimer, which is required for high affinity binding of IgG (Raghavan *et al.*, 1994; 1995b), or by direct contact between Fc and the "secondary" FcRn molecule of the FcRn dimer (Figure 1) (Weng *et al.*, 1997). Similarly, residues 219-224 of the secondary, but not the primary, FcRn molecule are in a position to contact Fc (Weng *et al.*, 1997).

Because of the low resolution of the available FcRn/Fc cocrystal structure, we cannot identify specific FcRn residues at the IgG interface with certainty. To further characterize the epitope on FcRn, we designed, constructed, and expressed mutants of rat FcRn at the predicted interfaces with IgG and with the second FcRn in the receptor dimer. We have quantitatively characterized the IgG binding interaction for each of these FcRn mutants using a biosensor based assay (Raghavan *et al.*, 1994, 1995a,b; Vaughn & Bjorkman, 1997). In this assay, soluble FcRn immobilized on a biosensor surface reproduces the affinity for IgG and the pH dependent interaction observed for membrane bound FcRn *in vivo* or on transfected cells (Mackenzie, 1984; Raghavan *et al.*, 1994). We have used the assay to demonstrate that high affinity binding of IgG requires both FcRn dimerization and receptor immobilization (Raghavan *et al.*, 1995b; Vaughn & Bjorkman, 1997). Here we identify several residues on rat FcRn that exert a major effect on binding affinity for murine or rat IgG, discuss the implications for pH dependent FcRn/IgG binding

and FcRn dimerization, and compare the results to other known receptor-ligand and protein-protein interaction systems.

Results

ß2m mutants at the FcRn-Fc interface

Using the FcRn/Fc cocrystal structure (Burmeister *et al.*, 1994b), we identified FcRn residues predicted to contact Fc. Most are located on the α2 domain of the primary receptor, with fewer contributions from the α1 and ß2m domains of the primary receptor and the α3 domain of the secondary (dimer-related) receptor. To verify the contacts between Fc and the primary FcRn predicted by the low resolution cocrystal structure, we constructed eight FcRn mutants.

The cocrystal structure predicts that the N-terminal portion of ß2m contacts the Fc C_H2 domain (Figure 1, 2A). To test this hypothesis we examined the binding of three mutants: ßI1A, ßQ2A, and ß-1Y (Table 1). In order to avoid potential exchange of mutant rat ß2m for endogenous hamster ß2m or bovine ß2m in the medium, these mutations were introduced into a lipid-linked version of rat ß2m that associates with the truncated FcRn heavy chain at the cell surface. This form of lipid-linked wild type FcRn was previously shown to bind IgG with the known physiological pH dependence (Gastinel *et al.*, 1992). The affinity of these mutants for radiolabeled IgG was evaluated using a cell binding assay (Table 2). The binding response at equilibrium was plotted as a function of the log of the concentration of IgG and fit to a model assuming one class of binding sites (Figure 3A). The binding behavior of FcRn at the cell surface may be more complicated (see Vaughn & Bjorkman, 1997 for a discussion), but the data from the cell binding assays are too noisy to reliably fit more complicated binding models. However, the affinity derived using the cell binding assay agrees with high affinity binding constants obtained using a biosensor assay (K_D = 24 nM, cell binding assay; $K_{D,1}$ = 24 nM, biosensor assay (Vaughn & Bjorkman, 1997); in both cases a rat IgG2a monoclonal antibody against CD4 was used). When the

mutants were examined using the cell binding assay, we find that substitution of the N-terminal Ile of ß2m with alanine (ßI1A), or extension of the N-terminus by one additional residue (ß-1Y), eliminates significant IgG binding at concentrations up to 0.9 μM, corresponding to a $\Delta\Delta G$ of > 2 kcal/mol (Table 2). However, substitution of Gln-2 of the ß2m domain with alanine (ßQ2A) results in binding similar to wild type FcRn (Table 2; Figure 3A,B), although the total binding response is increased presumably because the ßQ2A mutant is expressed at a higher level than the wild type construct as shown by FACS analysis (data not shown).

FcRn heavy chain mutants at the FcRn-Fc interface

In order to more completely characterize the binding, we used a surface plasmon resonance assay to measure the binding affinities between IgG and soluble forms of wild type and mutant receptors. Biosensor analyses of the interaction of IgG with soluble FcRn immobilized on a biosensor chip show non-linear behavior in Scatchard plots (Raghavan *et al.*, 1995a,b). We recently demonstrated that the interaction of IgG with immobilized FcRn is best described as two classes of non-interacting FcRn/IgG complexes: a slow dissociating population with an affinity in the range of values calculated in studies using membrane-bound FcRn (Mackenzie, 1984; Raghavan *et al.*, 1994), and a fast dissociating population with lower affinity (Vaughn & Bjorkman, 1997). As previously described (Vaughn & Bjorkman, 1997), plots of the net equilibrium response versus the log of the concentration of injected ligand were analyzed using linear regression to derive the percent of FcRn/IgG complexes comprising each population (f_1 and f_2), the high and low affinity binding constants ($K_{D,1}$ and $K_{D,2}$ respectively), and the maximum combined binding response ($R_{max,tot}$; Table 2).

Two mutations to the FcRn heavy chain were made in order to test the importance of potential aromatic and/or aliphatic contacts predicted from the cocrystal structure: W133A and 84-86 (Table 1). FcRn Trp-133 is exposed to solvent in the structure of FcRn

alone (Burmeister *et al.*, 1994a), and is in a position where it could interact with Ile-253 of Fc which was identified as a critical residue on Fc for interaction with FcRn (Kim *et al.*, 1994a,b,c; Raghavan *et al.*, 1995a; Medesan *et al.*, 1997) (Figure 2A). We find that IgG binding to the W133A mutant is extremely weak even at μM concentrations (Figure 4A). Thus the affinity of this mutant for IgG is > 8 μM corresponding to a ΔΔG of > 4 kcal/mol (Table 2). The 84-86 mutation (Table 1) encompasses three of the four amino acids in the α1 domain that are predicted to be within 5 Å of the Fc ligand in the cocrystal structure (Figure 2A). We find that replacement of these residues with the corresponding residues from class I MHC molecules (Kabat *et al.*, 1991) results in a binding affinity similar to wild type (Figure 4A; Table 2).

Much of the pH dependence of the FcRn-Fc interaction has been assigned to the titration of histidine residues on the Fc ligand (Raghavan *et al.*, 1995a). There are several acidic residues on the α2 domain of the receptor that could interact electrostatically with the protonated form of these histidines. Glu-117 is positioned near Fc His-310, Glu-132 and Glu-135 are near Fc His-435, and Asp-137 is in the vicinity of Fc His-435 (Figure 2B). Three mutations (E117S, E132Q&E135Q, and D137N) were constructed to test the functional importance of these acidic residues (Table 1). Neither E117S nor E132Q&E135Q bind IgG significantly at concentrations up to 8 μM (Figure 4B; Table 2). The D137N mutant binds IgG slightly at μM concentrations, but the binding affinity is also > 8 μM (Figure 4B; Table 2). For each mutant, the calculated high affinity binding is reduced by greater than 1000-fold, corresponding to a ΔΔG of more than 4 kcal/mol.

FcRn mutants at the dimer interface

In order to examine the effects on IgG binding of mutations at the FcRn dimer interface, we made mutations at two additional positions within FcRn. Based on the crystal structures of FcRn alone and the FcRn/Fc complex (Burmeister *et al.*, 1994a,b), Gly-191 is positioned such that side chains introduced at this position should interact with position

191 of the dimer related FcRn molecule (Figure 2C). We constructed two mutants (G191E and G191H) to examine the effect of substitution at position 191 (Table 1). Both mutations have a slight (~4-fold) effect on the high affinity binding constant ($K_{D,1}$) when FcRn is coupled at densities greater than 2500 RU (Figure 5A; Table 2). Both mutants also show a reduction in the total number of binding sites ($R_{max,tot}$) and the fraction of high affinity binding sites (f_1) compared to wild type FcRn. IgG binding is further reduced when the FcRn concentration on the chip is lowered by coupling at lower densities. Under these conditions, high affinity binding is further reduced (6- to 10-fold) and the fraction of high affinity and total number of binding sites are again reduced relative to wild type FcRn (Figure 5B; Table 2).

We next examined the effects of mutating ß2m residue Glu-89. This residue is in position to form a salt bridge with either His-250 or His-251 of the dimer-related FcRn heavy chain (Figure 2C). We previously showed that mutation of His-250 and His-251 results in a 6-fold reduction in affinity for IgG (Raghavan *et al.*, 1994). Two mutations were constructed (ßE89H and ßE89K) to test the role of Glu-89 in dimer formation and IgG binding (Table 1). Similar to the mutations at Gly-191, substitution of Glu-89 with either a histidine or a lysine results in a slight reduction in high affinity IgG binding, and a reduction in the fraction of high affinity IgG binding sites (Figure 5C; Table 2). Unlike the Gly-191 mutations, however, the total number of binding sites is not reduced, and the effect on affinity is largely independent of coupling density (Figure 5D; Table 2).

Discussion

Functionally critical residues for protein-protein interactions can be mapped by site directed mutagenesis followed by determination of mutant binding affinities. This is an especially powerful method when high resolution structures are available to identify the residues at the receptor-ligand interface. One of the best characterized protein-protein interfaces is the interaction between human growth hormone (hGH) and its receptor

(hGHR). Wells and colleagues have systematically changed all the residues that compose the crystallographically observed interface between the hormone and its receptor (De Vos *et al.*, 1992) to alanines, and find that only a small subset of the amino acids at the interface (approximately 5 of the 24-31 residues) are responsible for most of the binding affinity (reviewed in (Wells & DeVos, 1996). Thus there is a distinction between the "functional epitope" (those residues that exert a major effect upon the binding affinity; $\Delta\Delta G > 2$ kcal/mol for substitution of a single amino acid to alanine) and the "structural binding site" (all residues at the interface).

In the case of the interaction between FcRn and IgG, the structural binding site cannot be identified with certainty using the available low resolution FcRn/Fc cocrystal structure (Burmeister *et al.*, 1994b). The IgG binding site was tentatively identified as primarily formed from a surface of the α2 domain with additional potential contributions from residues in the α1 domain, the top surface of the ß2m domain, and/or the α3 domain of a dimer related molecule (Burmeister *et al.*, 1994b). Because the complex structure was determined using crystals that diffracted to only about 6.5 Å and a portion of the Fc C_H2 domains was disordered in the final electron density maps, we sought experimental confirmation of the IgG binding site on FcRn. The identification of several amino acid substitutions that substantially disrupt IgG binding within the structural epitope predicted from the low resolution cocrystal structure provides this confirmation. We have identified several amino acid mutations (W133A, E117S, D137N, E132Q&E135Q, ßI1A and ß-1Y) that result in a decrease in the free energy of binding of more than 2 kcal/mol (Table 2). These mutants, and all mutants in this study, are correctly folded as assayed by monoclonal antibody reactivity and heterodimer assembly (see Methods). Thus FcRn heavy chain residues Trp-133, Glu-117, Asp-137, either Glu-132, Glu-135 or both, as well as Ile-1 and the N–terminus of ß2m comprise much of the functional IgG binding epitope.

Well characterized functional binding epitopes for protein-protein interfaces often include surface exposed hydrophobic residues that make important contributions to the free

energy of binding. For example, hydrophobic interactions contribute to the binding energy in several antibody-antigen interactions (Kelley & O'Connell, 1993; Tsumoto *et al.*, 1995; Dall'Acqua *et al.*, 1996). In addition, the binding affinity for the hGH/hGHR interaction arises primarily from hydrophobic interactions, with electrostatic interactions being less important (Wells & DeVos, 1996). For hGHR, the largest contributions to the free energy of binding come from Trp-104 and Trp-169. Replacement of either residue with an alanine results in a loss of binding free energy of more than 4.5 kcal/mol. The next three largest contributions also are made by hydrophobic residues (Ile-103, Ile-105, and Pro-106), each with loss of binding free energy of 1.5 to 3.5 kcal/mol. For the hormone, both polar and hydrophobic residues show significant decreases in binding free energy when substituted with alanine residues. Interestingly, several of the polar residues (e.g., Lys-172, Thr-175, and Arg-43) use the aliphatic portions of their side chains to contact the receptor.

There is also a strong hydrophobic component to the interaction between FcRn and its IgG ligand. Previous reports have implicated Ile-253 as part of the ligand's functional epitope (Kim *et al.*, 1994a,b,c; Raghavan *et al.*, 1995a; Medesan *et al.*, 1997). Here we have shown that Trp-133 is part of the receptor's functional epitope. From the crystal structure of the complex, these two hydrophobic side chains are known to be positioned near each other (Figure 2A). Thus Ile-253 of the ligand and Trp-133 of the receptor are likely to form the hydrophobic core of a binding interface similar to those seen for hGH-hGHR and in several antibody-antigen interactions (Kelley & O'Connell, 1993; Tsumoto *et al.*, 1995; Dall'Acqua *et al.*, 1996; Wells & DeVos, 1996).

In addition to hydrophobic effects, the FcRn-Fc interface relies on strong electrostatic interactions to provide binding free energy. It was previously shown that His-310 and one or more of Histidine residues 433, 435, and 436 of the Fc ligand are necessary for full binding affinity and in vivo function (Kim *et al.*, 1994a,b,c; Raghavan *et al.*, 1994; 1995a; Medesan *et al.*, 1997). Here we have identified three FcRn mutations, E117S, D137N, and E132Q&E135Q, that dramatically reduce binding affinity. Since

these substitutions are conservative, most replacing only the negatively charged carboxylate group with a neutral amide group, it is likely that the disrupted interactions are salt bridges. In the FcRn/Fc cocrystal structure, each of the mutated acidic residues from FcRn are near one or more of the implicated Fc histidine residues (Figure 2B), suggesting that the protonated histidines form a pH-dependent salt bridge to the corresponding acidic residues on FcRn.

The approximately wild type binding of the 84-86 mutant, suggests that these residues within the FcRn α1 domain do not contribute to the functional IgG binding site, while the substantially reduced binding of ßI1A and ß-1Y demonstrates that the ß2m light chain does. The hydrophobic Ile side chain at the N-terminus of ß2m is positioned near the side chains of Fc residue 309 (Leu, Val, Gln, or Met in rat, murine, and human IgG's; (Kabat *et al.*, 1991)) and Fc residue 311 (Gln or Arg in rat, murine, and human IgG's; (Kabat *et al.*, 1991)), and could form a hydrophobic interaction with the aliphatic portions of one or the other of these sidechains. Extension of the N-terminus by one residue by the addition of a bulky tyrosine residue (ß-1Y) could reduce binding through a steric hindrance. Alternatively, the N-terminal extension could affect binding by blocking a specific interaction with the N-terminal amino group. In proteins, α-NH_2 groups have a pKa that is generally ~8 (Fersht, 1985). In FcRn, the presumably protonated α-NH_2 group of ß2m is positioned where it can form a hydrogen bond with the backbone carbonyl of residue 115 on the heavy chain and also a pH dependent salt-bridge with Glu-117. Thus the protonated α-NH_2 group of ß2m could help position Glu-117 of the heavy chain to form an anionic binding site for His-310 of the Fc ligand.

Inhibition studies using anti-ß2m specific monoclonal antibodies previously suggested the involvement of the FcRn ß2m domain in binding to IgG (Raghavan *et al.*, 1994). This suggestion is confirmed by the present demonstration that the N-terminal region of ß2m constitutes a functional epitope for ligand binding. Crystal structures show that ß2m interacts similarly with the heavy chains of class I MHC molecules and FcRn

(Bjorkman & Parham, 1990; Burmeister *et al.*, 1994a). In both cases, the ß2m and α3 immunoglobulin-like domains of FcRn and class I MHC molecules are related by a 152° +/- 7° rotation followed by a ~13 Å translation that positions the ß2m domain underneath the α1-α2 domain platform (Burmeister *et al.*, 1994a and references therein). The conservation of this asymmetric α3-ß2m interaction serves different functional purposes since the ß2m position in FcRn is critical for interaction with its IgG ligand, yet the same ß2m position is found in MHC molecules, which do not function as receptors for IgG.

The present study extends the results from previous work indicating that two FcRn molecules dimerize, as observed in FcRn and FcRn/Fc crystals (Burmeister *et al.*, 1994a,b), to form the high affinity binding site for a single IgG. We previously reported that FcRn mutants with alterations that specifically affect the interaction of IgG with FcRn dimers but not with monomers (residues 250 and 251 or the loop comprising residues 219-224; Figure 1) showed reduced affinities in biosensor assays and in measurements of labeled IgG binding to cell surface FcRn (Raghavan *et al.*, 1994). Here we report two additional regions that affect FcRn dimerization and/or the interaction of Fc with the FcRn dimer. Mutations at FcRn residue 191, which interacts with its counterpart on the dimer related receptor, result in a lower affinity and fewer high affinity binding sites. These effects are enhanced at lower receptor density, suggesting that mutation of this residue exerts its effect through interference with FcRn dimer formation. By contrast, mutation of ß2m residue Glu-89 results in a slight reduction in binding affinity which is not dependent upon FcRn coupling density and is not accompanied by a significant reduction in the number of binding sites. These results suggest that ß2m Glu-89 interacts primarily with the IgG ligand directly rather than the dimer-related FcRn heavy chain. Disorder of the Fc C_H2 domain makes it difficult to identify potential contacts for Glu-89 from the cocrystal structure (Burmeister *et al.*, 1994b). However, a direct interaction between the Fc C_H2 domain and residues at the dimer interface near ß2m Glu-89 (FcRn His 250 and His 251) was suggested by modeling studies using a computational docking algorithm to predict the

orientation of the Fc C_H2 domain when bound to FcRn (Weng *et al.*, 1997). If Fc becomes distorted upon binding to the FcRn dimer as predicted by the modeling studies, ß2m Glu-89 could contact the C_H2 domain.

Conclusions

We have designed and constructed several amino acid substitutions on FcRn to map its binding site for IgG. The identification of several mutations that reduce the IgG affinity confirm and further define the IgG binding site on FcRn that was identified at low resolution in the FcRn-Fc cocrystal structure (Burmeister *et al.*, 1994b). These functionally important IgG binding epitopes on FcRn complement previously reported binding epitopes on Fc (Kim *et al.*, 1994a,b,c; Raghavan *et al.*, 1994; 1995a; Medesan *et al.*, 1997). Ile-253 of Fc and Trp-133 of FcRn are likely to form the core of a strong hydrophobic interaction, while Glu-117, Glu-132, Glu-135 and Asp-137 on the receptor provide anionic binding partners for the protonated forms of His-310, His-433, His-435 and His 436 of the ligand. Finally, amino acid substitutions for Gly-191 at the dimer interface display an FcRn concentration dependent effect on IgG affinity, providing additional evidence that FcRn dimerization is necessary for normal high affinity IgG binding.

Methods

Reagents

1B5, a mouse IgG1 monoclonal antibody against human Zn-α2-glycoprotein (Sánchez *et al.*, 1997) whose interaction with wild type FcRn has been previously characterized (Vaughn & Bjorkman, 1997), was used for biosensor binding assays. Anti-CD4 (rat IgG2a) used in the cell binding assays was purchased from Boehringer Mannheim. Its interaction with wild type FcRn has also been characterized in a biosensor assay (Vaughn & Bjorkman, 1997). Two mouse IgG1 anti-FcRn monoclonal antibodies,

1G3 and 4C11 (Raghavan *et al.*, 1994), were used for immunoaffinity chromatography, enzyme-linked immunosorbent assays (ELISAs), immunoprecipitations, and fluorescence activated cell sorting (FACS). Rabbit anti-human ß2m and peroxidase-conjugated anti-mouse, as well as goat FITC-conjugated anti-rabbit antibodies were purchased from Boehringer Mannheim. Iodobeads were obtained from Pierce. ^{125}I (specific activity ~100 mCi/ml) was obtained from Amersham in the form of sodium iodide. N-ethyl-N'-(3-diethylaminopropyl)-carbodiimide (EDC), N-hydroxysuccinimide (NHS), BIAcore surfactant P20, and CM5 sensor chips were obtained from BIAcore AB. CNBr-activated Sepharose and PD-10 columns were purchased from Pharmacia.

Construction and expression of mutant FcRn molecules

Locations for FcRn mutants were chosen using the crystal structures of FcRn alone (Protein Data Bank entry 1FRU) and a complex between FcRn and Fc (Protein Data Bank entry 1FRT). For expression of soluble mutant FcRn heterodimers, the cDNAs encoding the truncated FcRn heavy chain (residues 1-269) (Gastinel *et al.*, 1992) or rat ß2m were altered by site directed mutagenesis (Kunkel *et al.*, 1987). After verifying the sequence of the altered cDNAs, the mutant cDNAs were subcloned into the expression vector pBJ5-GS which carries the glutamine synthetase gene as a means of selection and amplification in the presence of the drug methionine sulfoximine (Bebbington & Hentschel, 1987). Cotransfection of FcRn and ß2m expression vectors into Chinese hamster ovary (CHO) cells, selection, and amplification were carried out as described (Gastinel *et al.*, 1992; Raghavan *et al.*, 1994). Cell supernatants were screened for FcRn heterodimer expression by a sandwich ELISA, using either the FcRn heavy chain-specific monoclonal antibody 1G3 or 4C11 as the capture antibody and a polyclonal antiserum against human ß2m to detect positive samples as described (Raghavan *et al.*, 1995b), and confirmed by immunoprecipitation with the other antibody. Mutant proteins that retained functional binding to IgG were purified from the supernatants of the highest expressing clones by pH

dependent binding to a rat IgG column (Gastinel *et al.*, 1992). Mutants that did not bind IgG sufficiently for IgG-affinity chromatography were purified using an immunoaffinity column constructed with an anti-FcRn monoclonal antibody. Purified 1G3 antibody was covalently attached to CNBr-activated Sepharose following the manufacturer's protocol. Binding and elution conditions for FcRn binding to the 1G3 column were identified using a biosensor assay of wild type FcRn interacting with amine coupled 1G3 at pH 8 (see below). Supernatants from cells expressing wild type or mutant FcRn proteins were passed over the 1G3 column at pH 7.5, which was subsequently washed with ~10 column volumes of 50 mM sodium phosphate (pH 7.5 - 8.5) and eluted with 50 mM sodium phosphate (pH 3.0). Eluates were immediately neutralized with 1 M disodium phosphate. These elution conditions did not affect the ability of wild type FcRn to bind again to the 1G3 column or the behavior of wild type FcRn in subsequent biosensor assays (data not shown).

For expression of membrane bound FcRn mutants, mutations were introduced into a previously described lipid-linked version of rat ß2m that pairs with the truncated FcRn heavy chain at the surface of transfected cells (Gastinel *et al.*, 1992). The lipid-linked ß2m protein consists of the phosphatidylinositol anchoring signal of decay-accelerating factor (DAF) (residues 311-347; (Caras *et al.*, 1987)) fused to the final amino acid of ß2m (ß2m-DAF). Altered ß2m-DAF cDNAs were sequenced and subcloned into the PBJ5-GS expression vector, which was co-transfected into CHO cells along with the expression vector encoding wild type soluble FcRn. After two to four weeks, populations were screened for heterodimer expression by immunostaining at pH 8.0 with the anti–FcRn antibody 1G3 and FITC-conjugated goat anti-mouse secondary antibody. High expressing lines were isolated by single cell FACS. Cell sorting and analysis was performed on a Coulter Epics Elite flow cytometer using Coulter Elite software version 3.0.

The correct folding of each of the FcRn mutants used in this study was demonstrated by several experiments. First, each of the mutants is either expressed on the

cell surface or secreted, therefore none of the mutations results in intracellular retention as would be expected for misfolded proteins. Second, all mutants assemble into heterodimers, as verified either by SDS-PAGE analysis of purified protein and in a sandwich ELISA for secreted mutants or by cell surface reactivity with an anti-FcRn heavy chain monoclonal antibody for the mutations introduced into lipid-linked ß2m and expressed as heterodimers with soluble FcRn heavy chains (data not shown). Finally, each mutant retains the immunoreactivity of wild type FcRn for monoclonal antibodies generated against correctly folded wild type FcRn (4C11 and 1G3; Raghavan *et al.*, 1994). All secreted mutants were selected using a sandwich ELISA and immunoprecipitation employing 4C11 and 1G3, non-IgG binding mutants were purified on a 1G3 immunoaffinity column, and cells expressing lipid-linked mutants were isolated by flow cytometry using 1G3. The correct folding of each mutant was expected since each of the mutations were introduced into residues that are solvent exposed in the crystal structure of FcRn (Burmeister *et al.*, 1994a).

Purification and Iodination of IgG

Purified anti CD4 was iodinated using iodo-beads according to the manufacturer's protocol. Briefly, one to two beads were rinsed in 1 ml of 100 mM sodium phosphate buffer pH 6.0, dried on filter paper and added to a mixture of 20 µl of ^{125}I in 180 µl of the same buffer. After five minutes, 0.5 ml (0.4 mg) of purified IgG was added and the mixture was allowed to incubate for approximately 15 minutes at room temperature. Unreacted ^{125}I was removed by gel filtration using a PD-10 column.

Cell binding assays

Cells expressing wild type FcRn/ß2m-DAF or mutant FcRn/ß2m-DAF were grown to confluence in tissue culture plates and assayed for IgG binding as described (Raghavan *et al.*, 1994). Cells were detached, pelleted, washed and resuspended in binding buffer

(Hank's balanced salt solution, 10 mM HEPES, 0.25% bovine serum albumin, pH 6.0) to a concentration of approximately 3 X 10^6 cells/ml. In triplicate assays 3 X 10^5 to 5 X 10^5 cells were mixed with various amounts of ^{125}I labeled IgG and binding buffer to a total volume of 0.5 ml. The samples were incubated for at least 2 hours at room temperature, then pelleted and the supernatants removed and set aside. Cell pellets were washed with 1.0 ml of cold binding buffer. The levels of radioactivity in the supernatants and cell pellets were measured using a Beckman gamma 5500 counter. Non-specific binding was determined by similar treatment of untransfected CHO cells. The concentration of free IgG was determined from the radioactivity in the supernatant and the specific activity of the labeled IgG. The binding response was similarly calculated from the radioactivity in the washed cell pellet.

Biosensor experiments

A BIAcore biosensor system (Biacore AB) was used to evaluate the interaction of secreted mutant and wild type FcRn proteins with IgG as previously reported (Vaughn & Bjorkman, 1997) and references therein). Briefly, wild type or mutant FcRn proteins were immobilized to a biosensor chip surface using standard amine coupling chemistry as described in the BIAcore manual, and different concentrations of purified IgG were injected over the immobilized FcRn. IgG concentrations were determined spectrophotometrically using an extinction coefficient at 280 nm of 216000 M^{-1} cm^{-1} (IgG; Fasman, 1989) . Sensor chip surfaces were regenerated by injecting a pulse of 50 mM phosphate, 150 mM NaCl, pH 8. Variation in coupling densities was achieved by varying the chip activation step from 4 to 7 minutes.

Because systematic errors can contribute to the uncertainty of K_D determinations (including the slight variations in the pH of the binding buffer, the specifics of the coupling reaction, the concentration of the ligand, and the specific batch and purification state of the ligand), K_D values can be more accurately compared for experiments conducted in parallel

on the same chip. For each experiment, wild type FcRn, one or two mutants, and buffer without protein were coupled in one of the four available flowcells. The same dilution series of ligand and a buffer blank were passed over each flow cell, and the response at 10 minutes (taken as the equilibrium response) was recorded after subtraction of the buffer response. A modest response was observed for higher ligand concentrations (> ~62 nM) in mock-coupled flow cells, reaching a maximum of ~200 RU at the highest ligand concentration of 8 μM. This blank response, most likely due to either the bulk refractive index contribution of the ligand and/or a nonspecific low affinity interaction with the dextran matrix of the chip, was subtracted from the equilibrium responses recorded for FcRn coupled flow cells to yield a net equilibrium response.

Calculation of binding affinities and changes in the free energy of binding

For both the cell binding and biosensor assays, the equilibrium binding response was plotted as a function of the log of the free IgG concentration. These data were fit to either a model of one or two noninteracting binding sites by nonlinear regression as previously described (Vaughn & Bjorkman, 1997). In each case in which a model of two non-interacting sites is used, the two site model produces a lower cross-validated residual (Vaughn & Bjorkman, 1997) than the one site model. K_D and R_{max} (response corresponding to complete binding) values are presented when a single class of non-interacting sites was modeled, and $K_{D,1}$ (high affinity binding constant), $K_{D,2}$ (low affinity binding constant), f_1 (fraction of total binding sites corresponding to the high affinity class of binding sites) and $R_{max,tot}$ (response corresponding to complete occupancy of both classes of binding sites) values are presented when two classes of non-interacting sites when modeled (Table 2). For each of these parameters, standard errors are also reported as determined in the KaleidaGraph implementation of the Levenberg-Marquardt algorithm, which reflect the precision of individual curve fittings (Table 2). The reproducibility of the derived affinities is +/- ~20% as evaluated by comparing the six independent K_D values

reported for wild type FcRn from experiments conducted on different biosensor chips (Table 2). $\Delta\Delta G$ values were calculated as $2.303RT \log[K_{mut}/K_{w.t.}]$ for the high affinity binding constant ($K_{D,1}$) where R is the gas constant (1.99×10^{-3} kcal mol^{-1} K^{-1}) and T is the absolute temperature (295 K). Results from biosensor experiments in Table 2 correspond to the interaction of wild type and mutant FcRn proteins with the 1B5 monoclonal IgG. Similar results were obtained for experiments on FcRn mutants that interact directly with IgG using the anti-CD4 IgG (data not shown).

Acknowledgments

We thank Rochelle Diamond and the Caltech Flow Cytometry facility for help with FACS and Luis Sanchez and Zsuzsa Hamburger for critical reading of the manuscript. This work was supported by a grant from the NIH (AI/GM41239 to P.J.B.) and a Camille and Henry Dreyfuss Teacher Scholar Award (P.J.B.)

Abbreviations: ß2m, ß2-microglobulin; CHO, Chinese hamster ovary; DAF, Decay Accelerating Factor; EDC, N-ethyl-N'-(3-diethylaminopropyl)-carbodiimide; ELISA, enzyme linked immunosorbent assay; FcRn, Fc receptor, neonatal; hGH, human growth hormone; hGHR, human growth hormone receptor; IgG, Immunoglobulin G; K_D, equilibrium dissociation constant; MHC, major histocompatibility complex; NHS, N-hydroxysuccinimide; RU, Resonance Units.

References

Bebbington, C. R. & Hentschel, C. C. G. (1987). The use of vectors based on gene amplification for the expression of cloned genes in mammalian cells. In DNA Cloning: A Practical Approach, D. M. Glover, eds. (Oxford: IRL Press). 163-188.

Bjorkman, P. J. & Parham, P. (1990). Structure, function and diversity of class I major histocompatibility complex molecules. Ann. Rev. Biochem. **90**, 253-288.

Burmeister, W. P., Gastinel, L. N., Simister, N. E., Blum, M. L. & Bjorkman, P. J. (1994a). Crystal structure at 2.2 Å resolution of the MHC-related neonatal Fc receptor. Nature **372**, 336-343.

Burmeister, W. P., Huber, A. H. & Bjorkman, P. J. (1994b). Crystal structure of the complex of rat neonatal Fc receptor with Fc. Nature **372**, 379-383.

Caras, I. W., Weddell, G. N., Davitz, M. A., Nussenzweig, V. & Martin, D. W. (1987). Signal for attachment of a phospholipid membrane anchor in decay accelerating factor. Science **238**, 1280-1283.

Dall'Acqua, W., Goldman, E. R., Eisenstein, E. & Mariuzza, R. A. (1996). A mutational analysis of the binding of two different proteins to the same antibody. Biochemistry **35**, 9667-9676.

De Vos, A. M., Ultsch, M. & Kossiakoff, A. (1992). Human Growth Hormone and Extracellular Domain of its Receptor: Crystal Structure of the Complex. Science **255**, 306-312.

Fasman, G. D. (1989). Practical Handbook of Biochemistry and Molecular Biology. In eds. (Boca Raton, FL: CRC Press, Inc.). 265.

Fersht, A. (1985). Enzyme Structure and Mechanism, 2nd edition. (New York, NY: W. H. Freeman and Company).

Gastinel, L. N., Simister, N. E. & Bjorkman, P. J. (1992). Expression and crystallization of a soluble and functional form of an Fc receptor related to class I histocompatibility molecules. Proc. Natl. Acad. Sci USA **89**, 638-642.

Junghans, R. P. (1997). Finally! The Brambell Receptor (FcRB). Mediator of Transmission of Immunity and Protection from Catabolism for IgG. Immunol. Res. **16**, 29-57.

Kabat, E. A., Wu, T. T., Perry, H. M., Gottesman, K. S. & Foeller, C. (1991). Sequences of proteins of immunological interest. (Bethesda,MD: U.S. Department of Health and Human Services).

Kelley, R. F. & O'Connell, M. P. (1993). Thermodynamic analysis of an antibody functional epitope. Biochemistry **32**, 6828-6835.

Kim, J.-K., Tsen, M.-F., Ghetie, V. & Ward, E. S. (1994a). Catabolism of the murine IgG1 molecule: Evidence that both CH2-CH3 domain interfaces are required for the persistence of IgG1 in the circulation of mice. Scand. J. Immunol. **40**, 457-465.

Kim, J.-K., Tsen, M.-F., Ghetie, V. & Ward, E. S. (1994b). Localization of the site of the murine IgG1 molecule that is involved in binding to the murine intestinal Fc receptor. Eur. J. Immunol. **24**, 2429-2434.

Kim, J. K., Tsen, M. F., Ghetie, V. & Ward, E. S. (1994c). Identifying amino acid residues that influence plasma clearance of mouse IgG1 fragments by site directed mutagenesis. Eur. J. Immunol. **24**, 542-548.

Kunkel, T. A., Roberts, J. D. & Zakour, R. A. (1987). Rapid and efficient site directed mutagenesis without phenotypic selection. Meth. Enzymol. **154**, 367-382.

Mackenzie, N. (1984). Fc receptor-mediated transport of immunoglobulin across the intestinal epithelium of the neonatal rodent. Immunol. Today **5**, 364-366.

Medesan, C., Matesoi, D., Radu, C., Ghetie, V. & Ward, E. S. (1997). Delineation of the amino acid residues involved in transcytosis and catabolism of mouse IgG. J. Immunol. **158**, 2211-2217.

Raghavan, M. & Bjorkman, P. J. (1996). Fc receptors and their interactions with immunoglobulins. Ann. Rev. Cell Biol. **12**, 181-220.

Raghavan, M., Chen, M. Y., Gastinel, L. N. & Bjorkman, P. J. (1994). Identification of interaction sites in the class I MHC-related Fc receptor/immunoglobulin G complex. Immunity **1**, 303-315.

Raghavan, M., Bonagura, V. R., Morrison, S. L. & Bjorkman, P. J. (1995a). Analysis of the pH dependence of the neonatal Fc receptor/Immunoglobulin G interaction using antibody and receptor variants. Biochemistry **34**, 14649-14657.

Raghavan, M., Wang, Y. & Bjorkman, P. J. (1995b). Effects of receptor dimerization on the interaction between the class I MHC related Fc receptor and immunoglobulin G. Proc. Natl. Acad. Sci. USA **92**, 11200-11204.

Rodewald, R. (1976). pH-dependent binding of immunoglobulins to intestinal cells of the neonatal rat. J. Cell Biol. **71**, 666-670.

Rodewald, R. & Kraehenbuhl, J.-P. (1984). Receptor-mediated transport of IgG. *J.* Cell Biol. **99**, S159-S164.

Sánchez, L. M., López-Otín, C. & Bjorkman, P. J. (1997). Characterization and crystallization of human Zn-α2-glycoprotein, a soluble class I MHC homolog. Proc. Natl. Acad. Sci. USA **94**, 4626-4630.

Simister, N. E. & Mostov, K. E. (1989). An Fc receptor structurally related to MHC class I antigens. Nature **337**, 184-187.

Simister, N. E. & Rees, A. R. (1985). Isolation and characterization of an Fc receptor from neonatal rat small intestine. Eur. J. Immunol. **15**, 733-738.

Tsumoto, K., Ogasahara, K., Ueda, Y., Watanabe, K., Yutani, K. & Kumagai, I. (1995). Role of Tyr residues in the contact region of anti-lysozyme monoclonal antibody HyHEL10 for antigen binding. *J.* Biol. Chem. **270**, 18551-18557.

Vaughn, D. E. & Bjorkman, P. J. (1997). High affinity binding of the neonatal Fc receptor to its IgG ligand requires receptor immobilization. Biochemistry **36**, 9374-9380.

Wells, J. A. & DeVos, A. M. (1996). Hematopoietic receptor complexes. Ann. Rev. Biochem. **65**, 609-634.

Weng, Z., Gulukota, K., Vaughn, D. E., Bjorkman, P. J. & DeLisi, C. (1997). Computational determination of the structure of rat Fc bound to the neonatal Fc receptor. ms. submitted.

Table 1. FcRn mutants

Mutant	Domain	Position(s)	Mutation
Fc-FcRn Interface			
ßI1A	ß2m-DAF	1	I -> A
ßQ2A	ß2m-DAF	2	Q -> A
ß-1Y	ß2m-DAF	N-terminus	add Y
W133A	α2	133	W -> A
84-86	α1	84-86	NQI -> GYY
E117S	α2	117	E -> S
E132Q&E135Q	α2	132 and 135	Both E -> Q
D137N	α2	137	D -> N
Dimer Interface			
G191E	α3	191	G -> E
G191H	α3	191	G -> H
ßE89H	ß2m	89	E -> H
ßE89K	ß2m	89	E -> K

Table 2. Characterization of IgG binding to FcRn mutants

Mutant	$K_{D,1}$ (nM)	f_1 (%)	$K_{D,2}$ (μM)	$R_{max,tot}$ (RU)	ΔΔG (kcal/mol)	F
Fc-FcRn Interface:						
Wild Type	24 ± 4			0.129 ± 0.008[a]		
ßI1A	>> 900			N.B.	>> 2	
ßQ2A	10 ± 2			0.60 ± 0.04[a]	-0.5	
ß-1Y	>> 900			N.B.	>> 2	
Wild Type	12 ± 2	43 ± 2	1.1 ± 0.3	910 ± 30		
W133A	> 8000			130[c]	> 4	
84-86	6.0 ± 0.6	62 ± 2	0.9 ± 0.2	1430 ± 30	-0.4	
Wild Type	4.9 ± 0.4	66 ± 2	0.7 ± 0.2	1890 ± 30		
D137N	> 8000			250[c]	> 4	
E117S	>> 8000			N.B.	>> 4	
E132Q&E135Q	>> 8000			N.B.	>> 4	
Dimer Interface:						
Wild Type	6.3 ± 0.4	60 ± 1	0.9 ± 0.1	1410 ± 20		
G191E	25 ± 5	41 ± 3	2.2 ± 0.7	650 ± 40	0.8	
G191H	21 ± 4	39 ± 2	1.9 ± 0.5	740 ± 30	0.7	
Wild Type	10. ± 1	54 ± 3	0.9 ± 0.2	580 ± 20		
G191E	57 ± 5	41 ± 1	4.4 ± 0.9	370 ± 20	1.1	
G191H	90 ± 30	37 ± 4	5 ± 4	350 ± 60	1.4	
Wild Type	6.7 ± 0.6	54 ± 2	0.8 ± 0.1	1250 ± 20		
ßE89K	19 ± 2	43 ± 3	1.2 ± 0.2	1180 ± 30	0.6	
ßE89H	22 ± 2	46 ± 2	1.4 ± 0.2	1310 ± 20	0.7	
Wild Type	7 ± 1	54 ± 3	0.6 ± 0.2	880 ± 20		
ßE89K	27 ± 2	38 ± 2	1.7 ± 0.5	720 ± 30	0.8	
ßE89H	22 ± 2	37 ± 3	1.5 ± 0.4	660 ± 20	0.7	

N.B. = no binding detected

[a] Arbitrary units on the same relative scale

[b] Affinity measurements done using lipid-linked FcRn at the cell surface

[c] Observed binding response at highest IgG concentration (8 μM)

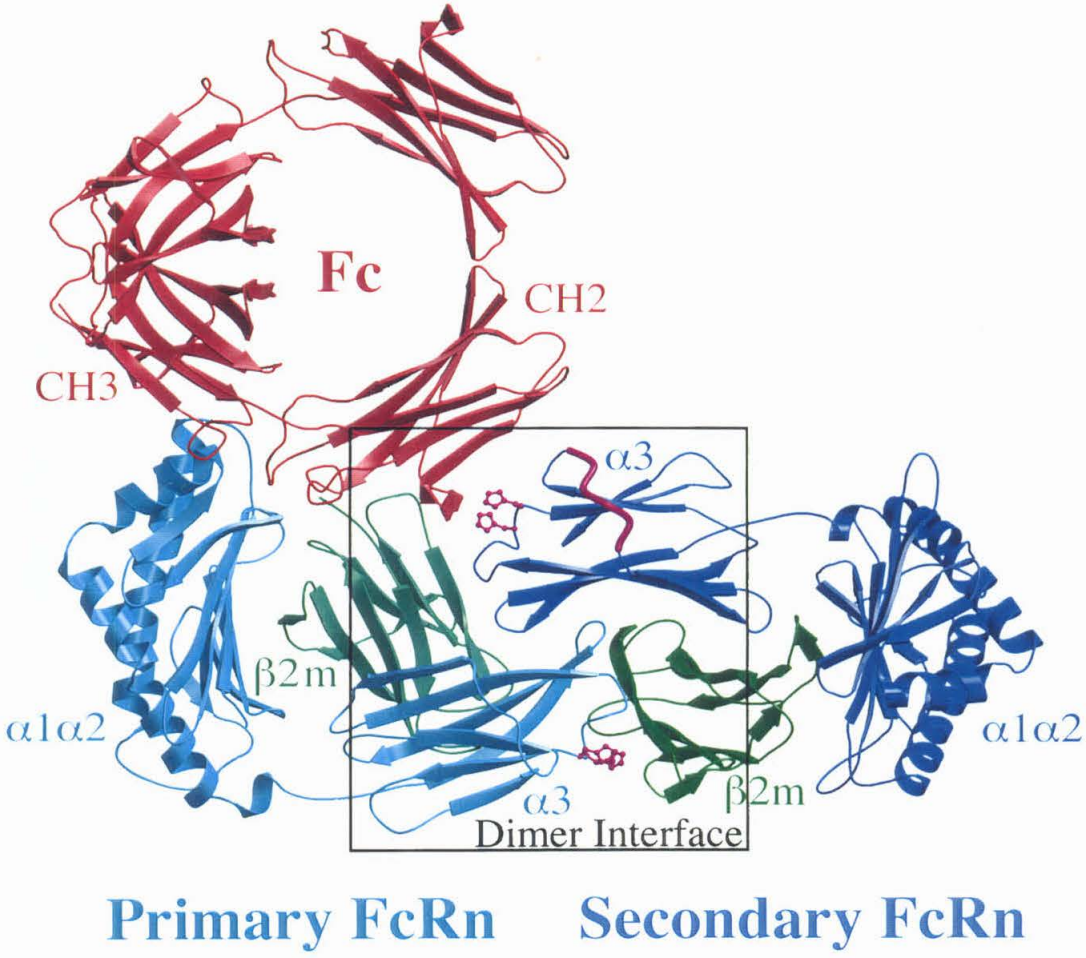

Figure 1. Ribbon diagram of the cocrystal structure of the FcRn dimer binding to its Fc ligand. The high affinity binding site for IgG is formed by a homodimer of two FcRn molecules identified as the "Primary FcRn" (cyan and light green) and the "Secondary FcRn" (blue and dark green). Each FcRn molecule is composed of a multidomain heavy chain (cyan or blue) and a single domain light chain (β2m; green). The Fc ligand (red) interacts with the heavy chain α2 domain and β2m domain of the primary FcRn, and the heavy chain α3 domain of the secondary receptor. Previously characterized FcRn heavy chain mutations that affect ligand binding (see text for details) are shown in magenta. The FcRn dimer interface shown as a close-up in Figure 2C is indicated by a black box.

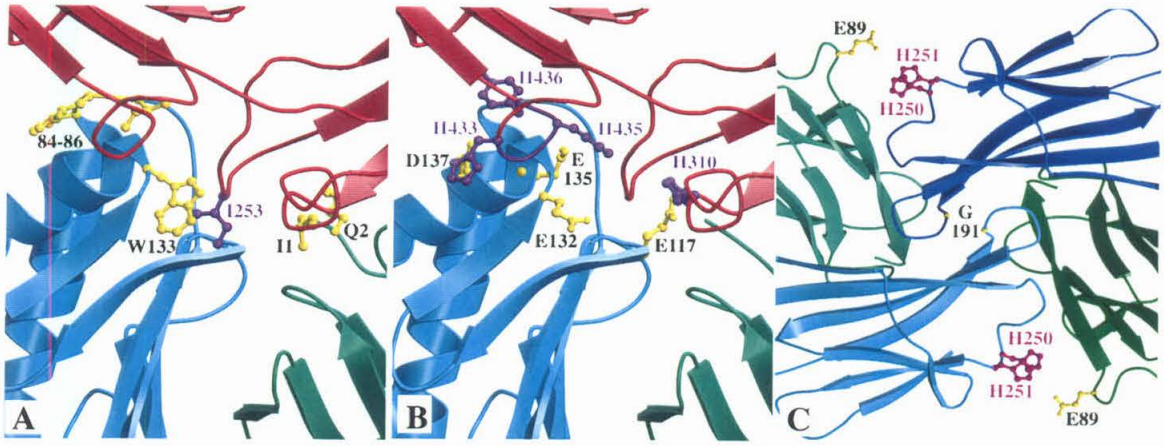

Figure 2. Close-up views of the mutated amino acids on FcRn. Orientations are the same as shown in Figure 1 (panels A and B) or rotated by 45° about a horizontal axis (panel C). Substituted amino acids are highlighted in yellow (mutations described and characterized in this text) or magenta (previously characterized mutations). Other colors are as described for Figure 1. Highlighted positions are: (A) Ile-1 (I1) and Gln-2 (Q2) of β2m, amino acids 84 to 86 (84-86) and Trp-133 (W133) of the FcRn heavy chain, and Fc Ile-253 (I253); (B) His-310 (H310), His-433 (H433), His-435 (H435), and His-436 (H436) of the Fc and Glu-117 (E117), Glu-132 (E132), Glu-135 (E135), and Asp-137 (D137) of the FcRn heavy chain; and (C) Gly-191 (G191), His-250 (H250), His-251 (H251) of the FcRn heavy chain, and Glu-89 (E89) of β2m.

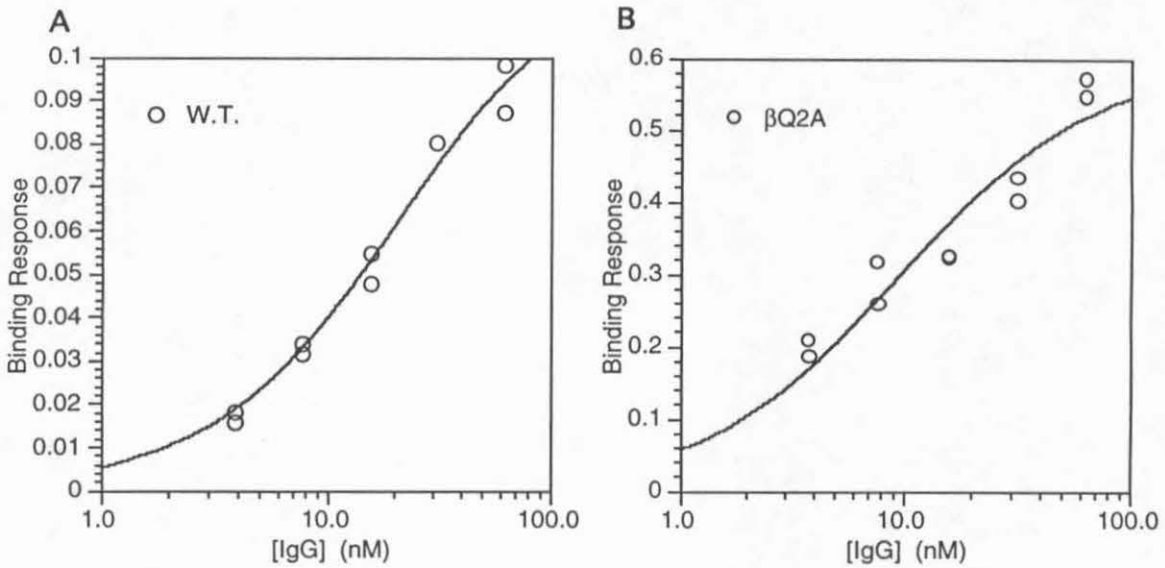

Figure 3. IgG binding to ß2m mutants at the FcRn-Fc interface. Equilibrium IgG binding to membrane associated wild-type and mutant βQ2A FcRn is plotted as a function of the log of the IgG concentration. The best fit binding curves, modelled as a single class of non-interacting binding sites, correspond to the values reported in Table 2. Two additional mutants (βI12A and β-1Y) showed no significant binding at IgG concentrations of ≤ 0.9 μM (data not shown).

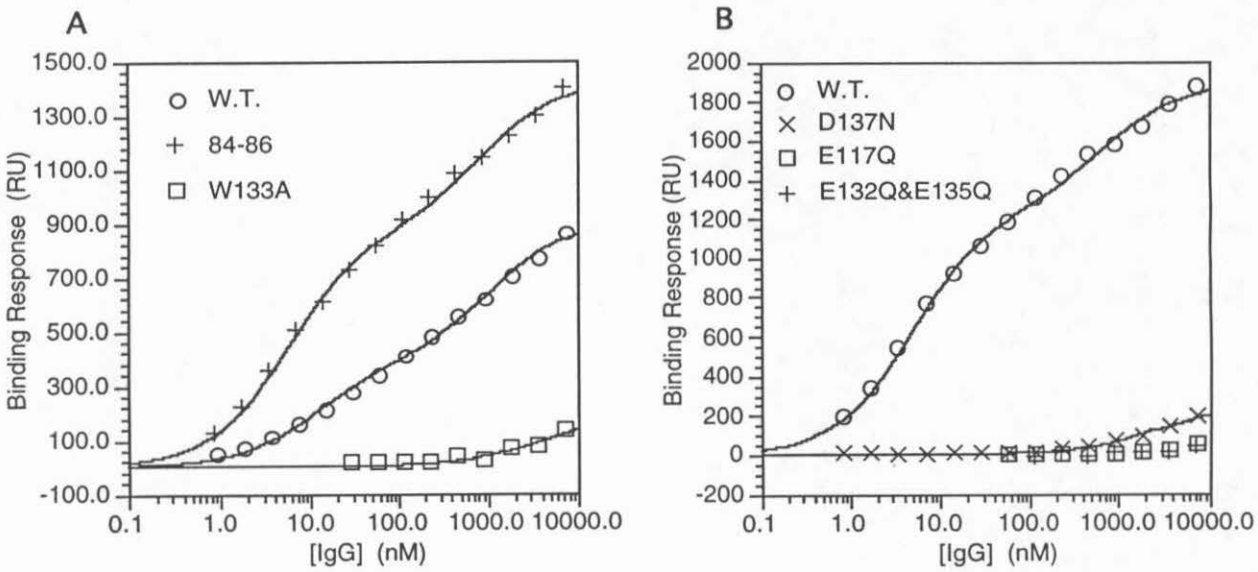

Figure 4. IgG binding to FcRn heavy chain mutants at the FcRn-Fc interface. Equilibrium IgG binding to wild-type and mutant FcRn proteins immobilized on a biosensor chip is plotted as a function of the log of the IgG concentration. The best fit binding curves, modelled as two classes of non-interacting binding sites, correspond to the values reported in Table 2.

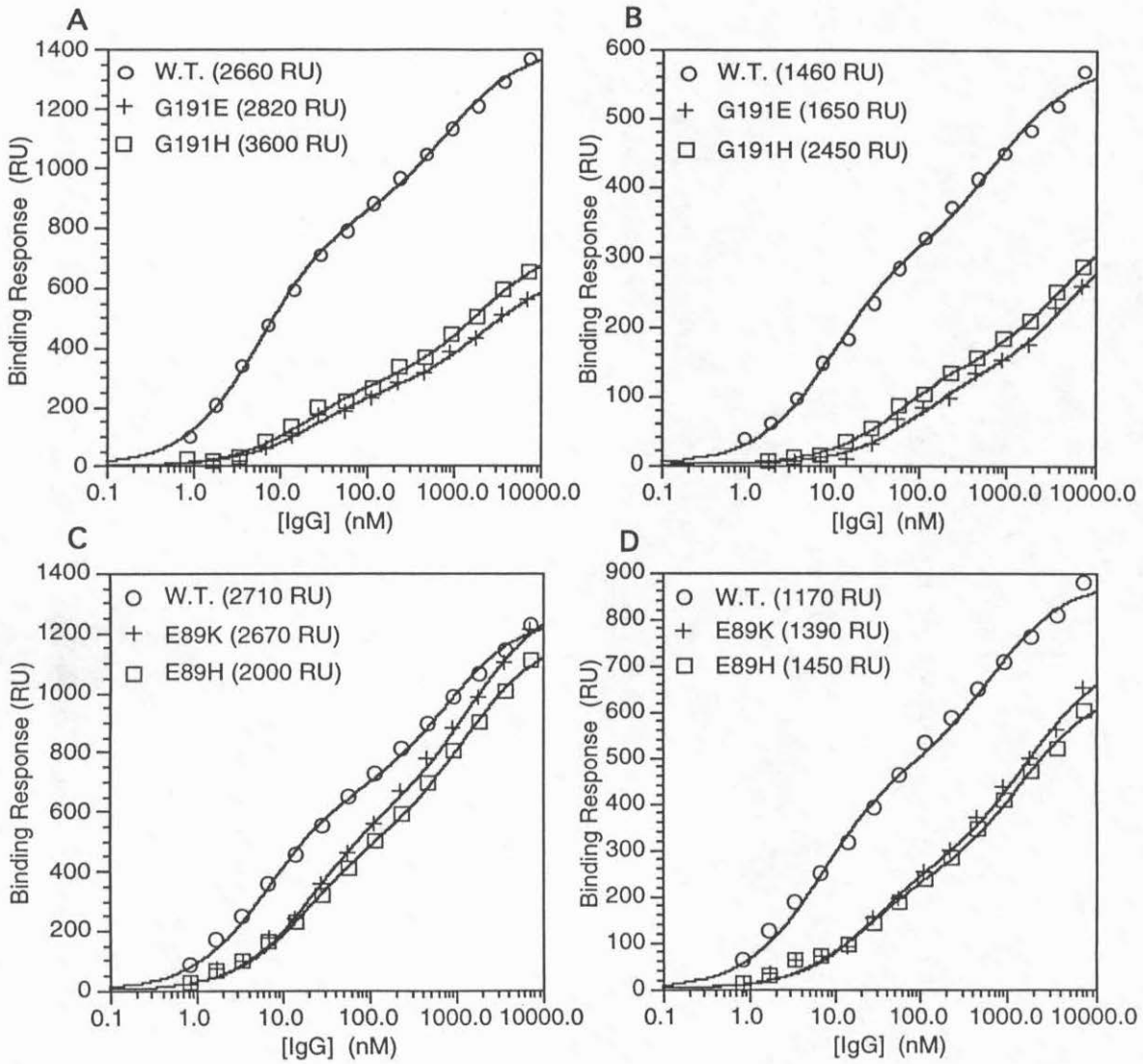

Figure 5. IgG binding to FcRn mutants at the dimer interface. Equilibrium IgG binding to wild-type and mutant FcRn proteins immobilized on a biosensor chip is plotted as a function of the log of the IgG concentration. The best fit binding curves, modelled as two classes of non-interacting binding sites, correspond to the values reported in Table 2. Experiments were performed at high (panels A and C) and low (panels B and D) coupling densities. Values for coupling densities are indicated in parentheses.

Structural basis of pH dependent antibody binding by the neonatal Fc receptor

Daniel E. Vaughn and Pamela J. Bjorkman

Background: The neonatal Fc receptor (FcRn) binds immunoglobulin G (IgG) with nanomolar affinity at pH 6, but shows no detectable binding at pH 7.5. At pH 6, FcRn is more thermally stable and the dissociation rate of its light chain is an order of magnitude slower than at pH 8.0.

Results: We determined the structure of FcRn at pH 8 and compared it to a further refined version of the pH 6.5 structure. Extensive ordered carbohydrate is observed at both pH values. The two structures are very similar; thus the pH dependence of FcRn's stability and affinity for IgG can be attributed to chemical properties of the structures themselves rather than mechanisms that rely on conformational changes.

Conclusions: FcRn dimerization, required for high affinity binding of IgG, is facilitated by reciprocal interactions in which carbohydrate from one receptor binds to protein residues from the dimer-related receptor to form a "carbohydrate handshake". The pH dependence of FcRn stability and binding to IgG are mediated by electrostatic interactions involving histidines. These interactions are more favorable for protonated histidines, which predominate at acidic pH values.

Introduction

The neonatal Fc receptor (FcRn) binds immunoglobulin G (IgG) in two important physiological processes (reviewed in [1]). Mammals, and probably amniotes in general, transmit maternal IgG molecules to pre- or postnatal offspring in order to provide the newborn with humoral immunity to antigens encountered by the mother. This passively acquired IgG is critical during the first few weeks of life before the newborn develops a fully functional immune system. Depending on the species, FcRn mediates the transcytosis of maternal IgG across fetal and/or neonatal tissues in this acquisition of passive immunity. FcRn also functions in the adult, where it is involved in the maintenance of high serum IgG levels. FcRn rescues IgG from a default degradative pathway by binding IgG in endocytic vesicles of the cells that degrade serum proteins and mediating the return of IgG to the bloodstream. Both of these processes are facilitated by pH dependent IgG binding to FcRn [2,3]. At pH 6.5, FcRn binds IgG with nanomolar affinity while IgG binding to FcRn is not detectable at pH 7.5 [4].

The sharp pH dependence of FcRn binding to IgG is an unusual and characteristic feature of this protein-protein interaction. At least part of the pH dependence of the interaction comes from histidines at the C_H2-C_H3 domain interface of the IgG ligand [4-9]. Thus the FcRn binding site on IgG has evolved to interact in a pH dependent manner with FcRn. It is noteworthy that other Fc receptors (i.e., the various FcγRs of the immunoglobulin gene superfamily, none of which show pH dependent IgG binding) bind to a different region of IgG, involving the hinge and the hinge-proximal portion of the C_H2 domain (reviewed in [10]). This region is distant from the C_H2-C_H3 domain interface containing the conserved histidines implicated in FcRn binding. Several other proteins bind to IgG at the junction between the C_H2 and C_H3 domains. These include protein A [11], protein G [11,12], and rheumatoid factor autoantibodies [13]. One or more of the conserved histidines have been shown to be contact residues in complexes of these proteins

with IgG. Nonetheless, only the interaction of FcRn shows a sharp pH dependent binding profile.

In addition to the pH dependence of IgG binding, FcRn shows other pH dependent properties. FcRn is more stable at pH 6 compared to pH 8 as assayed in thermal denaturation profiles [14]. Furthermore, the dissociation rate of the FcRn light chain from the heavy chain is an order of magnitude slower at pH 6 than at pH 8 [14]. Taken together, these results suggest that the interaction between the two chains of the FcRn heterodimer is altered over this narrow pH range.

FcRn shows structural and sequence similarity to class I major histocompatibility complex (MHC) molecules (reviewed in [10]). The FcRn light chain, ß2-microglobulin (ß2m), is the same polypeptide that associates with class I MHC heavy chains [15]. The heavy chains of both FcRn and class I MHC molecules consist of three extracellular domains, α1, α2, and α3, followed by a transmembrane region and a short cytoplasmic sequence [16,17]. The 2.2 Å crystal structure of a soluble form of rat FcRn corresponding to the ligand-binding extracellular region was solved at pH 6.5 [18]. In each of three crystal forms used in the FcRn structure determination, a dimer of FcRn heterodimers mediated by contacts between the α3 and ß2m domains was observed (hereafter referred to as the "FcRn dimer"). FcRn dimerization is required for the formation of the physiological high affinity IgG binding site [19]. The FcRn dimer was also observed in the crystal structure of a 2:1 complex of FcRn and the Fc fragment of IgG determined at an effective resolution of 6.5 Å [20]. The low resolution FcRn/Fc cocrystal structure revealed the approximate IgG binding site on FcRn, which was further defined by evaluating the IgG affinities of a series of FcRn mutants [21].

Here we report the structure of rat FcRn at pH 8. This structure determination reveals an extensive carbohydrate mediated interaction between the dimer related FcRn molecules that was not originally interpretable at pH 6.5 [18]. We also present a further refined structure of FcRn at pH 6.5 that includes the additional carbohydrate structure, and

discuss the physiological relevance of this interaction. The pH 8 and 6.5 structures are compared with specific attention to the pH dependence of FcRn stability and affinity for IgG. We propose a mechanism for pH dependent antibody binding to FcRn based on these structures and the body of structure/function literature concerning this interaction.

Results & Discussion

Solution of the pH 8 FcRn structure and refinement of pH 6.5 and pH 8 structures

FcRn crystallizes in space group $C222_1$ both at pH 6.5 and at pH 8, although the unit cell dimensions are slightly different (Table 1). The pH 8 and pH 6.5 crystals both diffract weakly and suffer from extensive radiation damage when data are collected at room temperature, therefore data for the new pH 8 structure were collected from cryopreserved crystals using synchrotron radiation, as had been done previously for the pH 6.5 crystals [18]. The pH 8 crystals diffract to approximately 2.7 Å resolution (effective resolution is 3 Å for $F > 3\sigma$), as compared to a 2.2 Å nominal and 2.4 Å effective resolution limit for the pH 6.5 crystals (Table 1).

The pH 8 structure was solved by molecular replacement using the pH 6.5 coordinates. The asymmetric units in both crystals include two FcRn molecules forming the FcRn dimer, and a third unpaired FcRn molecule referred to as the FcRn monomer. In both crystal forms, the FcRn monomer is not as well ordered as the FcRn molecules that form the dimer, as evidenced by higher average B factors (Table 1). To facilitate comparison of potentially small differences between the new structure at pH 8 and the previously determined structure at pH 6.5, the pH 6.5 structure was re-refined using more stringent application of non-crystallographic symmetry (NCS) restraints as recently recommended [22]. NCS restraints were set at 300 kcal mol^{-1} A^{-2} for the whole molecule until regions that did not obey the NCS were identified manually. Later in the refinement,

the NCS unrelated regions were not restrained, while the restraint weight for the NCS related regions was optimized to minimize the free R factor. The NCS unrelated regions are mainly interdomain linkers, at crystal contacts, or at the FcRn dimer interface. The conformations of the three NCS related FcRn molecules are similar (1.0 Å and 0.8 Å r.m.s. difference for all protein atoms in the pH 6.5 and pH 8 structures respectively). Within each domain, the regions which obey the NCS are nearly identical (0.3 Å and 0.1 Å r.m.s. difference for all protein atoms in the pH 6.5 and pH 8 structures respectively).

In both structures, all 269 heavy chain and 99 light chain residues are observed in each of the three NCS related molecules, as well as a total of 18 sugar residues and three 2-mercaptoethanol molecules covalently bound to the proteins. The newly refined pH 6.5 structure includes 480 water and two sulfate molecules, while the pH 8 structure includes 189 water and two sulfate molecules. Both structures have good model geometry, including >80% of the main chain phi-psi angles in the most favored regions of a Ramachandran plot and no residues in disallowed regions as defined in Procheck ([23]; Table 1). Both structures also adequately account for the observed diffraction data, with R_{free} values less than 30% (Table 1).

Comparison of FcRn crystal structures at pH 6.5 and pH 8

The structure of FcRn at pH 8 is similar, but not identical, to the pH 6.5 structure. The two crystal forms are not isomorphous; each refined model having an R-factor > 50% when calculated using the diffraction amplitudes of the other data set. Rigid body refinement, treating the FcRn dimer and the unpaired FcRn molecule as separate rigid bodies to account for differences in the crystal packing interactions, reduces the R-factor from 53% to 41% for the pH 6.5 structure refined against the pH 8 data. When each of three domains (α1 plus α2, α3 and ß2m) is treated as a separate rigid body, the R-factor is further reduced to 34.6%. When the pH 6.5 and pH 8 FcRn dimers have been

superimposed to align corresponding α1α2 platforms, the ß2m and α3 domains of the same FcRn are rotated 1.2° and 1.1° respectively and the dimer related FcRn is rotated 3.0° (Figure 1) . Thus, there are minor differences in both the interdomain and intermolecular packing. Within each domain the structures are very similar (less than 1 Å r.m.s. difference for all protein atoms within each domain), although there are a few sidechains that adopt alternate rotamers, most notably His-250 in the FcRn dimer (discussed below).

Implications for pH dependent FcRn stability and ligand binding

Although FcRn is more stable at pH 6 than at pH 8 [14], the crystal structures determined under acidic and alkaline conditions are very similar. The absence of large structural differences eliminates explanations that rely on conformational changes, allosteric effects or induced fits, and suggests that the pH dependent differences in stability and affinity for IgG are properties of the residues within the structures themselves. Histidines are likely to be involved in pH dependent protein interactions at pH values near neutral. The pK_a for histidine in model compounds is 6.6 [24]. However, the actual pK_a depends on the environment of the histidine side chain, most significantly on the solvent accessibility and the proximity of charged species (reviewed in [25]). Thus an imidazole group buried in the hydrophobic interior of a protein tends to have a $pK_a > 6.6$, whereas proximity to a negative charge generally lowers the pK_a. The usual range of pK_a values observed for histidines in proteins is 5 to 8 [24].

FcRn contains ten histidine residues, six located on the heavy chain and four on ß2m [16]. Electrostatic interactions between histidines and neighboring electronegative oxygen atoms are listed in Table 2. Within an FcRn molecule, there are two interdomain salt bridges (His-168 of the α2 domain to Glu-54 of the α1 domain, and His-237 of the α3 domain to the C-terminal carboxylate group of ß2m), and numerous other interdomain electrostatic bonds involving histidines (Figure 2). In these electrostatic bonds, the Nδ1 or

Nε2 proton of histidine interacts with an oxygen atom carrying either a formal or partial negative charge. These interactions are more favorable for fully protonated histidines and thus stabilize FcRn at pH 6.5 relative to pH 8. Four of the interactions are between ß2m and the FcRn heavy chain (His-10, His-237, ß2m His-13, and ß2m His-31; Table 2) thus directly stabilizing the association of the FcRn heavy and light chains at acidic relative to alkaline pH. This subset of histidine-mediated interactions accounts, at least in part, for the observed pH dependent difference in the rate of ß2m exchange [14], while all the interactions listed in Table 2 potentially contribute to increased FcRn stability at pH 6. FcRn and class I MHC molecules share the same light chain, ß2m. Only one of the ß2m histidines forms an inter-subunit salt bridge. Of the six histidine residues on the FcRn heavy chain, only His-258 is conserved in class I molecules, which do not show pH dependent differences in stability [14]. Thus distinct structural features of FcRn cause its pH dependent properties, and these features involve interactions with specific side chains rather than a major rearrangement of domains or a large conformational change.

The pH dependence of FcRn's interaction with IgG can also be attributed to chemical properties of the FcRn and Fc structures themselves rather than mechanisms that rely on conformational changes. The structures of the FcRn dimer at pH 6.5 and at pH 8 are essentially the same as the structure of the Fc-bound FcRn dimer in the low resolution FcRn/Fc cocrystal structure [20]. Although IgG is flexible in solution [26] and presumably undergoes a loss of entropy upon FcRn binding due to trapping FcRn-bound Fc in one of its many solution conformations [27], there is no evidence that Fc undergoes a pH dependent conformational change [14]. As is the case for the pH dependent stability of FcRn, the pH dependence of IgG binding also appears to be mediated primarily by histidines. We propose the following mechanism for pH dependent IgG binding by FcRn (Figure 3a). At pH 8, most solvent exposed histidine residues will be deprotonated and carry no net charge, while at pH 6.5 and below, these residues will generally be protonated and carry a net positive charge. For each positively charged histidine, there is a

complementary anionic binding pocket, and thus these histidines form several pH dependent salt bridges. Specifically, there are three anionic binding sites on FcRn that accomodate histidines on Fc, and two anionic binding sites (one on each ß2m molecule) that accept histidines on the dimer related FcRn molecule. We believe that the cooperative effect of these several pH dependent salt bridges are sufficient to explain the dramatic difference in IgG affinity between FcRn at pH $\leq$ 6.5 and FcRn at pH $\geq$ 7.5.

On IgG, histidine residues critical for FcRn binding have been identified by mutagenesis and subtype studies. One of these is His-310. A triple site directed mutant of human IgG4 (Leu-309, His-310, and Gln-311 each to Gly) decreases the affinity for IgG from 22 nM to 1.9 µM [4], and a murine IgG1 mutant (His-310 to Ala) shows greatly reduced transcytosis and protection from catabolism [9]. Histidine residues within loop 433-436 of IgG have also been implicated, although the specific residues appear to vary among IgG isotypes. For human IgG4, His-433 but not His-435 is necessary for high affinity IgG binding [4], while for murine IgG1 both His-435 and His-436 but not His-433 are necessary for both optimal *in vitro* FcRn binding and *in vivo* FcRn function [9].

FcRn residues that are critical for IgG binding line three negatively charged pockets (Figure 3b). Critical residues were identified by site directed mutagenesis of FcRn side chains that are near Fc in the low resolution structure of the FcRn/Fc complex [20]. Substitution of FcRn heavy chain residues Glu-117 with Ser, Trp-133 with Ala, Asp-137 with Asn, or both Glu-132 and Glu-135 with Gln, reduces the affinity for a monoclonal murine IgG1 from a K_D of 5 nM to a K_D more than 8 µM, a change in the free energy of binding of > 4 kcal/mol [21]. Similarly, substitution of ß2m Ile-1 with Ala, or extension of the ß2m N-terminus one residue by addition of a tyrosine reduces the binding affinity to levels that are undetectable for 1 µM IgG ($K_D >> 1\mu M$) [21]. The pockets lined by these residues are negatively charged, and could form anionic binding sites for protonated histidines. Although the resolution of the FcRn/Fc cocrystal structure is insufficient to

visualize the interaction of individual Fc histidines with anionic pockets on FcRn, they are in positions where they could form pH dependent salt bridges [20].

Formation of the FcRn dimer is also required for high affinity binding of IgG [19]. The interaction of FcRn residues His-250 and His-251 with Glu-89 on ß2m of the dimer related molecule stabilizes this interaction, and can be directly compared in the structures of FcRn at pH 6.5 and pH 8 (Figure 3c, d). Mutation of His-250 and His-251 to the corresponding MHC class I residues (Gln and Asn) decreases IgG affinity ~6 fold, while replacement of Glu-89 of ß2m with either His or Lys decreases IgG affinity ~3 fold, corresponding to changes in the free energy of binding of 1.1 and 0.7 kcal/mol respectively [7,21]. Thus the dimer related histidine salt bridges are less critical for IgG binding than the salt bridges between histidines on the ligand and anionic sites on the receptor. Nonetheless, these interactions are necessary for optimal IgG binding even though FcRn forms essentially the same dimer at pH 6.5 and at pH 8. There are slight differences at these sites between the pH 6.5 structure and that at pH 8 that might account for these effects. At pH 6.5, both histidine 250 and 251 extend across the dimer interface and interact with Glu-89 of ß2m (Figure 3c), while at pH 8 only His-251 extends across the dimer interface (Figure 3d). At pH 8, the alternative conformation of His-250 allows it to form a salt bridge with the terminal carboxylate of the same heavy chain (Figure 2), and this conformation is seen in the FcRn monomer at both pH 6.5 and 8.

Carbohydrate mediated dimer interface

Several studies show that the FcRn dimer is required to form the high affinity binding site for a single IgG. A 2:1 receptor:ligand stoichiometry was observed for rat FcRn interacting with IgG in solution and in crystals of the receptor/Fc complex [20,28]. Site directed FcRn mutants with alterations that specifically affect the interaction with FcRn dimers, but not with monomers, show reduced affinities for IgG [7,21]. The role of FcRn

dimerization in its interaction with IgG was directly tested by introducing cysteines at positions that either facilitated or hindered receptor dimerization when FcRn was coupled to a biosensor chip using thiol chemistry [19]. High affinity binding (K_D = 22 nM), similar to the affinity observed under physiological conditions [29], was found when FcRn was coupled in the orientation facilitating dimerization, but the affinity was reduced over 100-fold when receptor dimerization was hindered [19].

There is an extensive interface between dimer related FcRn molecules. The α3 domain from each molecule interacts with both the α3 and ß2m domains from the dimer related molecule, while the only direct interaction between ß2m domains is made between the side chains of Glu-74. The dimer is approximately two-fold symmetric with each molecule interacting through the loops connecting strands A and B and strands E and F of the α3 domain, and the G strand of ß2m. However, the dyad symmetry is not exact; e.g., two sulfate molecules bind to one α3 domain of the dimer but not the other.

In addition to the protein-protein interactions, much of the FcRn dimer interface is formed by interactions involving carbohydrates. We originally calculated that FcRn dimerization buries approximately 2100 Å^2 of surface area (1068 Å^2 contributed from each FcRn monomer) using the pH 6.5 structure that included three sugar residues from each molecule [18]. After interpretation of additional carbohydrate density at the dimer interface, we now calculate that dimerization buries 2600 Å^2 of surface area in the pH 6.5 structure, of which 1100 Å^2 are buried by carbohydrate. N-linked carbohydrate from one α3 domain binds to an otherwise exposed hydrophobic surface on the dimer related α3 domain (Figure 4a,b). Combined with the reciprocal interaction, this forms a "carbohydrate handshake" that could rationalize previously reported results that are in apparent contradiction. While the stoichiometry of rat FcRn with Fc or IgG is 2:1 [20,28], presumably reflecting the interaction of Fc with the FcRn dimer, the stoichiometry of mouse FcRn interacting with Fc in solution was observed to be 1:1 [30]. In the latter study, a soluble form of mouse FcRn was expressed in insect cells in which N-linked

carbohydrate structures differ from their mammalian counterparts. Proteins expressed in mammalian cells undergo additional processing steps on N-glycosides to add complex carbohydrate antennae relative to proteins expressed in insect cells, which stop carbohydrate processing at an earlier high mannose step [31,32] (Figure 4c). The rat FcRn structure, which was solved using protein expressed in Chinese hamster ovary (CHO) cells, reveals intimate contacts between the α1,6-linked antennae and dimer related hydrophobic amino acids that would not be possible if the carbohydrate moiety was of the high mannose type: e.g., the glucosamine group of Nag-509 penetrates into a pocket in the α3 domain formed by residues Arg-216, Ser-221, Leu-242, Val-244, and Tyr-252 (Figure 4b). Thus differences between the high mannose N-glycoside of mouse FcRn and the complex carbohydrate of rat FcRn could affect the propensity of FcRn to dimerize. Indeed, we observe that soluble mouse FcRn expressed in CHO cells interacts with Fc with a 2:1 stoichiometry (L.M. Sánchez and P.J.B., unpublished results). Thus, it is likely that the complex carbohydrate antennae make specific contacts that facilitate formation of the high affinity 2:1 FcRn/IgG complex.

Although ordered N-glycoside sugars have been observed on other glycoprotein structures, it is unusual for more than about three sugar residues to be ordered. Exceptions include the structures of (i) a legume lectin, in which a plant-specific heptasaccharide is ordered at a crystal contact [33], (ii) the adhesion domain of CD2, in which a high mannose N-glycan stabilizes the protein fold [34], and (iii) the Fc fragment of IgG, in which complex oligosaccharides occupy the space between the dimer-related C_H2 domains [11]. In both Fc and FcRn, the N-glycoside core and much of one antenna (Figure 4c) are modeled in each structure, with the other antenna being disordered. For Fc, it is the α1,3-linked antenna that is ordered, while the α1,6-linked antenna is seen in FcRn.

Amongst these examples of ordered carbohydrate in protein structures, the FcRn carbohydrate is the only glycoside that facilitates a physiologically relevant dimerization. The ordered carbohydrate on Fc is the most comparable to that of FcRn, because in both

cases the carbohydrate includes residues specific to complex oligosaccharides, and is at a homodimer interface that obeys approximate two-fold symmetry. However, the Fc carbohydrate is not required for dimerization or function, as nonglycosylated Fc expressed in bacteria forms dimers that retain full *in vivo* function [5,6], perhaps because the glycoside in Fc primarily contacts other carbohydrate molecules on the dimer related molecule [11]. By contrast, the carbohydrate at the FcRn dimer interface makes contacts to dimer related protein residues (Figure 4a,b). Binding of the distal sugar residues to the dimer related FcRn presumably stabilizes the carbohydrate structure and allows its visualization in the electron density maps. Indeed, these sugars are disordered at both pH 6.5 and pH 8 on the FcRn monomer that lacks a dimer-related partner.

Biological implications

The pH dependent interaction between FcRn and IgG is necessary for*in vivo* transport of IgG between acidic and basic pH environments. The structure of FcRn does not change significantly between pH 6.5 and 8, even though FcRn shows decreased stability at alkaline versus acidic pH [14]. A network of electrostatic bonds between the N∂1 or Nε2 proton of histidines and oxygen atoms carrying either a formal or partial negative charge makes a set of interactions that are more favorable under acidic conditions that favor protonation of the histidine residue. We propose that these interactions contribute to the observed pH dependent stability of FcRn. Thus for FcRn, structural changes that lead to increased or decreased stability can be explained by subtle features rather than major conformational changes. As a second example of a system in which stability differences are not revealed as large conformational changes, class II MHC molecules that bind the CLIP peptide of the invariant chain are less stable than class II complexes with conventional peptide antigens, yet the crystal structures of both types of complexes are nearly identical [35].

The characteristic feature of the FcRn/IgG interaction is its sharp pH dependence, which allows FcRn to bind IgG in early endosomes (pH ~6.2) and release IgG at the cell surface (pH ~7.5). The use of titratable salt bridges by FcRn to bind IgG at pH 6.5 but not pH 8 is a simple but elegant mechanism that provides the necessary pH dependent affinity for FcRn to carry out its IgG transport functions *in vivo*. The lack of a conformational change between the FcRn structures solved at permissive and non-permissive pH conditions for ligand binding is in contrast to the classical pH dependent binding interaction of oxygen to hemoglobin. Hemoglobin undergoes a conformational transition between an "R" and "T" state that is influenced by the binding of numerous small molecules. Thus FcRn's pH dependent IgG affinity illustrates a molecular mechanism for sharply pH dependent binding that does not involve allosteric effects or conformational changes.

To our knowledge, the FcRn/IgG interaction is the first detailed molecular mechanism of a receptor binding to a protein ligand with physiological pH dependence. Many other receptor-ligand pairs also make use of sharply pH dependent affinities to achieve the desired intracellular routing. For example, low density lipoprotein binds its receptor extracellularly at pH ~7.5 and is released under the slightly acidic conditions of the early endosomes (pH ~ 6.2) [36]. Similarly, apo-transferrin binds to the transferrin receptor in acidic endosomes, but is released at the cell surface [37]. In the case of FcRn, most of the affinity for its ligand is achieved by the interactions between protonated histidines and anionic binding pockets [21]. By contrast, for other well-characterized protein-protein interactions, hydrophobic contacts provide much of the free energy of binding [38-41]. The predominance of electrostatic interactions involving titratable histidines in the binding of IgG by FcRn provides a mechanism to achieve sharply pH dependent receptor-ligand affinity that might be generally applicable.

Materials and Methods

Crystallization and cryopreservation

FcRn was expressed and purified as previously described [42]. Crystals were grown at 22°C in hanging drops by combining 2 µl protein solution (~20 mg/mL FcRn, 20 mM PIPES pH 6.5, and 0.02% NaN_3) with 2 µl reservoir solution (15% PEG 3000, 100 mM Tris pH 8.0, 100 mM $(NH_4)_2SO_4$ pH 8.0, and 30% ethylene glycol). Crystals grew to a mature size of about 0.5 mm x 0.5 mm x 0.3 mm in approximately two weeks. The crystals belong to space group $C222_1$ with unit cell dimensions a = 122.6, b = 193.1, c = 149.0 Å. These crystals suffered from severe radiation damage at room temperature, so diffraction data were collected at cryogenic temperatures. The crystal could be flash cooled either in liquid nitrogen or in a -170°C nitrogen stream, although better results (higher resolution diffraction and lower mosaic spread) were obtained by initially cooling the crystals in a -120 to -140°C nitrogen stream and slowly (over about 10 minutes) reducing the temperature of the nitrogen stream to -170°C.

Data collection and processing

X-ray diffraction data of the pH 8 FcRn crystals were collected on beamline A1 at the Cornell High Energy Synchrotron Source (CHESS) on the Princeton 1K CCD detector (Table 3). Despite cryopreservation, the FcRn crystals decayed noticeably over the course of a data collection and therefore data were collected from five crystals. All data processing was done with version 1.5 of the HKL suite [43]. Several alternate data reduction strategies were examined (inclusion of different subsets of the five crystals, various statistical criteria for the rejection of individual observations and/or exclusion of invididual data frames) and assayed by the merging statistics of Friedel mates. Strategies that

improved traditional measures of data quality (i.e., R_{merge}) without a corresponding reduction in the agreement between Friedel mates were abandoned. The final scaled data set includes data from three crystals, and while several whole images were discarded because of beam drift or crystal decay, no observations were discarded based on statistical assays or because of negative intensities. The average redundancy of 3.4 was comparable for all resolution bins.

Structure solution and refinement

Electron density fitting was done using the program "O" [44]. All crystallographic refinement was done using X-PLOR [45] with a maximum likelihood target function [46], a flat bulk solvent correction, and no low resolution or sigma cutoff applied to the data. As previously done for the pH 6.5 structure [18], a randomly selected 5% of pH 8 structure factor amplitudes were excluded from automated refinement and used to compute a "free" R factor (R_{free}) [47] throughout refinement. The chemical restraints included only repulsive terms with weights chosen to minimize the R_{free} value; no electrostatic terms were included. Thus the refinement was independent of the assumed protonation state of each titratable residue.

FcRn packs similarly in the pH 8 and pH 6.5 crystals, but there is a significant change in the pH 8 unit cell (Table 1). The initial search model for the pH 8 crystals was the pH 6.5 structure without solvent molecules that had been subjected to simulated annealing (3000 K) [48] with strong NCS restraints (300 kcal mol^{-1} A^{-2}). Initial molecular replacement maps revealed carbohydrate structure that was not modeled in original pH 6.5 structure [18]. The pH 8 structure was built to include the N-glycoside, refined against the high pH data, and the model was then returned to the acidic pH crystal form by rigid body refinement. The additional sugar residues showed strong density, and the higher resolution data provided significant new information. Several rounds of rebuilding and refinement

against the pH 6.5 data were carried out. At this point the final pH 6.5 structure without water molecules was again rigid body refined against the pH 8 data. This structure was than subjected to positional and individual B-factor refinement, and water molecules were placed to generate the final pH 8 structure. For both structures, ordered water positions were identified by selecting peaks within hydrogen bonding distance to polar or charged atoms at 1.5σ above the average density in a 2Fo-Fc SigmaA weighted map. Throughout refinement of both pH 8 and pH 6.5 structures, NCS restraints were applied to each domain separately with weights chosen to minimize the R_{free} value. Residues that do not obey the NCS were identified manually during map interpretation and not restrained. Specifically, these regions are the four N-terminal residues of the heavy chain, the two N-terminal residues of the light chain, the interdomain linkers (residues 84-89 and 177-182 of the heavy chain), residues 39-45 (involved in a crystal contact), and residues that comprise the dimer interface (177-182, 189-193, and 246-252 or the heavy chain and the side chain of Glu-74 on ß2m).

The programs "O" [44] and Procheck [23] were used for model assesment. Figures were generated using Molscript [49] and Raster-3D [50] (Figures 1, 2, and 4a), "O" (Figures 3c,d and 4b), and GRASP [51] (Figure 3b).

Acknowledgments

We thank Art Chirino for help with data collection, valuable discussions and critical reading of the manuscript, Luis Sánchez for sharing unpublished results, Axel Brünger for providing test versions of his software, and Steve Mayo for the use of computational resources. We thank the MacChess staff and operators at CHESS for help with data collection and the crystallographers at Caltech. This work was supported by a Camille and Henry Dreyfuss Teacher Scholar Award (P.J.B.) and a grant from the NIH (AI/GM41239

to P.J.B.). Coordinates for both the pH 8 and further refined pH 6.5 FcRn structures will be deposited in the Brookhaven protein data bank.

References

1. Junghans, R.P. (1997). Finally! The Brambell Receptor (FcRB). Mediator of Transmission of Immunity and Protection from Catabolism for IgG. *Immunol. Res.* **16**, 29-57.

2. Rodewald, R. (1976). pH-dependent binding of immunoglobulins to intestinal cells of the neonatal rat. *J. Cell Biol.* **71**, 666-670.

3. Rodewald, R. & Kraehenbuhl, J.-P. (1984). Receptor-mediated transport of IgG. *J. Cell Biol.* **99**, S159-S164.

4. Raghavan, M., Bonagura, V.R., Morrison, S.L. & Bjorkman, P.J. (1995). Analysis of the pH dependence of the neonatal Fc receptor/Immunoglobulin G interaction using antibody and receptor variants. *Biochemistry* **34**, 14649-14657.

5. Kim, J.K., Tsen, M.F., Ghetie, V. & Ward, E.S. (1994). Identifying amino acid residues that influence plasma clearance of mouse IgG1 fragments by site directed mutagenesis. *Eur. J. Immunol.* **24**, 542-548.

6. Kim, J.-K., Tsen, M.-F., Ghetie, V. & Ward, E.S. (1994). Catabolism of the murine IgG1 molecule: Evidence that both CH2-CH3 domain interfaces are required for the persistence of IgG1 in the circulation of mice. *Scand. J. Immunol.* **40**, 457-465.

7. Raghavan, M., Chen, M.Y., Gastinel, L.N. & Bjorkman, P.J. (1994). Identification of interaction sites in the class I MHC-related Fc receptor/immunoglobulin G complex. *Immunity* **1**, 303-315.

8. Kim, J.-K., Tsen, M.-F., Ghetie, V. & Ward, E.S. (1994). Localization of the site of the murine IgG1 molecule that is involved in binding to the murine intestinal Fc receptor. *Eur. J. Immunol.* **24**, 2429-2434.

9. Medesan, C., Matesoi, D., Radu, C., Ghetie, V. & Ward, E.S. (1997). Delineation of the amino acid residues involved in transcytosis and catabolism of mouse IgG. *J. Immunol.* **158**, 2211-2217.

10. Raghavan, M. & Bjorkman, P.J. (1996). Fc receptors and their interactions with immunoglobulins. *Ann. Rev. Cell Biol.* **12**, 181-220.

11. Deisenhofer, J. (1981). Crystallographic refinement and atomic models of a human Fc fragment and its complex with fragment B of protein A from *Staphylococcus aureus* at 2.9- and 2.8-Å resolution. *Biochemistry* **20**, 2361-2370.

12. Sauer-Eriksson, A.E., Kleywegt, G.J., Uhlen, M. & Jones, T.A. (1995). Crystal structure of the C2 fragment of streptococcal protein G in complex with the Fc domain of human IgG. *Structure* **3**, 265-278.

13. Artandi, S.E., Calame, K.L., Morrison, S.L. & Bonagura, V.R. (1992). Monoclonal IgM rheumatoid factors bind IgG at a discontinuous epitope comprised of amino acid loops from heavy-chain constant-region domains 2 and 3. *Proc. Natl. Acad. Sci. USA* **89**, 94-98.

14. Raghavan, M., Gastinel, L.N. & Bjorkman, P.J. (1993). The Class I MHC-related Fc receptor shows pH Dependent stability differences correlating with Immunoglobulin binding and release. *Biochemistry* **32**, 8654-8660.

15. Simister, N.E. & Rees, A.R. (1985). Isolation and characterization of an Fc receptor from neonatal rat small intestine. *Eur. J. Immunol.* **15**, 733-738.

16. Simister, N.E. & Mostov, K.E. (1989). An Fc receptor structurally related to MHC class I antigens. *Nature* **337**, 184-187.

17. Bjorkman, P.J. & Parham, P. (1990). Structure, function and diversity of class I major histocompatibility complex molecules. *Ann. Rev. Biochem.* **90**, 253-88.

18. Burmeister, W.P., Gastinel, L.N., Simister, N.E., Blum, M.L. & Bjorkman, P.J. (1994). Crystal structure at 2.2 Å resolution of the MHC-related neonatal Fc receptor. *Nature* **372**, 336-343.

19. Raghavan, M., Wang, Y. & Bjorkman, P.J. (1995). Effects of receptor dimerization on the interaction between the class I MHC related Fc receptor and immunoglobulin G. *Proc. Natl. Acad. Sci. USA* **92**, 11200-11204.

20. Burmeister, W.P., Huber, A.H. & Bjorkman, P.J. (1994). Crystal structure of the complex of rat neonatal Fc receptor with Fc. *Nature* **372**, 379-383.

21. Vaughn, D.E., Milburn, C.M., Penny, D.M., Martin, W.L., Johnson, J.L. & Bjorkman, P.J. (1997). Identification of critical IgG binding epitopes on the neonatal Fc receptor. *J. Mol. Biol.* in press.

22. Kleywegt, G.J. & Jones, T.A. (1995). Where freedom is given, liberties are taken. *Structure* **3**, 535-540.

23. Laskowski, R.A., MacArthur, M.W., Hutchinson, E.G. & Thornton, J.M. (1992). Stereochemical quality of protein structure coordinates. *Proteins* **12**, 345-364.

24. Fersht, A. (1985). *Enzyme Structure and Mechanism, 2nd edition*. W. H. Freeman and Company, New York, NY.

25. Matthew, J.B., Gurd, F.R.N., Garcia-Morena E., B., Flanagan, M.A., March, K.L. & Shire, S.J. (1985). pH dependent processes in proteins. *CRC Crit. Rev. in Biochem.* **18**, 91-197.

26. Zheng, Y., Shopes, B., Holowka, D. & Baird, B. (1992). Dynamic conformations compared for IgE and IgG1 in solution and when bound to receptors. *Biochemistry* **31**, 7446-7456.

27. Weng, Z., Gulukota, K., Vaughn, D.E., Bjorkman, P.J. & DeLisi, C. (1997). Computational determination of the structure of rat Fc bound to the neonatal Fc receptor. ms. submitted.

28. Huber, A.H., Kelley, R.F., Gastinel, L.N. & Bjorkman, P.J. (1993). Crystallization and Stoichiometry of Binding of a Complex between a Rat Intestinal Fc Receptor and Fc. *J. Mol. Biol.* **230**, 1077-1083.

29. Mackenzie, N. (1984). Fc receptor-mediated transport of immunoglobulin across the intestinal epithelium of the neonatal rodent. *Immunol. Today* **5**, 364-366.

30. Popov, S., Hubbard, J.G., Kim, J.-K., Ober, B., Ghetie, V. & Ward, E.S. (1996). The stoichiometry and affinity of interaction of murine Fc fragments with the MHC class I - related receptor, FcRn. *Mol. Immunol.* **33**, 521-530.

31. Luckow, V.A. & Summers, M.D. (1988). Trends in the development of baculovirus expression vectors. *Biotechnology* **6**, 47-55.

32. Jenkins, N., Parekh, R.B. & James, D.C. (1996). Getting the glycosylation right - Implications for the biotechnology industry. *Nature Biotech.* **14**, 975-981.

33. Shaanan, B., Lis, H. & Sharon, N. (1991). Structure of a legume lectin with an ordered N-linked carbohydrate in complex with lactose. *Science* **254**, 862-866.

34. Wyss, D.F., Choi, J.S., Li, J., Knoppers, M.H., Willis, K.J., Arulanandam, A.R.N., Smolyar, A., Reinherz, E.L. & Wagner, G. (1995). Conformation and function of the N-linked glycan in the adhesion domain of human CD2. *Science* **269**, 1273-1278.

35. Ghosh, P., Amaya, M., Mellins, E. & Wiley, D.C. (1995). The structure of an intermediate in class II MHC maturation - CLIP bound to HLA-DR3. *Nature* **378**, 457-462.

36. Brown, V.I. & Green, M.I. (1991). Molecular and cellular mechanisms of receptor-mediated endocytosis. *DNA and Cell Biol.* **10**, 399-409.

37. De Silva, D.M., Askwith, C.C. & Kaplan, J. (1996). Molecular mechanisms of iron uptake in eukaryotes. *Physiol. Rev.* **76**, 31-47.

38. Kelley, R.F. & O'Connell, M.P. (1993). Thermodynamic analysis of an antibody functional epitope. *Biochemistry* **32**, 6828-6835.

39. Tsumoto, K., Ogasahara, K., Ueda, Y., Watanabe, K., Yutani, K. & Kumagai, I. (1995). Role of Tyr residues in the contact region of anti-lysozyme monoclonal antibody HyHEL10 for antigen binding. *J. Biol. Chem.* **270**, 18551-18557.

40. Dall'Acqua, W., Goldman, E.R., Eisenstein, E. & Mariuzza, R.A. (1996). A mutational analysis of the binding of two different proteins to the same antibody. *Biochemistry* **35**, 9667-9676.

41. Wells, J.A. & DeVos, A.M. (1996). Hematopoietic receptor complexes. *Ann. Rev. Biochem.* **65**, 609-634.

42. Gastinel, L.N., Simister, N.E. & Bjorkman, P.J. (1992). Expression and crystallization of a soluble and functional form of an Fc receptor related to class I histocompatibility molecules. *Proc. Natl. Acad. Sci USA* **89**, 638-642.

43. Otwinowski, Z. & Minor, W. (1997). Processing of x-ray diffraction data collected in oscillation mode. *Methods in Enzymology* **276**, 307-326.

44. Jones, T.A., Bergdoll, M. & Kjeldgaard, M., Ed. (1993). Crystallographic computing and modeling methods in molecular design. New York, Springer.

45. Brünger, A.T., Kuriyan, J. & Karplus, M. (1987). Crystallographic R factor refinement by molecular dynamics. *Science* **235**, 458-460.

46. Pannu, N.S. & Read, R.J. (1996). Improved structure refinement through maximum likelihood. *Acta Cryst.* **A52**, 659-668.

47. Brünger, A.T. (1992). Free R value: a novel statistical quantity for assessing the accuracy of crystal structures. *Nature* **355**, 472-475.

48. Brünger, A.T., Krukowski, A. & Erickson, J.W. (1990). Slow-cooling protocols for crystallographic refinement by simulated annealing. *Acta Cryst.* **A46**, 585-593.

49. Kraulis, P.J. (1991). MOLSCRIPT: a program to produce both detailed and schematic plots of protein structures. *J. Appl. Crystallogr.* **24**, 946-950.

50. Merritt, E.A. & Murphy, M.E.P. (1994). Raster3D Version 2.0, a program for photorealistic molecular graphics. *Acta Cryst. D.* **50**, 869-873.

51. Nicholls, A., Bharadwaj, R. & Honig, B. (1993). GRASP - Graphical representation and analysis of surface properties. *Biophys. J.* **64**, A166-A166.

52. Kleywegt, G.J. & Jones, T.A. (1996). Xdlmapman and Xdldataman - Programs for reformatting, analysis and manipulation of biomacromolecular electron density maps and reflection data sets. *Acta Cryst.* **D52**, 826-828.

Table 1

Data collection and refinement statistics.

	pH 8	pH 6.5
Crystal		
Unit Cell ($C222_1$)	122.6 x 193.1 x 149.0 Å	126.5 x 191.7 x 149.6 Å†
Resolution	30 - 2.7 Å	25 - 2.2 Å†
Effective resolution ($\mathbf{F} > 3\sigma$)*	3.0 Å	2.4 Å
R_{merge}	11.3 %	7.2 %†
Completeness	90.0 %	86 %†
Number of observations	149 543	436 000†
Number of unique reflections	43 936	83 821†
Refinement		
Resolution		6-2.2
R_{cryst}	27.8 %	23.60%
R_{free}	29.7 %	27.7%
Number of scattering atoms		
Protein	8921	8877
Carbohydrate	198	198
Water	189	626
Sulfate	10	10
2-mercaptoethanol	12	12
Model geometry		
R.m.s. deviation from ideality		
Bonds	0.004 Å	0.009 Å
Angles	0.8°	1.4°
Ramachandran plot quality‡		
most favored	83.3 %	90.0 %
additionally allowed	16.1 %	10.0 %
generously allowed	0.6 %	0.0 %
disallowed	0.0 %	0.0 %
B factors		
r.m.s.d. bonded	2.2 $Å^2$	5.2 $Å^2$
Average		
Overall	71.8 $Å^2$	49.6 $Å^2$
FcRn Dimer (protein)	69.5 $Å^2$	42.6 $Å^2$
FcRn Monomer (protein)	80.5 $Å^2$	60.4 $Å^2$
Carbohydrate	106.9 $Å^2$	75.5 $Å^2$
Solvent	53.3 $Å^2$	56.0 $Å^2$

*As defined in [52], the resolution at which a complete data set would have the same number of reflections as the number of observed reflections with an amplitude greater than 3σ.

†As previously reported [18]

‡As defined in Procheck [23]

Table 2

pH dependent electrostatic interactions.

Proton Donor			Distance	Proton Acceptor		
Residue	Domain	Atom	(Å)	Residue	Domain	Atom
His-10	α1	Nδ1	3.5	Ser-55	ß2m	Oγ
			3.5	Phe-56	ß2m	O
His-168	α2	Nδ1	3.5	Glu-54	α1	Oε1
			2.8	Glu-54	α1	Oε2
His-237	α3	Nε2	3.2	Met-99	ß2m	OT
His-250	α3	Nε2	2.7	Glu-89	ß2m*	Oε1
His-250†	*α3*	*Nε2*	*3.2*	*Leu-269*	*α3*	*OT*
His-251	α3	Nε2	3.1	Glu-89	ß2m*	Oε1
His-251†	*α3*	*Nε2*	*2.7*	*Glu-89*	*ß2m**	*Oε1*
			2.9	*Glu-89*	*ß2m**	*Oε2*
His-258	α3	Nδ1	3.9	Glu-180	α2-α3	O
		Nε2	2.9	Pro-207	α3	O
His-13	ß2m	Nδ1	4.0	Ser-204	α3	Oγ
His-31	ß2m	Nε2	3.0	Gln-93	α2	Oε1
His-67	ß2m	Nε2	4.0	Glu-50	ß2m	Oε1
His-84	ß2m	Nε2	2.9	Pro-32	ß2m	O

* Interacts with the dimer-related molecule.

† Interactions shown are for the pH 6.5 structure. Interactions that are different (> 0.5 Å) for the pH 8 structure are shown in italics.

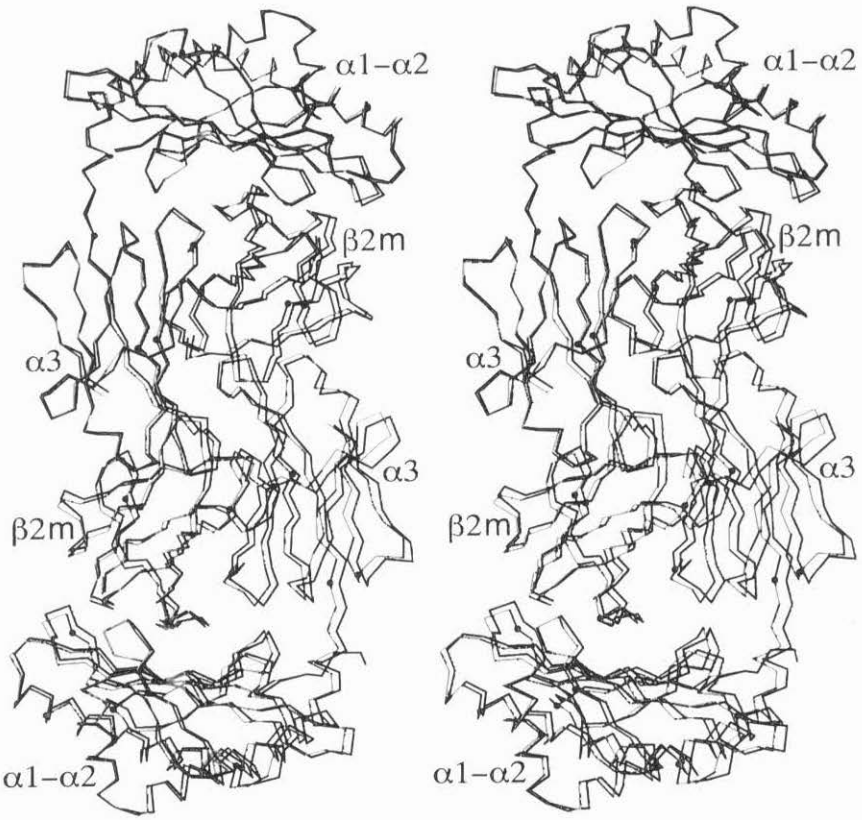

Figure 1: pH dependent domain movements in the FcRn dimer. Cα traces of the pH 6.5 (black) and pH 8 (grey) FcRn dimer superimposed to optimize the alignment of the α1α2 platform of the top FcRn molecule show small domain movements. Every twentieth Cα position for the pH 8 structure is represented as a black sphere.

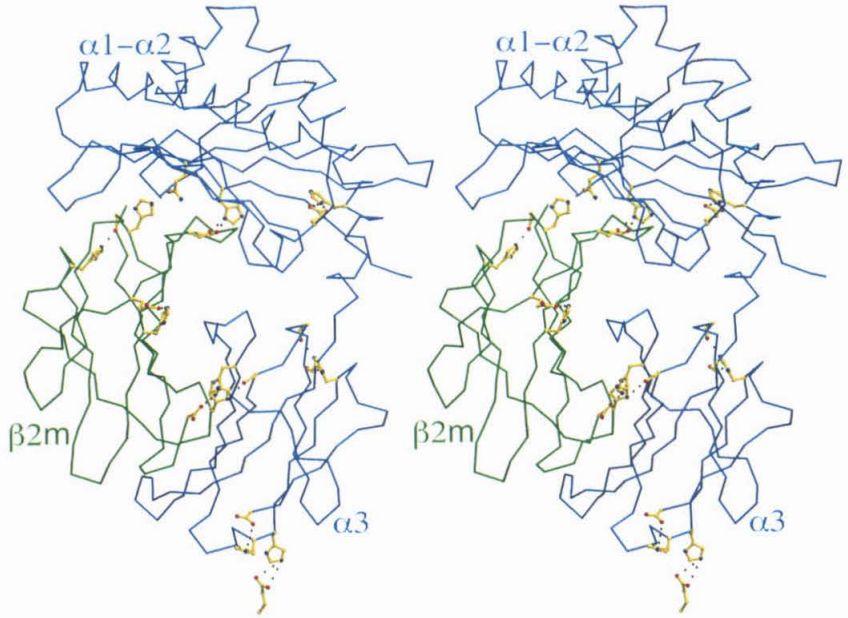

Figure 2: Histidine mediated stabilization of FcRn. FcRn is stabilized in part by a network of pH sensitive electrostatic interactions (see text for details), many of which occur between the FcRn heavy chain (blue) and light chain (green). All ten histidine residues and their electrostatic bonding partners are shown. The isolated glutamate at the bottom of the figure is Glu-89 from the dimer related FcRn.

Figure 3: Mechanism for pH dependent IgG binding. a) Schematic representation of the association (pH 6; left) and dissociation (pH 7.5; right) of the high affinity FcRn/Fc complex. At pH 6.0 to 6.5, positively charged histidines on Fc (top) interact favorably with negatively charged residues on FcRn (bottom). High affinity binding is additionally facilitated by stabilization of the FcRn dimer through the interaction between positively charged histidines on the FcRn heavy chain with a negatively charged residue on the dimer related ß2m subunit. At pH 7.5 and above, the histidines are neutral, destabilizing the FcRn dimer and allowing dissociation of the Fc/FcRn complex. b) Stereo figure of the IgG binding surface on FcRn. Negatively charged regions are red and positively charged regions are blue. Three anionic binding pockets for the protonated Fc histidines (A, B, and C) are lined by amino acids that are required for IgG binding (see text for details). c) The pH 6.5 interaction of His-250 and His-251 with the dimer-related ß2m Glu-89 shown with electron density from a 2Fo-Fc SigmaA weighted electron density map contoured at 1.5σ. d) The comparable interaction at pH 8 with His-250 adopting an alternate conformation.

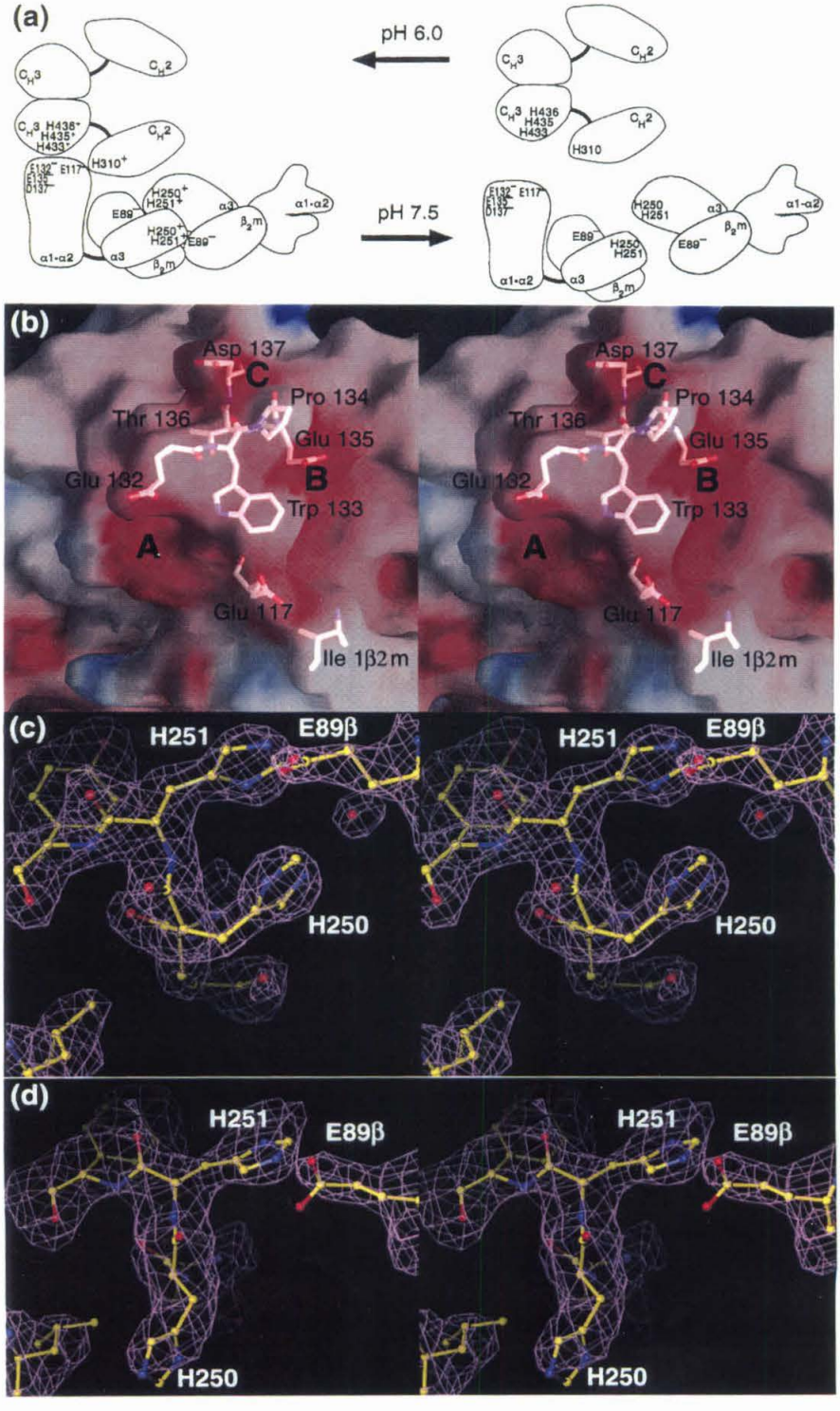
(a)
pH 6.0
pH 7.5
(b)
Asp 137
Pro 134
Thr 136
Glu 135
Glu 132
Trp 133
Glu 117
Ile 1β2m
(c)
H251
E89β
H250
(d)
H251
E89β
H250

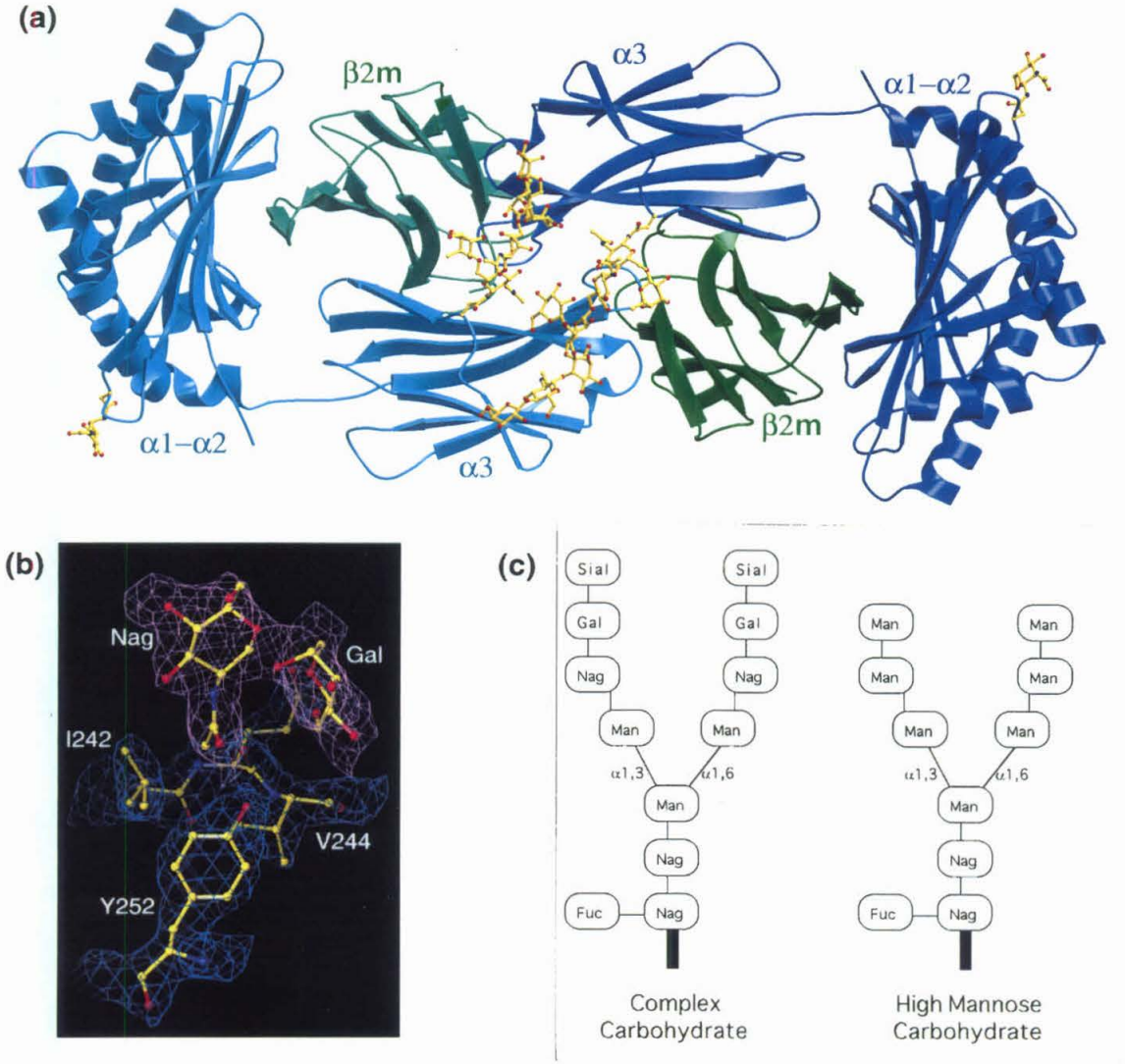

Figure 4: Ordered carbohydrate at the dimer interface. a) Ribbon diagram of the FcRn dimer including the ordered carbohydrate. At the center of the figure, ordered glycoside covalently attached to one monomer interacts extensively with the dimer related molecule. b) Two sugar residues (Nag and Gal of the complex carbohydrate antenna) are shown binding to a hydrophobic patch on the dimer related FcRn at pH 6.5. The electron density for a 2Fo-Fc SigmaA weighted map is contoured at 1σ for the carbohydrate (pink) and at 1.5σ for the protein (blue). There is clear electron density for the N-acetyl group on the Nag that interacts with Ile-242, Val-244, and Tyr-252. c) Schematic structures of typical complex and high mannose carbohydrates.

Neuron, Vol. 16, 261–273, February, 1996, Copyright ©1996 by Cell Press

The (Greek) Key to Structures of Neural Adhesion Molecules

Review

Daniel E. Vaughn* and Pamela J. Bjorkman*†
*Division of Biology
†Howard Hughes Medical Institute
California Institute of Technology
Pasadena, California 91125

Cells need to adhere specifically to cellular and extracellular components of their environment to carry out diverse physiological functions. Examples of such functions within the nervous system include neurite extension, synapse formation, and the myelination of axons. The ability to recognize multiple environmental cues and to undergo specific adhesion is critical to each of these complex cellular functions. Recognition and adhesion are mediated by cell adhesion molecules (CAMs), which bind to macromolecules expressed on neighboring cells or in the extracellular matrix (ECM).

A detailed understanding of how CAMs mediate cellular adhesion will ultimately require site-directed mutagenesis to identify critical amino acids involved in specific recognition, quantitative functional assays to evaluate binding interactions, and high resolution three-dimensional structures to provide a context for the interpretation of these data. Three-dimensional structures of macromolecules are obtained by protein crystallographic or multidimensional nuclear magnetic resonance (NMR) techniques. In the case of adhesion molecules, structural biologists have adopted a "divide and conquer" approach in which structures of stable protein fragments are determined. These structures, which are the focus of this review, illustrate the basic architecture of several CAM building block domains and, in some cases, provide information about inter- and intramolecular interactions. There are several reasons why it is difficult, if not impossible, to determine the three-dimensional structure of an entire CAM. First, no one has succeeded in growing crystals of a protein with characteristics of a typical CAM (a large extracellular region connected to a cytoplasmic domain by a single membrane-spanning region). For this reason, crystallographers generally concentrate on the soluble extracellular portions of CAMs. However, the extracellular portions of most neural CAMs contain multiple copies of one or more domain motifs organized into long flexible structures that are too large to tackle using current NMR technology (Wagner et al., 1992) and generally do not produce well-ordered crystals (Kwong et al., 1990). These constraints combine to preclude structure determinations of the entire extracellular regions of larger CAMs.

Here we review the structures of the CAM domains relevant to cell adhesion events in the nervous system, focusing on the three motifs for which three-dimensional structures are available: immunoglobulin (Ig) superfamily domains, fibronectin type III (Fn-III) domains, and the domains found in cadherins. In the nervous system, members of the Ig superfamily mediate calcium-independent homophilic and heterophilic binding. Their extracellular regions include one or more domains with sequence similarity to antibodies (Williams and Barclay, 1988; Yoshihara et al., 1991). Many neural CAM Ig superfamily members include Fn-III domains arranged in tandem with Ig-like domains (Figure 1). Three-dimensional structures are available for domains of several classes of Ig-like domains and for Fn-III domains; thus, one can mentally (or using computer graphics; e.g., see Figure 4) piece together the likely structures of the extracellular regions of many neural CAMs. Cadherins are also important neural CAMs, forming homophilic adhesion interfaces in the presence of calcium (Geiger and Ayalon, 1992). Two recent structures of cadherin domains provide a clue about how the adhesive interface is formed.

The classification of Ig-like domains has evolved since the first description of the Ig superfamily (Williams and Barclay, 1988) because of many recent structure determinations. Studies by Chothia and colleagues (e.g., Harpaz and Chothia, 1994) suggest that some of the original classifications of Ig superfamily domains need to be reconsidered. We review this work briefly and present a structure-based sequence alignment of Ig superfamily domains (Figure 2; Tables 1 and 2) to allow the reader to classify Ig-like domains correctly. Alignments based on structurally equivalent residues often differ from those generated using sequence information alone, especially when the sequences share a low percent identity, as is the case for alignments of Ig-like domains. Thus, when analyzing a sequence for the design and interpretation of mutagenesis experiments, one should use a structure-based sequence alignment such as that provided in this review. Consultation of this sort of alignment is also the most accurate method for identifying conserved sequences in a family of related proteins. Molecular biologists often use such information in the design of primers for polymerase chain reaction-based experiments to probe for new members of a family.

In this review, we also present the tertiary structures of Ig superfamily, Fn-III, and cadherin building blocks. These structures share a common β-sheet folding topology called a "Greek key." We introduce this protein fold using topology diagrams of representative members of each domain family (Figure 3). Topology diagrams are representations of protein structures commonly used for illustrating the connectivity between individual secondary structural elements (i.e., β strands and α helices). Figure 3 is designed to allow the reader to compare the variations in β-strand topology that result in different structures for the various members of each family. In addition, conserved features of each domain type are indicated on the topology diagram, allowing the reader to correlate the location of particular residues in the sequences of related domains with their likely positions in three-dimensional structures. The topology diagram for each type of domain can be compared to the schematic ribbon diagram directly below it. Ribbon diagrams are constructed by fitting a smoothed curve through the position of a single atom representing each residue, and stylistic features (such as depicting β strands as arrows and helices as spirals) aid the viewer in interpreting the structure. Figures 1 and 3 thus depict the structures of CAMs with increasing levels of complexity and realism:

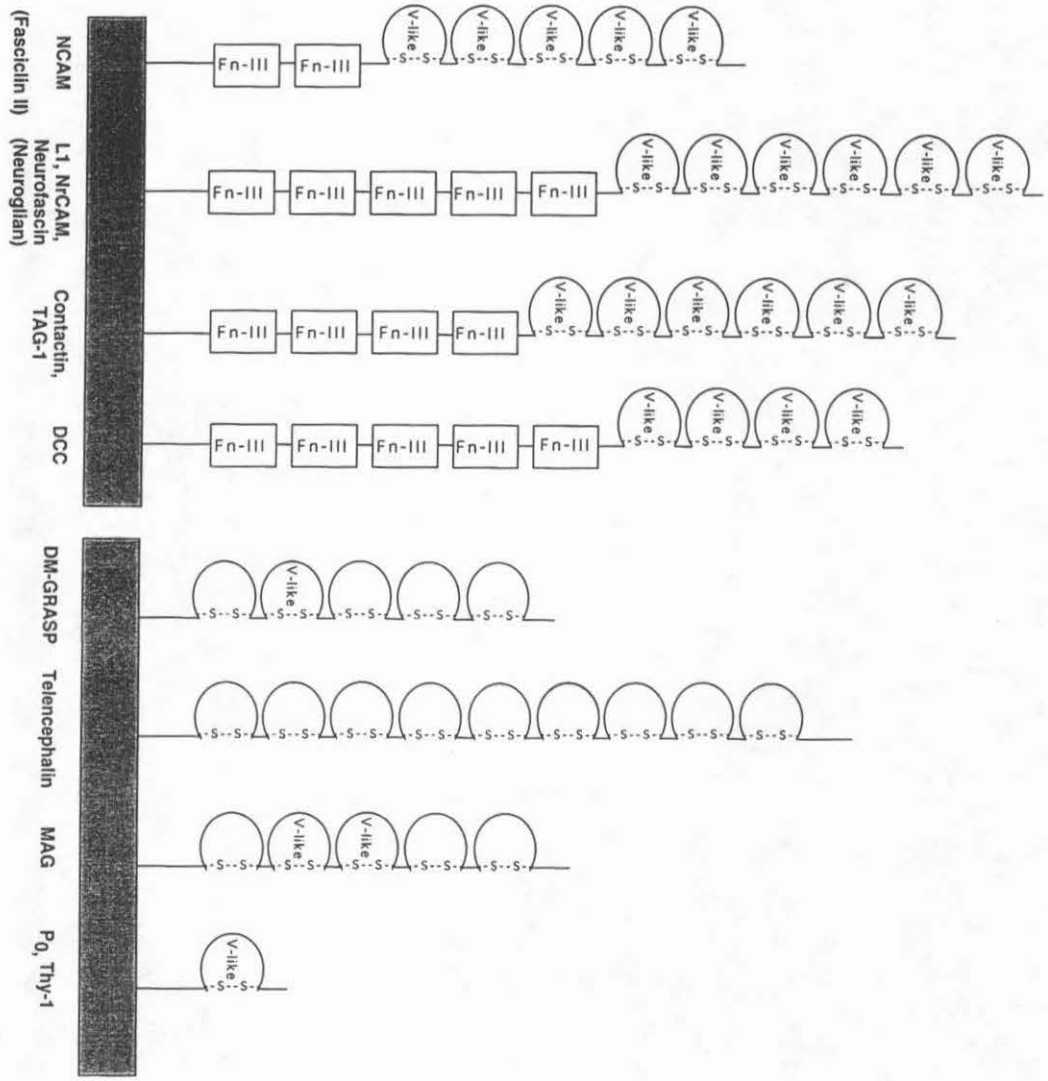

ɟure 1. Domain Organization of Neural Ig Superfamily CAMs

·like and Fn-III domains are indicated for the extracellular regions of vertebrate CAMs; structural homologs in insects are listed in parentheses. e domains are classified based upon a comparison of their sequences to the structure-based sequence alignments in Figure 2. No ıssification is listed for those domains that do not show a clear agreement to one of the consensus sequences.

at is, many of the domains that are commonly schema- ed as ovals, rectangles, or loops (e.g., Figure 1) have own three-dimensional structures.

Structures of individual domains, however, do not re- al how domains are arranged within the whole mole- le. Because of the necessity of the divide and conquer proach, we know less about this aspect of CAM struc- ·e. Figure 4 summarizes the available structural infor- ıtion about the relevant interactions of tandem do- ıins within a CAM. In the case of most neural CAMs, we understand even less about intermolecular recognition, since the ligands for many neural adhesion molecules are unknown and there is little available information about particular residues involved in homotypic and heterotypic adhesion. Thus, the interpretation of many of the structural studies related to neural adhesion molecules awaits the gathering of additional data on their functional interactions. However, clues from some of the individual structures provide hints about the likely nature of a few of these interactions. We describe these

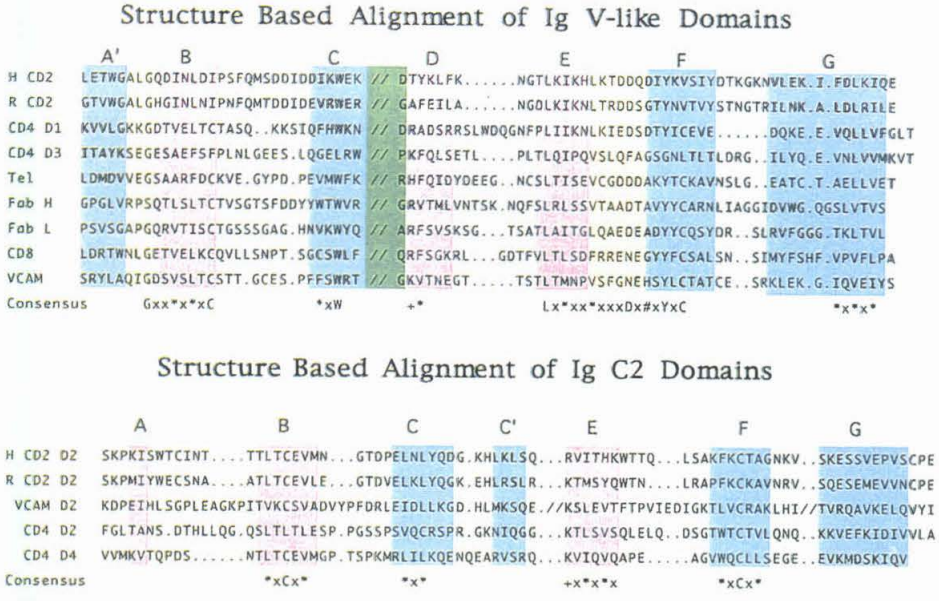

Figure 2. Structure-Based Sequence Alignments

Structural alignment of residues is based upon the pairwise superposition of V-like and C2 domains (Tables 1 and 2). Gaps in one sequence compared with the others are indicated by dots. β strands are colored red (ABE-containing sheet) or blue (GFC-containing sheet). Structurally conserved loops characteristic of V-like domains (connecting strands A' to B and E to F) are colored yellow. Sequences between strands C and D are not listed in the Ig-like domain sequences (indicated by double slashes and colored green) because the high degree of variability between structures makes alignment impossible. Consensus primary sequence patterns are identified at the bottom of the sequences: an asterisk indicates a hydrophobic amino acid; a plus sign represents a basic amino acid; a number sign indicates a glycine, alanine, or aspartate; and an "x" indicates any amino acid.

structures to give the neurobiologist a glimpse of what will eventually become a structural framework for understanding the molecular basis of neural adhesion.

The Greek Key Folding Topology

β-pleated sheets are a common structural element in globular proteins. Within a sheet, β strands adopt an almost fully extended conformation, aligned so that hydrogen bonds form between main chain atoms of residues within adjacent strands. When β strands are arranged in an antiparallel fashion, as is the case for the neural CAM building blocks reviewed here, the result is usually two β sheets that are packed against each other. Side chains from both sheets contribute to a hydrophobic core at the interface between the sheets, and because every second residue of a β strand points to the same side of the sheet, hydrophobic residues tend to occur at every second position in the primary sequences of β strands arranged in a two-sheet structure (Figures 2 and 3).

A common folding topology for domains containing one or two antiparallel β sheets is called a Greek key because of the similarity in the connectivity of the β strands to a repeating unit of an ornamental pattern

Table 1. Superposition of Ig V-like Domains

	VCAM D1	CD4 D1	CD4 D3	CD8	Telokin	V_H	V_L
CD2 D1	1.5 (65)	1.6 (75)	2.0 (75)	1.3 (64)	1.5 (62)	1.3 (67)	1.3 (67)
VCAM D1		1.2 (64)	1.7 (67)	1.6 (63)	1.6 (75)	1.8 (71)	1.5 (76)
CD4 D1			1.4 (68)	1.5 (74)	1.5 (76)	1.4 (78)	1.5 (78)
CD4 D3				1.5 (54)	1.2 (66)	1.9 (73)	1.6 (63)
CD8					1.6 (71)	1.3 (93)	1.3 (83)
Telokin						1.4 (70)	1.6 (83)
V^H							1.3 (83)

The rms deviations (Å) for different pairwise superpositions of carbon-α atoms of Ig V-like domains are listed. For each combination, the number of carbon-α atoms used in the calculation of the rms deviation is listed in parentheses. Regions containing five or more adjacent carbon-α atoms that superimposed within 3.8 Å were used to generate the rms deviations listed. V_H and V_L domain coordinates were obtained from the protein database file 7fab.

Table 2. Superposition of Ig C2 Domains

	VCAM D2	CD4 D2	CD4 D4
CD2 D2	1.3 (59)	1.6 (54)	1.6 (56)
VCAM D2		1.9 (48)	1.6 (61)
CD4 D2			1.8 (41)

The rms deviations (Å) for different pairwise superpositions of carbon-α atoms of Ig C2 domains are listed. For each combination, the number of carbon-α atoms used in the calculation of the rms deviation is listed in parentheses. Regions containing five or more adjacent carbon-α atoms that superimposed within 3.8 Å were used to generate the rms deviations listed. V_H and V_L domain coordinates were obtained from the protein database file 7fab.

used in ancient Greece (Richardson, 1977; middle of Figure 3). The presence of a Greek key fold in a protein does not imply a common evolutionary origin or function with another Greek key protein. For example, Ig variable domains and the enzyme superoxide dismutase have the same folding topology, but no sequence or functional similarity (Richardson et al., 1976).

We use the Ig constant domain depicted in Figure 3 as the archetypal Greek key fold. β strands are labeled with consecutive letters starting with the N-terminal strand. For other domains, extra strands are labeled with primes (e.g., C′ and C″ of Ig variable domains) to preserve the nomenclature for analogous β strands. Throughout all figures, the β sheet including strands A, B, and E is red, and the sheet containing strands G, F, and C is blue. Throughout the review, we refer to the different sheets by the letters of the strands they contain; for example, an Ig C1 domain contains an ABDE sheet (or ABDE face) and a GFC sheet.

The Ig Superfamily

Many cell–cell interactions in the nervous system are mediated by Ig superfamily members, which are defined as molecules that contain domains with sequence similarity to the variable or constant domains of antibodies (Williams and Barclay, 1988; Yoshihara et al., 1991). Many Ig superfamily molecules consist of tandem Ig-like domains connected in series with multiple copies of a second building block domain called an Fn-III repeat (shown schematically in Figure 1). Current structural information about domains in Ig superfamily members comes mainly from structures of molecules that function in the immune system. However, to date, any two molecules that share detectable sequence similarity have been found to adopt the same folding topology. Thus, one can use the structures of the immunologically relevant molecules as first order models for the structures of Ig superfamily domains in neural CAMs. In this section, we describe the three-dimensional structures of some of the CAM domains depicted schematically in Figure 1.

Structures of Ig Superfamily Domains

Ig-like domains have traditionally been identified at the primary sequence level by the presence of two cysteine residues separated by 55 to 75 amino acids (which form a disulfide bond in the folded structures), and a so-called "invariant" tryptophan residue located 10–15 residues C-terminal to the first conserved cysteine (Davies and Metzger, 1983; Williams and Barclay, 1988; Kabat et al., 1991). However, some Ig superfamily domains lack these features but still adopt an Ig-like fold (e.g., CD4 domain 3; Brady et al., 1993).

On the basis of sequence and structural similarities, Ig superfamily member domains were divided into three sets; C1, C2, and V-like (Williams and Barclay, 1988). The C1 set includes antibody-constant and topologically equivalent domains. The C2 set has a slightly different organization of β strands within the two sheets as compared with the C1 set. The V-like (variable-like) set includes Ig variable and structurally similar domains. Recently, Harpaz and Chothia defined another structural set called the "I" set (Harpaz and Chothia, 1994), which can be regarded as a shortened V-like domain (Wagner and Wyss, 1994). For the purposes of this review, we will group the I set of superfamily members together with other V-like domains. Because of the presence of Fn-III modules in a number of Ig superfamily neural adhesion molecules (Yoshihara et al., 1991), we include a discussion of Fn-III domain structure in this section although these domains are not part of the Ig superfamily.

Ig C1 Domains

C1 domains consist of seven β strands arranged into two antiparallel sheets: one consisting of strands A, B, D, and E (red in Figure 3), and the other consisting of strands G, F, and C (blue in Figure 3; Davies and Metzger, 1983). The two sheets are connected by a disulfide bond between strands B and F. In an antibody, constant domains are found in the F_c region and the C-terminal domains of the F_{ab}. Constant-like, or C1 set domains, are also found in the membrane proximal domains of major histocompatibility complex antigens and T cell receptors (Chothia et al., 1988; Bjorkman and Parham,

Figure 3. Structures of Building Block Domains

The border separating diagrams of antibody domains (top) and from neural CAM domains (bottom) shows a typical Greek key pattern as seen in vases and other early Greek art. Topology (above the fold name) and ribbon (below the fold name) diagrams are presented for each building block structure. The ABE-containing sheets are red and the GFC-containing sheets are blue. In the topology diagrams, strands are identified by letters. Amino acids that have equivalent positions in all structures of the domain type are indicated by a closed circle, by the one-letter code if the identity of the amino acid is conserved, by the symbol ϕ for hydrophobic residues, or by the symbol ψ for hydrophilic residues. β-sheet hydrogen bonding is indicated by dashed lines. Regions of irregular secondary structure are indicated by open rectangles. Yellow highlights the antigen binding loops in the Ig variable domain, the structurally conserved loops in the V-like domains (A′ to B and E to F loops), the integrin-binding RGD loop present in some Fn-III domains, and the A strand of N-cadherin domain 1 that mediates formation of the strand dimer. The part of the V-like domain that shows the most variability between structures (connection between strands C and D) is highlighted in green. Ribbon diagrams were prepared using Molscript (Kraulis, 1991) and rendered with Raster 3D (Merritt and Murphy, 1994) from coordinates available from the PHB (7fab for Ig constant and variable domains, 1ten for Fn-III) or provided by the authors (VCAM-1 coordinates from E. Y. Jones for V-like and C2 domains, and N-cadherin domain 1 coordinates from L. Shapiro for Cad).

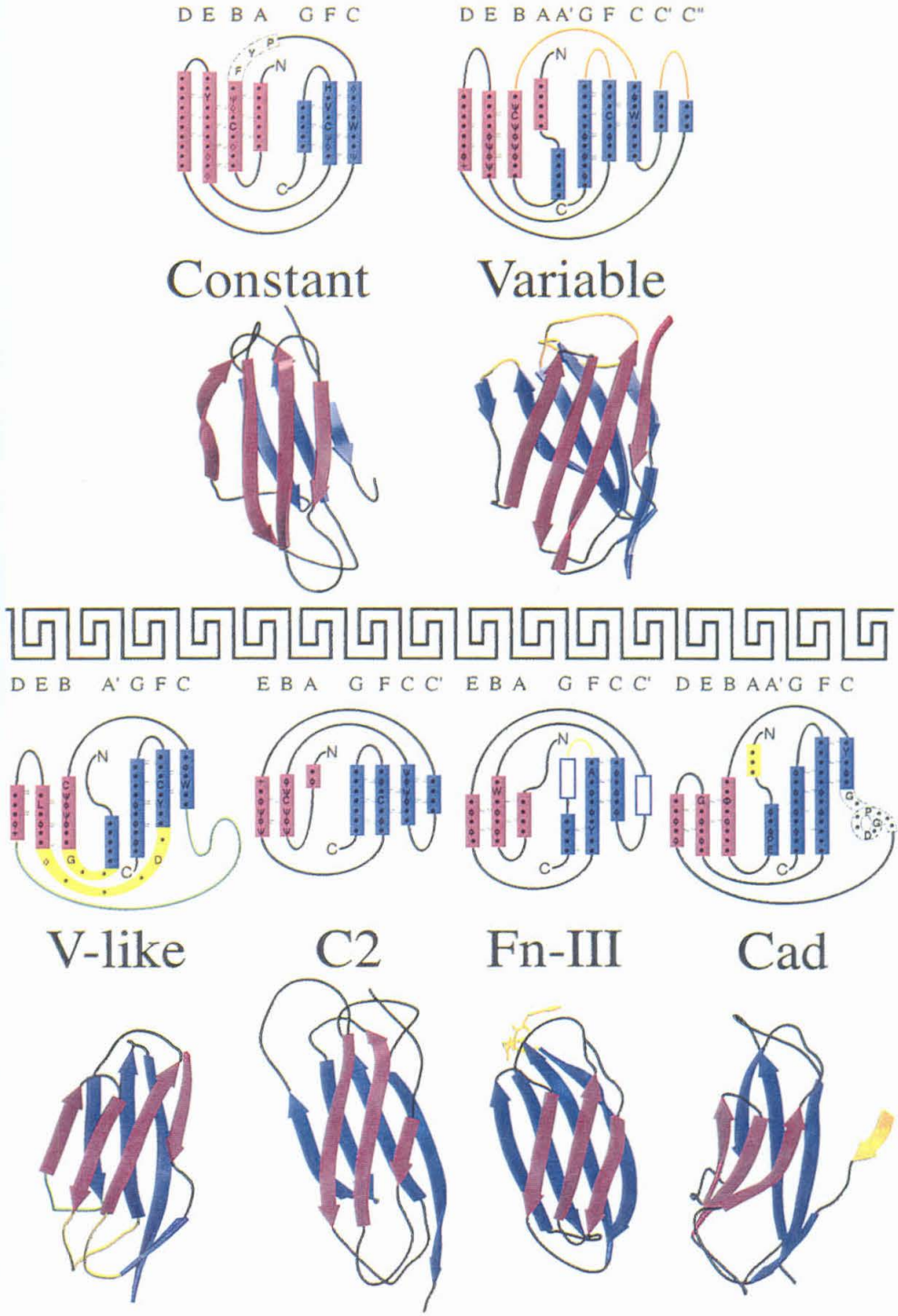
D E B A G F C
D E B A A' G F C C' C"
Constant
Variable
D E B A' G F C
E B A G F C C'
E B A G F C C'
D E B A A' G F C
V-like
C2
Fn-III
Cad

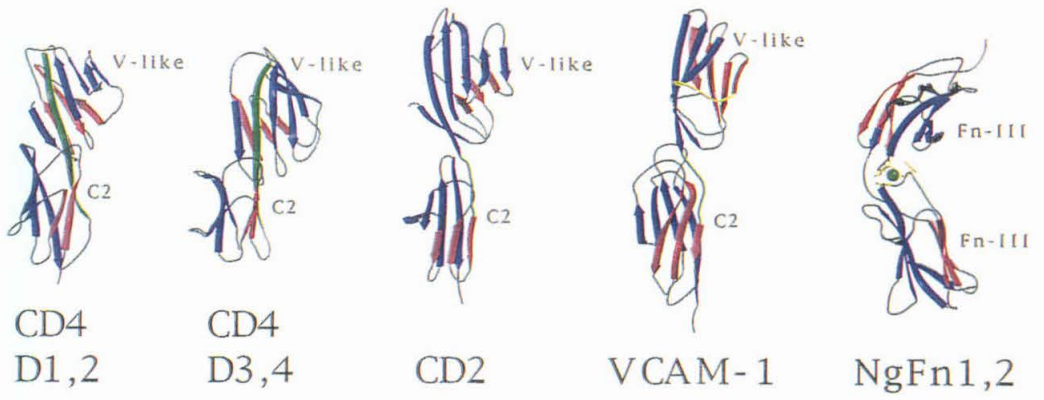

Figure 4. Tandem Domain Interfaces in CAMs

Ribbon diagrams are shown for tandem domain structures. The ABED sheet is red and the A'GFCC'C'' sheet is blue. In the two diagrams of CD4, the strand that continues from the first domain into the second domain is highlighted in green. For the CD2 and VCAM-1 diagrams, the short interdomain connecting sequence is highlighted in green. A metal ion between the neuroglian Fn-III domains (NgFn1,2) is shown in green. The integrin binding loop in VCAM-1 and residues within the metal binding site in NgFn1,2 are highlighted in yellow. These figures were prepared with Molscript (Kraulis, 1991) and rendered with Raster 3D (Merritt and Murphy, 1994) from coordinates obtained from the protein database (3cd4 for CD4 D1,2; 1cid for CD4 D3,4; 1hgf for CD2, and 1cfb for NgFn1,2) or provided by E. Y. Jones for VCAM-1.

1990; Bentley et al., 1995). To date, this fold has not been found as a component of a CAM (Wagner and Wyss, 1994).

Ig C2 Domains

The C2 and C1 folding topologies are similar, except for the "sheet switching" of one β strand (strand D of the ABED sheet [red] in a C1 domain becomes strand C′ in a C2 domain to form a GFCC′ sheet; blue). β strands in Ig C2 domains are somewhat shorter than in C1 domains (~6 compared with ~9 residues) and lack many of the conserved sequence patterns at the N-terminal end of the β barrel (see Figure 2). C2 domains have been seen in the structures of three Ig superfamily members (Table 2): the second domain of the immune system adhesion molecule CD2 (Jones et al., 1992; Bodian et al., 1994), the second domain of vascular cell adhesion molecule-1 (VCAM-1; Jones et al., 1995), and the second and fourth domains of the T cell coreceptor CD4 (Ryu et al., 1990; Wang et al., 1990; Brady et al., 1993).

Ig V-like Domains

Variable domains of immunoglobulins are the prototype for the V-like domains of adhesion molecules. This fold is found in the VH and VL domains of antibodies (Davies and Metzger, 1983) and the N-terminal domains of T cell receptor α and β chains (Chothia et al., 1988; Bentley et al., 1995). The folding topology is similar to the Ig constant fold or C1 set. However, two additional β strands (C′ and C′′) extend the GFC face (blue). For antibodies and T cell receptors, two variable domains pair to form an antigen binding site composed of residues within the loops connecting strands B and C, strands C′ and C′′, and strands F and G (yellow in Figure 3). Close examination of the hydrogen bonding patterns in Ig variable domains shows that the C-terminal portion of the A strand is hydrogen bonded to the GFC-containing sheet (blue). This portion of the strand is called A′ (Figure 3).

V-like domains in Ig superfamily members are folded similarly to Ig variable domains (Table 1). V-like domain structures do not always include the C′ and C′′ strands that distinguish Ig variable from Ig constant domains. Structures with V-like domains include the T cell coreceptors CD4 (first and third domains; Ryu et al., 1990; Wang et al., 1990; Brady et al., 1993) and CD8 (Leahy et al., 1992a), the N-terminal domains of two adhesion molecules (CD2 and VCAM-1; Jones et al., 1992; Bodian et al., 1994; Jones et al., 1995), and telokin, the C-terminal domain of the myosin light chain kinase (Holden et al., 1992).

Primary Sequence–Based Classification of Ig-like Domains in CAMs

One way to compare three-dimensional structures of proteins is to superimpose the coordinates of their carbon-α atoms. For proteins adopting the same fold, a structural core of residues can be identified as one whose carbon-α atoms superimpose upon their counterparts. The overall rms deviation among core residues of related proteins varies inversely with the percent sequence identity: i.e., core residues in proteins related by a high percent identity (≥60%) superimpose well (generally within 1 Å rms deviation), whereas core residues in more distantly related proteins (20%–30% sequence identity) superimpose with a larger average rms deviation (~2 Å; Chothia and Lesk, 1986). For pairwise superpositions of Ig V-like and Ig C2 domains, we present the number of core residues and their rms deviations in Tables 1 and 2. A large structural core of residues superimpose well within each subset of Ig-like domains, whereas a much smaller structural core is identified when Ig V-like domains are superimposed upon Ig C2 domains.

We generated structure-based sequence alignments for Ig V-like and Ig C2 domains by aligning residues within the appropriate structural cores (Figure 2). The alignments reveal a consensus of primary sequence features that can be used to predict if a protein will adopt

a C2 fold versus a V-like fold. Many neural CAM domains were initially classified as C2 primarily on the basis of the number of residues separating the cysteine residues (Yoshihara et al., 1991). However, an examination of the sequences in light of the consensus sequences of V-like and C2 domains indicates that many neural CAM domains are more likely to adopt a V-like fold (Harpaz and Chothia, 1994). For example, the sequences of all of the Ig-like domains of the NCAM, L1, and contactin/TAG-1 families match the V-like consensus sequence better than the C2 consensus sequence (Figure 1).

The differences between Ig V-like and C2 domains at the primary and tertiary structure levels can be summarized as follows: first, in V-like domains, the C-terminal portion of the A strand (A′) is part of the GFC face (blue) and connects to the B strand via a conserved type II β turn (yellow in Figure 3; Harpaz and Chothia, 1994). This turn is usually identifiable in the primary structure by a sequence motif that includes a glycine seven residues before the first of the characteristic cysteines (Figure 2). Another distinguishing sequence motif is found at the region connecting the E and F strands of V-like domains compared to C2 domains (yellow in Figures 2 and 3).

Fn-III Modules

Fn-III domains were originally identified as a repeating motif of ~90 amino acids in the ECM protein fibronectin (Hynes, 1990). This common structural motif has been estimated to occur in up to 2% of all animal proteins (Bork and Doolittle, 1992). Structures of single Fn-III modules from the ECM proteins tenascin (Leahy et al., 1992b) and fibronectin (Main et al., 1992), as well as a tandem pair of domains from the Drosophila neural CAM neuroglian (Huber et al., 1994) and domains 7–10 of fibronectin (Leahy et al., 1996) have been reported. The β-sheet domain topology of the Fn-III motif is identical to Ig C2 domains (Figure 3), although domains with these folds are not related by primary sequence. This topology is also shared by the bacterial chaperone PapD (Holmgren and Bränden, 1989) and the human growth hormone receptor (De Vos et al., 1992); thus, a number of proteins with diverse functions have converged upon this common fold.

Arrangements of Domains within a Molecule

Recognition of a ligand may not be confined to a single CAM domain; thus, multidomain structures are important for understanding ligand binding. The structures of tandem Ig-like domains from CD4, CD2, and VCAM-1 and a structure of tandem Fn-III repeats provide examples of how adjacent domains within a neural CAM can be arranged (Figure 4).

Crystals of the entire extracellular domain of CD4 diffract poorly (Kwong et al., 1990); thus, separate structures of domains 1 and 2 (D1D2; Ryu et al., 1990; Wang et al., 1990), then domains 3 and 4 (D3D4; Brady et al., 1993), were determined. In both the D1D2 and D3D4 structures, the G strand of the first domain continues to become the A strand of the second domain (G to A strand is green; Figure 4). The relative orientation of domains 1 and 2 in human CD4 is conserved in multiple crystal forms, suggesting there is little segmental flexibility between the first two domains (Ryu et al., 1994). The D3D4 interface is also likely to be rigid (Brady et al., 1993). Thus, the available structural data for CD4 suggests that segmental flexibility is mostly restricted to the junction between D2 and D3 (Kwong et al., 1990).

In the crystal structures of the two-domain extracellular regions of rat and human CD2, however, strand G from domain 1 does not continue directly into strand A of domain 2 (Jones et al., 1992; Bodian et al., 1994). Instead, the two domains are separated by a linker of six amino acids that adopts an extended conformation (green in Figure 4). There are significant differences in the relative domain orientations when the various structures of CD2 are compared, suggesting interdomain flexibility (Jones et al., 1992; Bodian et al., 1994). Similarly, an extended linker connects domains 1 and 2 of VCAM-1 (green in Figure 4), and the domain association is believed to be somewhat flexible (Jones et al., 1995).

The structure of a two-domain proteolytic fragment of neuroglian provides an example of the relative orientation of tandem Fn-III domains (Huber et al., 1994). The interface between the two Fn-III modules that were crystalized is believed to be rigid, consistent with the insensitivity of the two-domain fragment to proteolytic digestion. The hydrophobic interface includes a metal binding site, presumably involved in stabilizing the relative orientation between domains (Figure 4). Although metal binding may not be a universal feature at Fn-III domain interfaces (and was not seen in the recently determined crystal structure of domains 7–10 of fibronectin; Leahy et al., 1996), an interdomain metal site at the analogous position is predicted by sequence comparision to be present in the homologous vertebrate neural CAM L1 (Huber et al., 1994).

The two Fn-III domains in neuroglian are related by a near perfect twofold screw axis along the longest molecular dimension (~70 Å). Assuming this relative orientation is a general property of tandem Fn-III repeats, the tandem Fn-III domains in neuroglian and other neural CAMs can be modeled as a thin straight rod with two-domain zig-zag repeats (Huber et al., 1994). When combined with the dimensions of pairs of tandem Ig-like domains from CD4, CD2, and VCAM-1 (60–80 Å long, 20–30 Å wide), the model suggests that neuroglian is a long narrow molecule (20–30 Å in diameter) that could extend up to 400 Å from the cell surface if there were no significant bends between domains (Figure 5). However in photomicrographs, rotary-shadowed whole neuroglian (six Ig-like domains plus five Fn-III domains) appears to be a flexible rodlike molecule containing about four bends (Huber, 1994; H.P. Erickson, A.H. Huber, A.J. Bieber, and P.J.B., unpublished data). The mean total length is ~390 Å, consistent with a head-to-tail packing of the Ig-like domains and with the dimensions assumed for the neuroglian Ig-like and the Fn-III domains. The five-domain Fn-III portion of neuroglian is observed to bend in at least two positions. Analysis of the electron microscopy data supports a model in which the domain interface joining the first two Fn-III modules of neuroglian (the ones in the crystal structure) is rigid, but some of the other Fn-III interdomain interfaces are flexible and appear to exhibit considerable rotational freedom (Huber, 1994).

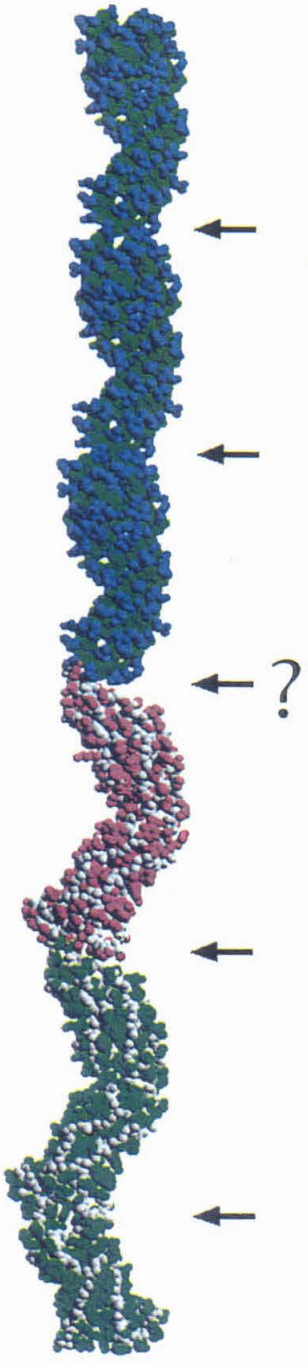

Figure 5. Hypothetical Model for the Alignment of Six Ig-like and Five Fn-III Domains in Series, as in Molecules of the L1 Family

Space-filling model in which atoms in Ig-like domains are blue (side-chain atoms) and green (main-chain atoms). Main-chain atoms in Fn-III domains are gray and side-chain atoms are pink (first two domains) or green (domains 3–5). Potential points of flexibility suggested by electron microscopic studies of neuroglian (see text) and by crystallographic and biochemical data on Ig superfamily molecules (e.g., Kwong et al., 1990) are noted by arrows. No structural information concerning the potential flexibility of the interface between Ig-like and Fn-III domains (indicated by a question mark) is available. This figure was generated using the program SETOR (Evans, 1993) and coordinates for CD4 D1D2 (3cd4) as a model for the six Ig-like domains and NgFn1,2 (1cfb) as a model for Fn-III repeats.

Thus, we have seen that the body of current structural knowledge is sufficient to piece together a general idea of the structures of neural CAMs in the Ig superfamily. The CD4, VCAM-1, and CD2 structures provide starting models for the structures of Ig-like domains in neural CAMs. The available structures of Fn-III modules provide the starting model for the remaining portion of neural CAMs that include these motifs. Both Ig-like and Fn-III modules in CAMs interact in a head-to-tail fashion, producing an extracellular region that is much longer than it is wide (e.g., Figure 5). Structural data on Ig-like as well as Fn-III repeats suggest that connections between domains can be rigid (as in the interface between the first two domains of CD4 or the first two Fn-III modules of neuroglian) or flexible (as in the first two domains of CD2). For each individual CAM, some interdomain connections are probably rigid while others are likely to allow adjacent domains to adopt multiple orientations with respect to each other. Presently, there is no way to predict which domain interfaces will be flexible or rigid based upon primary sequences alone, and even CAMs with related domain organization and sequences may show different points of flexibility. Although the functional significance of flexibility in neural CAM molecules is unknown, flexibility could allow molecules on different cells to adopt the specific conformations required for adhesive binding.

Ig Superfamily Adhesive Interactions

Neural CAMs of the Ig superfamily are involved in a variety of adhesive interactions, including homophilic binding, recognition of other Ig superfamily members, recognition by integrins, and binding to components of the ECM.

In homophilic adhesion, for example by NCAM or L1 family members, CAMs on one cell bind to partner molecules expressed on an adjacent cell (Rutishauser and Jessell, 1988). There are no structural data that directly address how this interaction occurs. However, packing in the crystals of rat and human CD2 provides a hint of what a homophilic interaction between V-like domains may resemble (Jones et al., 1992; Bodian et al., 1994). Although multiple crystal forms of rat and human CD2 show different crystal packing arrangements, a head-to-head interaction between the N-terminal V-like domains is conserved across space groups and species (Bodian et al., 1994). In this interaction, the A′GFCC′C″ faces (blue) from molecules packed head-to-head form a tightly packed interface (Figure 6). This interaction is consistent with molecules on different cells binding in an extended orientation, and could be a model for how homophilic adhesion is accomplished between V-like domains of Ig superfamily members.

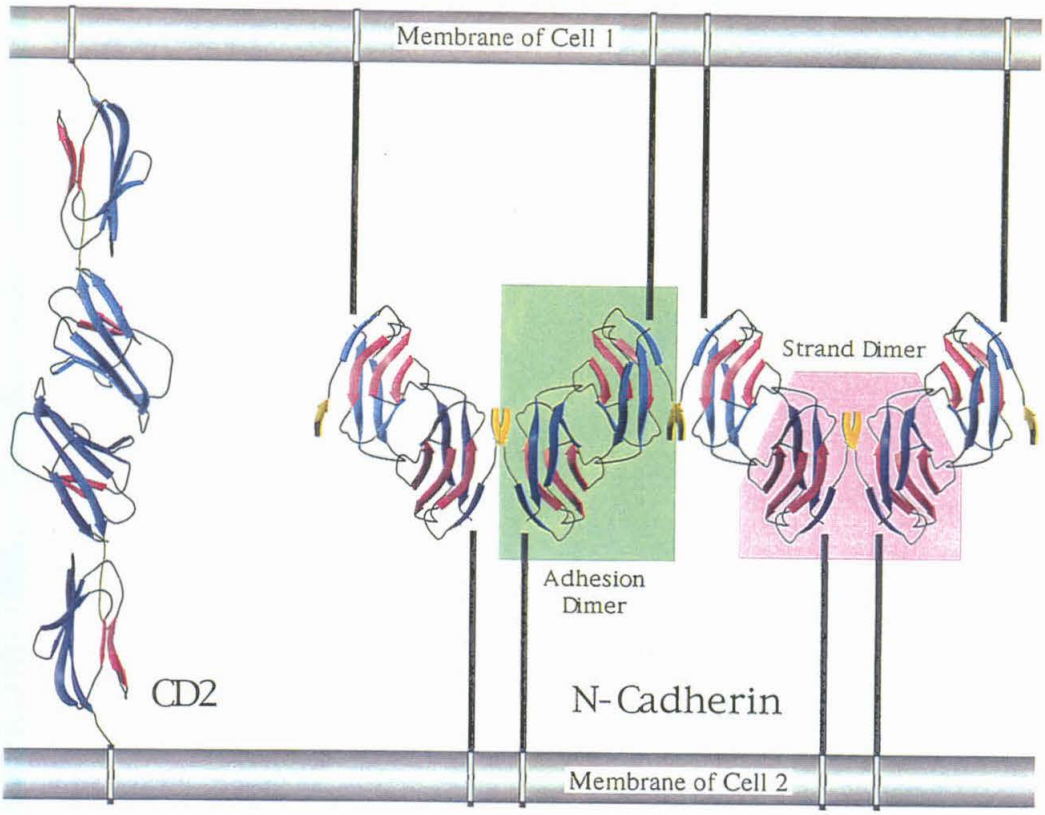

Figure 6. Models of Homophilic Adhesive Interactions for Ig V-like and Cadherin Domains

(Left) Ribbon diagram of the head-to-head interaction observed in crystals of CD2 domains 1 and 2 (Jones et al., 1992) serves as a model for homophilic and heterophilic interaction between Ig superfamily members.

(Right) The zipperlike structure observed in crystals of N-cadherin domain 1 (Shapiro et al., 1995a) as a model for cadherin-mediated cell–cell adhesion. Strand A, which interdigitates into the partner domain of the strand dimer, is highlighted in yellow.

Many Ig superfamily CAMs bind heterophilically to other superfamily members. In fact, CD2 itself binds to CD58, another Ig superfamily member. Site-directed mutagenesis studies (Withka et al., 1993) have mapped the CD58 binding site on CD2 to the same face observed in the crystallographic interaction between opposing CD2 molecules (the A'GFCC'C'' face; blue). Thus, the packing in the CD2 crystals may also be illustrative of heterophilic interactions between Ig superfamily members.

Structural information about the interaction of Ig superfamily domains with integrins comes from the VCAM-1 crystal structure (Jones et al., 1995). Mutagenesis studies implicate six residues of VCAM-1 domain 1 as critical for binding to the VLA-4 integrin (Osborn et al., 1994). Other leukocyte Ig superfamily integrin-binding molecules have been shown to bind to integrins via a similar sequence motif (hydrophobic, followed by a negative charge). The critical residues for VLA-4 binding are part of the GFC face (blue; Figures 3 and 4) and occur at the N-terminal portion of the loop connecting strands C and D (yellow; Figure 4). The GFC face of VCAM-1 is comparable to the GFCC'C'' face of CD2, which is implicated in heterophilic interactions (Jones et al., 1992; Bodian et al., 1994). It has therefore been suggested that the face containing β strands C, F, and G of the first domain of Ig superfamily members may be a site of intercellular adhesive interactions, regardless of the nature of the ligand (Jones et al., 1995). This detailed structural analysis of the VCAM-1/integrin interaction is relevant to nervous system molecules such as telencephalin, a VCAM-1 homolog expressed on a restricted set of dendrites that is predicted to bind integrins (Yoshihara and Mori, 1994).

In addition to Ig superfamily domains, integrins are also recognized by some Fn-III repeats in ECM proteins. This interaction is mediated by an Arg-Gly-Asp (RGD) sequence motif (Hynes, 1990). The RGD sequences of the Fn-III modules from the ECM proteins tenascin and fibronectin are located in a β hairpin loop between strands F and G (Leahy et al., 1992b, 1996; Main et al., 1992; yellow in Figure 3). Other than the common feature

of a negatively charged residue in the midst of a flexible loop, the conformation of the RGD loops in these ECM proteins does not resemble the conformation of the CD loop in the first domain of VCAM-1, which is critical for the interactions of V-like domains with integrins. However, both types of loops contain a negative charge, which could facilitate adhesion by completing a divalent cation-binding site on the integrin (Jones et al., 1995). Significant progress has been made in the field of integrin structure with the solution of the structure of the A domain of the α subunit of an integrin (Lee et al., 1995). However, further information about interactions between integrins and Ig superfamily or Fn-III domains awaits the solution of the structure of a heterodimeric integrin and/or a complex between an integrin and its ligand.

The Fn-III modules of most neural CAMs do not contain RGD sequences (Bork and Doolittle, 1992), and the function, if any, of the comparable loop in the Fn-III modules of CAMs is unknown. However, RGD sequences are found in what appears to be the F-to-G loop of a few neural CAMs such as TAG-1 (Furley et al., 1990), Ng-CAM (Brugoon et al., 1991), and neurofascin (Volkmer et al., 1992). In the case of neuroglian, the only neural CAM for which structural information is available, the Fn-III domains do not contain RGD sequences (Bieber et al., 1989). However, both FG loops are solvent-accessible β hairpin turns and are therefore available for intermolecular recognition (Huber et al., 1994).

Cadherins

Cadherins are single-pass transmembrane proteins that include an extracellular region formed by five repeats of 100 amino acids and a conserved cytoplasmic domain. The extracellular region functions in calcium-dependent homophilic cell adhesion, with the adhesive specificity residing primarily within the first repeat. The cytoplasmic domain meditates connections with actin filaments via catenin proteins. The combination of cadherin-mediated homophilic recognition and catenin-mediated cytoskeletal anchoring has been implicated in cell sorting and cell condensation events during morphogenesis. Different cadherins, such as P-, N-, R-, T-, and E-cadherin, are expressed in a wide variety of cell types. Since each member binds homophilically to the identical type, cells preferentially adhere to other cells bearing the same cadherin member (Takeichi et al., 1990; Geiger and Ayalon, 1992). In addition to the "classic" cadherins found in the zonula adherens cell–cell junctions of vertebrates, a protocadherin family with developmentally regulated expression is found in the brain (Sano et al., 1993), and proteins with tandem cadherin-like repeats are found in Drosophila (Mahoney et al., 1991) and in vertebrate desmosome junctions (Wheeler et al., 1991). Other proteins, such as the proto-oncogene c-ret (which functions in differentiation and/or proliferation in peripheral nerve cells and hematopoietic cells), consist of a cadherin-like extracellular region and an intracellular tyrosine kinase domain (Iwamoto et al., 1993).

The Cadherin Fold

The NMR structure of the first domain of E-cadherin and the crystal structure of the comparable N-cadherin domain were recently reported (Overduin et al., 1995; Shapiro et al., 1995a). Although there is no significant sequence similarity between cadherins and members of the Ig superfamily, the cadherin domain adopts a Greek key fold with ABED (red) and A′GFC (blue) β sheets, a topology similar to that of Ig V-like domains (Figure 3). However, unlike Ig V-like domains, the BC and CD loops include helical regions, and the AB and EF connections differ from their V-like counterparts. The cadherin domain is topologically similar to Ig V-like domains without showing the primary sequence characteristics that would make cadherins members of the Ig superfamily, much as Fn-III domains are topologically similar, yet not related by sequence, to Ig superfamily C2 domains. An analysis of Ig superfamily and cadherin sequences and intron patterns suggests the two types of structures converged upon a similar stable folding topology, rather than diverged from a common ancestor (Shapiro et al., 1995b).

The first domain of N-cadherin dimerizes in solution and in the crystal structure (Shapiro et al., 1995a). The dimer-related domains are oriented parallel to each other; thus, the same dimer could be formed on a cell surface. This dimer is called the "strand dimer" because the first four residues of each domain (A strands; yellow in Figures 3 and 6) interdigitate into the partner domain, forming hydrogen bonds with strand B. In particular, the tryptophan side chain at residue 2 is inserted into the hydrophobic core of the dimer-related molecule. An analysis of cadherin domain 1 sequences shows a notable conservation of residues at the strand dimer interface, and it therefore seems likely that all cadherin extracellular regions function as dimers (Shapiro et al., 1995a, 1995b). Domain 1 of E-cadherin, however, is reported to be monomeric (Overduin et al., 1995), a surprising result given the conservation of residues, including Trp 2, within the A and A′ strands of the two structures. Further studies will be required to assess the generalizability of the cadherin strand dimer as the functional unit for formation of adhesive interfaces.

Arrangements of Cadherin Domains within a Molecule

In addition to requiring calcium for adhesive interactions, cadherins show a calcium-dependent resistance to proteolytic degradation. A single amino acid change is sufficient to abolish calcium-mediated adhesion and protection from proteolysis, implying that calcium acts indirectly to regulate homophilic adhesion by modulating the protein structure (Ozawa et al., 1990). In both the NMR and X-ray cadherin structures (Overduin et al., 1995; Shapiro et al., 1995a), a calcium binding site is identified near the carboxyl terminus of the domain. The metal ions are incompletely coordinated in the single domain structures; thus, it is speculated that residues within the second domain complete the coordination. This hypothesis is supported by results of NMR and site-directed mutagenesis studies (Ozawa et al., 1990; Overduin et al., 1995). Homologous calcium binding sites are predicted at the interfaces between each tandem pair of cadherin domains (Overduin et al., 1995; Shapiro et al., 1995a), which could stabilize the interdomain junctions and thereby account for the observation of calcium-dependent resistance to proteolysis (Ozawa

et al., 1990). A model for the five-domain extracellular region of cadherins was constructed based upon the structure of the domain 1 strand dimer, with the relative positioning of successive domains dictated by the calcium ion coordination (Overduin et al., 1995; Shapiro et al., 1995a).

Homophilic Adhesion by Cadherins

Three different crystal forms of N-cadherin contain a linear zipper of cadherin dimers thought to reflect adhesive interactions between two cadherin-expressing cells (Figure 6) (Shapiro et al., 1995a). The zipper is formed by the combination of the strand dimer twofold symmetry axis with another twofold axis orthogonal to the first. The result is a continuous ribbon of cadherin protomers, in which the C-termini of successive dimers project in opposite directions, as if the dimers were emanating from two interacting cells. Thus, the packing in these crystals may be providing us with the first atomic resolution view of cell–cell adhesion. It is therefore instructive to examine the features of the interaction interface between cadherin protomers related by the antiparallel twofold symmetric interaction (termed the "adhesion dimer").

The main contact areas within the adhesion dimer interface include an interaction between the related C strands, the related CD loops, and the DE loop of one protomer with the FG loop of the partner. The interaction interface includes residues within strand F that had been implicated in cadherin subtype recognition. In general, the regions involved in adhesive contacts are distant from the Ca^{2+} binding site, another indication that the calcium dependence of cadherin adhesion arises from its stabilizing influence, rather than through a direct effect on the adhesive interface.

The adhesive interface is assumed to be relatively weak, since domain 1 of N-cadherin forms only dimers in solution, rather than higher order oligomers (Shapiro et al., 1995a). (The dimers formed in solution are assumed to correspond to the strand dimer rather than the adhesion dimer.) Indeed, a portion of the adhesion dimer interface is mediated by water molecules, as compared with the strand dimer interface, in which a strand from one domain interdigitates into the hydrophobic core of the partner. The adhesion zipper observed in the cadherin crystals illustrates a mechanism to overcome weak individual adhesive interactions through the cooperative binding of rows of molecules on each cell.

Conclusions

The Greek key β sandwich structure is a common motif in cell surface proteins involved in adhesive interactions. This folding topology serves as the building block for domains in neural CAMs, such as cadherin domains and the Ig-like and Fn-III domains of Ig superfamily members. Structure-based sequence alignments for domains from these proteins (Figure 2) (Leahy et al., 1992b; Huber et al., 1994) provide an important tool for relating primary sequences to three-dimensional structures.

The Greek key structural motif is usually found as an array of tandem repeats, arranged in a head-to-tail fashion to create a long rodlike structure in which some domain interfaces allow rotational freedom, while others are relatively rigid. The available structures of tandem repeats have demonstrated ways that serially arranged Ig-like domains can form rigid (e.g., CD4) or relatively rigid (e.g., CD2) interfaces. However, because only fairly inflexible interactions are amenable to structure determination, we have yet to visualize the domain interactions that provide CAMs with their greatest flexibility. To date, this inherent flexibility has hindered crystallization of entire multidomain extracellular regions. Similarly, intact antibodies resisted formation of well-ordered crystals for many years, and the "divide and conquer" approach was used to elucidate the mechanism of antibody function (Davies and Metzger, 1983). However, with the improvement of crystallization techniques, even a highly flexible intact antibody has been crystallized and used for an atomic resolution structure determination (Harris et al., 1992); thus providing hope that similar advances will allow crystallization of whole extracellular regions of large neural CAMs.

By combining the results of site-directed mutagenesis and structural studies, the molecular mechanism by which CAMs achieve homophilic and heterophilic adhesion is beginning to be elucidated. The face of V-like domains that includes strands G, F, and C has been implicated in two different adhesive interactions (Jones et al., 1992, 1995; Bodian et al., 1994), and this face was suggested to be the site of intercellular adhesive interactions, irrespective of the ligand that binds (Jones et al., 1995). In this regard, it is interesting that the location of the cadherin adhesion interface involves residues from the G, F, C, and D strands. However, adhesion by N-cadherin domain 1 is more of an edge-to-edge interaction than the face-to-face interaction observed in crystals of CD2 (Figure 6) (Jones et al., 1992; Shapiro et al., 1995a). The adhesive interface observed in the cadherin crystals illustrates one way in which cell adhesion is accomplished even with a very weak affinity adhesive interaction (i.e., mM or weaker). This example also suggests that weak adhesive interactions will be difficult to study biochemically, because they are stable only under conditions of high valency. However, in some cases, crystallization can overcome this difficulty, so that the weak adhesive interactions that normally occur only on the cell surface can exist within the crystal, owing to the high protein concentrations required for crystallization.

Many questions remain to be answered. At present, very little is known about the strength of different homophilic and heterophilic interactions. As more neural CAMs are available in purified forms, the affinities of specific homophilic and heterophilic interactions can be measured and the effects of introduced mutations can be quantitated. Complexes between partner molecules involved in heterophilic interactions can be crystallized, which will allow a visualization of the atomic specificity involved in different cellular recognition events. Indeed, some proteins that do not form well-ordered crystals by themselves can be induced to crystallize as a complex with another protein; thus cocrystallization may be one method to obtain the structures of entire neural CAM extracellular regions. As the powerful tools of molecular biology are combined with the knowledge of the binding affinities and the structures of neural CAMs, we may

approach an atomic resolution understanding of how the neural CAM building blocks are used by cells to accomplish their diverse adhesive interactions. A number of interesting structures are undoubtedly on the horizon, and we can look forward to a more complete picture of the mechanism of cell adhesion.

Acknowledgments

We thank Yvonne Jones and Lawrence Shapiro for providing coordinates of VCAM-1 and N-cadherin domain 1; Andrew Huber, Harold Erickson, and Allan Bieber for communicating results prior to publication; Arthur Chirino for help with figures; and Andrew Huber, Robert Lane, Henry Lester, Paul Patterson, Luis Sanchez, Jost Vielmetter, William Weis, and Kai Zinn for critical reading of the manuscript. Support was provided by a National Institutes of Health predoctoral fellowship (D. E. V.) and the Howard Hughes Medical Institute (P. J. B.).

References

Bentley, G.A., Boulot, G., Karjalainen, K., and Mariuzza, R.A. (1995). Crystal structure of the β chain of a T cell antigen receptor. Science *267*, 1984–1987.

Bieber, A.J., Snow, P.M., Hortsch, M., Patel, N.H., Jacobs, J.R., Traquina, Z.R., Schilling, J., and Goodman, C.S. (1989). Drosophila neuroglian: a member of the immunoglobulin superfamily with extensive homology to the vertebrate neural adhesion molecule L1. Cell *59*, 447–460.

Bjorkman, P.J., and Parham, P. (1990). Structure, function and diversity of class I major histocompatibility complex molecules. Ann. Rev. Biochem. *90*, 253–288.

Bodian, D.L., Jones, E.Y., Harlos, K., Stuart, D.I., and Davis, S.J. (1994). Crystal structure of the extracellular region of the human cell adhesion molecule CD2 at 2.5 Å resolution. Structure *2*, 755–766.

Bork, P., and Doolittle, R.F. (1992). Proposed acquisition of an animal protein domain by bacteria. Proc. Natl. Acad. Sci. USA *89*, 8990–8994.

Brady, R.L., Dodson, E.J., Dodson, G.G., Lange, G., Davis, S.J., Williams, A.F., and Barclay, A.N. (1993). Crystal structure of domains 3 and 4 of rat CD4: relation to the NH2-terminal domains. Science *260*, 979–983.

Brugoon, M.P., Grumet, M., Mauro, V., Edelman, G.M., and Cunningham, B.A. (1991). Structure of the chicken neuron–glia cell adhesion molecule, Ng-CAM: origin of the polypeptides and relation to the immunoglobulin superfamily. J. Cell Biol. *112*, 1017–1029.

Chothia, C., and Lesk, A.M. (1986). The relation between the divergence of sequence and structure in proteins. EMBO J. *5*, 823–826.

Chothia, C., Boswell, D.R., and Lesk, A.M. (1988). The outline structure of the T cell αβ receptor. EMBO J. *7*, 3745–3755.

Davies, D.R., and Metzger, H. (1983). Structural basis of antibody function. Annu. Rev. Immunol. *1*, 87–117.

De Vos, A.M., Ultsch, M., and Kossiakoff, A. (1992). Human growth hormone and extracellular domain of its receptor: crystal structure of the complex. Science *255*, 306–312.

Evans, S.V. (1993). SETOR: hardware lighted three-dimensional solid model representations of macromolecules. J. Mol. Graphics *4*, 134–138.

Furley, A.J., Morton, S.B., Manalo, D., Karagogeos, D., Dodd, J., and Jessel, T.M. (1990). The axonal gycoprotein TAG-1 is an immunoglobulin superfamily member with neurite outgrowth promoting activity. Cell *61*, 157–170.

Geiger, B., and Ayalon, O. (1992). Cadherins. Annu. Rev. Cell Biol. *8*, 307–332.

Harpaz, Y., and Chothia, C. (1994). Many of the immunoglobulin superfamily domains in cell adhesion molecules and surface receptors belong to a new structural set which is close to that containing variable domains. J. Mol. Biol. *238*, 528–539.

Harris, L.J., Larson, S.B., Hasel, K.W., Day, J., Greenwood, A., and McPherson, A. (1992). The three-dimensional structure of an intact monoclonal antibody for canine lymphoma. Nature *360*, 369–372.

Holden, H.M., Ito, M., Hartshorne, D.J., and Rayment, I. (1992). X-ray structure determination of telokin, the C-terminal domain of myosin light chain kinase, at 2.8 Å resolution. J. Mol. Biol. *277*, 840–851.

Holmgren, A., and Bränden, C.-I. (1989). Crystal structure of chaperone protein PapD reveals an immunoglobulin fold. Nature *342*, 248–251.

Huber, A.H. (1994). A biochemical and structural characterization of *Drosophila* neuroglian. Thesis, California Institute of Technology, Pasadena, California.

Huber, A.H., Wang, Y.-m.E., Bieber, A.J., and Bjorkman, P.J. (1994). Crystal structure of tandem type III fibronectin domains from Drosophila neuroglian at 2.1 Å. Neuron *12*, 717–731.

Hynes, R.O. (1990). Fibronectins (New York: Springer-Verlag).

Iwamoto, T., Taniguchi, M., Asai, N., Ohkusu, K., Nakashima, I., and Takahashi, M. (1993). cDNA cloning of mouse *ret* proto-oncogene and its sequence similarity to the cadherin superfamily. Oncogene *8*, 1087–1091.

Jones, E.Y., Davis, S.J., Williams, A.F., Harlos, K., and Stuart, D.I. (1992). Crystal structure at 2.8 Å resolution of a soluble form of the cell adhesion molecule CD2. Nature *360*, 232–239.

Jones, E.Y., Harlos, K., Bottomley, M.J., Robinson, R.C., Driscoll, P.C., Edwards, R.M., Clements, J.M., Dudgeon, T.J., and Stuart, D.I. (1995). Crystal structure of an integrin-binding fragment of vascular cell adhesion molecule-1 at 1.8 Å resolution. Nature *373*, 539–544.

Kabat, E.A., Wu, T.T., Perry, H.M., Gottesman, K.S., and Foeller, C. (1991). Sequences of proteins of immunological interest. (Bethesda, MD: U.S. Department of Health and Human Services).

Kraulis, P.J. (1991). MOLSCRIPT: a program to produce both detailed and schematic plots of protein structures. J. Appl. Crystallogr. *24*, 946–950.

Kwong, P.D., Ryu, S.E., Hendrickson, W.A., and Axel, R. (1990). Molecular characteristics of recombinant human CD4 as deduced from polymorphic crystals. Proc. Natl. Acad. Sci. USA *87*, 6423–6427.

Leahy, D.J., Axel, R., and Hendrickson, W.A. (1992a). Crystal structure of a soluble form of the human T cell coreceptor CD8 at 2.6 Å resolution. Cell *68*, 1145–1162.

Leahy, D.J., Hendrickson, W.A., Aukhil, I., and Erickson, H.P. (1992b). Structure of a fibronectin type III domain from tenascin phased by MAD analysis of the selenomethionyl protein. Science *258*, 987–991.

Leahy, D.J., Aukhil, I., and Erickson, H.P. (1996). 2.0 Å crystal structure of a four-domain segment of human fibronectin encompassing the RGD loop and synergy region. Cell *84*, 155–164.

Lee, J.-O., Rieu, P., Arnaout, M.A., and Liddington, R. (1995). Crystal structure of the A domain from the α subunit of integrin CD3 (CD11b/CD18). Cell *80*, 631–638.

Mahoney, P.A., Weber, U., Onofrechuk, P., Biessmann, H., Bryant, P.J., and Goodman, C.S. (1991). The *fat* tumor suppressor gene in Drosophila encodes a novel member of the cadherin gene superfamily. Cell *67*, 853–868.

Main, A.L., Harvey, T.S., Baron, M.J.B., and Campbell, I.A. (1992). The three-dimensional structure of the tenth type III module of fibronectin: an insight into RGD-mediated interactions. Cell *71*, 671–678.

Merritt, E.A., and Murphy, M.E.P. (1994). Raster3D Version 2.0, a program for photorealistic molecular graphics. Acta Crystallogr. (D) *50*, 869–873.

Osborn, L., Vassallo, C., Browning, B.G., Tizard, R., Haskard, D.O., Benjamin, C.D., Dougas, I., and Kirchhausen, T. (1994). Arrangement of domains and amino acid residues required for binding of vascular cell adhesion molecule-1 to its counter receptor VLA-4 (α4β1). J. Cell Biol. *124*, 601–608.

Overduin, M., Harvey, T.S., Bagby, S., Tong, K.I., Yau, P., Takeichi, M., and Ikura, M. (1995). Solution structure of the epithelial cadherin domain responsible for selective cell adhesion. Science *267*, 386–389.

Ozawa, M., Engel, J., and Kemler, R. (1990). Single amino acid substitutions in one Ca^{2+} binding site of uvomorulin abolish the adhesive function. Cell *63*, 1033–1038.

Richardson, J.S. (1977). β-sheet topology and the relatedness of proteins. Nature *268*, 495–500.

Richardson, J.S., Richardson, D.C., Thomas, K.A., Silverton, E.W., and Davies, D.R. (1976). Similarity of three-dimensional structure between the immunoglobulin domain and the copper, zinc superoxide dismutase subunit. J. Mol. Biol. *102*, 221–235.

Rutishauser, U., and Jessell, T.M. (1988). Cell adhesion molecules in vertebrate neural development. Physiol. Rev. *68*, 819–857.

Ryu, S.-E., Kwong, P.D., Truneh, A., Porter, T.G., Arthos, J., Rosenberg, M., Dai, X., Xuong, N.-h., Axel, R., Sweet, R.W., and Hendrickson, W.A. (1990). Crystal structure of an HIV-binding recombinant fragment of human CD4. Nature *348*, 419–426.

Ryu, S.-E., Turneh, A., Sweet, R.W., and Hendrickson, W.A. (1994). Structures of an HIV and MHC binding fragment from human CD4 as refined in two crystal lattices. Structure *2*, 59–74.

Sano, K., Tanihara, H., and Heimark, R.L. (1993). Protocadherins—a large familiy of cadherin-related molecules in the central nervous system. EMBO J. *12*, 2249–2256.

Shapiro, L., Fannon, A.M., Kwong, P.D., Thompson, A., Lehmann, M.S., Grubel, G., Legrand, J.F., Als-Nielsen, J., Colman, D.R., and Hendrickson, W.A. (1995a). Structural basis of cell–cell adhesion by cadherins. Nature *374*, 327–337.

Shapiro, L., Kwong, P.D., Fannon, A.M., Colman, D.R., and Hendrickson, W.A. (1995b). Considerations on the folding topology and evolutionary origin of cadherin domains. Proc. Natl. Acad. Sci. USA *92*, 6793–6797.

Takeichi, M., Inuzuka, H., Shimamura, K., Fujimori, T., and Nagafuchi, A. (1990). Cadherin subclasses: differential expression and their roles in neural morphogenesis. Cold Spring Harb. Symp. Quant. Biol. *55*, 319–325.

Volkmer, H., Hassel, B., Wolff, J.M., Frank, R., and Rathjen, F.G. (1992). Structure of the axonal surface recognition molecule neurofascin and its relationship to a neural subgroup of the immunoglobulin superfamily. J. Cell Biol. *118*, 149–161.

Wagner, G., and Wyss, D.F. (1994). Cell surface adhesion receptors. Curr. Opin. Struct. Biol. *4*, 841–851.

Wagner, G., Hyberts, S.G., and Havel, T.F. (1992). NMR structure determination in solution: a critique and comparison with X-ray crystallography. Annu. Rev. Biophys. Biomol. Struct. *21*, 167–198.

Wang, J., Yan, Y., Garrett, T.P.J., Liu, J., Rodgers, D.W., Garlick, R.L., Tarr, G.E., Husain, Y., Reinherz, E.L., and Harrison, S.C. (1990). Atomic structure of a fragment of human CD4 containing two immunoglobulin-like domains. Nature *348*, 411–419.

Wheeler, G.N., Buxton, R.S., Parker, A.E., Arnemann, J., Rees, D.A., King, I.A., and Magee, A.I. (1991). Desmosomal glycoproteins I, II, and III: novel members of the cadherin superfamily. Biochem. Soc. Trans. *19*, 1060–1064.

Williams, A.F., and Barclay, A.N. (1988). The immunoglobulin superfamily—domains for cell surface recognition. Annu. Rev. Immunol. *6*, 381–405.

Withka, J.M., Wyss, D.F., Wagner, G., Kister, A., Pallai, P., Recny, M.A., and Reinherz, E.L. (1993). The CD58 (LFA-3) binding site is a localized and highly charged surface area on the AGFCC′C″ face of the human CD2 adhesion domain. Proc. Natl. Acad. Sci. USA *90*, 11613–11617.

Yoshihara, Y., and Mori, K. (1994). Telencephalin: a neuronal area code molecule? Neurosci. Res. *21*, 119–124.

Yoshihara, Y., Oka, S., Ikeda., J., and Mori, K. (1991). Immunoglobulin superfamily molecules in the nervous system. Neurosci. Res. *10*, 83–105.

J. Mol. Biol. (1994) **241**, 483–487

Expression and Crystallization of a Soluble Form of *Drosophila* Fasciclin III

Roland K. Strong[1]†, Daniel E. Vaughn[1], Pamela J. Bjorkman[2] and Peter M. Snow[3]

[1]*Division of Biology and* [2]*Howard Hughes Medical Institute*
156–29 California Institute of Technology, Pasadena, CA 91125, U.S.A.

[3]*Department of Biological Sciences*
State University of New York, Albany, NY 12222, U.S.A.

A truncated form of *Drosophila* fasciclin III has been engineered by site-directed mutagenesis. Secreted fasciclin III is expressed at 35 to 40 mg/l in insect cells with baculovirus carrying the recombinant gene. Single crystals of purified soluble fasciclin III have been grown by vapor diffiusion *versus* polyethylene glycol 8000/sodium citrate at low pH. The space group is $P6_122$ or its enantiomorph $P6_522$, with unit cell dimensions $a = b = 140$ Å, $c = 260$ Å. Cryo-preserved crystals diffract to reciprocal lattice spacings beyond 3·0 Å.

Keywords: baculovirus expression; immunoglobulin superfamily; cell adhesion molecule; homophilic binding; crystallization

Fasciculation is a process in which neuronal growth cones extend along specific axonal surfaces, contributing to the development of appropriate axonal pathways in the embryonic nervous system (reviewed by Grenningloh *et al.*, 1990). Studies of growth cone guidance in the central nervous systems of insects (Raper *et al.*, 1983*a*,*b*,*c*; Bastiani *et al.*, 1984; Goodman *et al.*, 1984; Raper *et al.*, 1984) suggested that specific axon pathways are demarcated by different cell-surface recognition molecules. Four different membrane-associated glycoproteins, identified on subsets of fasciculating axons and associated glia, have been implicated in neuronal recognition and adhesion. Fasciclin I, II (Bastiani *et al.*, 1987) and IV (Kolodkin *et al.*, 1992), each initially identified in the grasshopper; fasciclin III (Patel *et al.*, 1987) and neuroglian (Bieber *et al.*, 1989), both originally characterized in *Drosophila*. The genes encoding each of these proteins were subsequently cloned (Harrelson & Goodman, 1988; Snow *et al.*, 1988; Zinn *et al.*, 1988; Patel *et al.*, 1987; Bieber *et al.*, 1989; Snow *et al.*, 1989; Kolodkin *et al.*, 1992). *In vitro* assays have demonstrated that fasciclin I and III are capable of mediating homophilic adhesion as demonstrated by cell aggregation and cell sorting (Snow *et al.*, 1989; Elkins *et al.*, 1990).

The extracellular region of fasciclin III has been predicted to be composed of three highly diverged immunoglobulin domains based upon limited sequence similarity with other members of the immunoglobulin superfamily (Williams & Barclay, 1988). The most amino-terminal of these domains (D1) is proposed to be V-type, while the two more carboxy-terminal domains (D2 and D3) are proposed to be of the C2-type (Grenningloh *et al.*, 1990).

The physical basis for interactions between cell surface adhesion molecules has not been well characterized. Crystal structures are available for CD2 and CD4, two members of the immunoglobulin superfamily (Ryu *et al.*, 1990; Wang *et al.*, 1990; Jones *et al.*, 1992). Regions of these two proteins involved in mediating molecular interactions have been identified by mutational analysis. For example, in the case of CD2, the GFCC′C″ face of the amino-terminal V-type domain has been implicated in mediating homophilic as well as heterophilic interactions with its counter-receptors (Jones *et al.*, 1992). It has been suggested that such an interaction may represent a structural paradigm for interactions between members of the immunoglobulin superfamily (Jones *et al.*, 1992).

In order to further understand homophilic interactions between adhesion molecules in the developing nervous system, we have initiated a series of studies to define the regions of fasciclin III important for homophilic specificity. On the basis of a computer-generated model of the amino-terminal domain (L. A. Castonguay, S. H. Bryant, P. M. S. & J. S. Fatrow, unpublished results), we are creating a

† Present address: Fred Hutchinson Cancer Research Center, 1124 Columbia Street, Seattle, WA 98104, U.S.A.

0022–2836/94/330483–05 $08.00/0

set of replacement mutants that will serve to crudely define those regions of the molecule important in mediating homophilic interactions. The crystal structure of the extracellular domain of fasciclin III would provide a context within which to interpret the effects of specific mutations in the protein, and provide a structural basis for understanding the mechanism of homophilic adhesion. In addition, determination of the crystal structure would allow a direct comparison with the model of the amino-terminal domain, allowing an assessment of the utility of the threading algorithm (Bryant & Lawrence, 1993), used in its construction. Here we describe the construction of a soluble form of the extracellular domains of fasciclin III, its expression, purification, and crystallization.

(a) *Construction of a soluble form of fasciclin III*

A cloned cDNA encoding the 80 kDa form of fasciclin III (Snow *et al.*, 1989) was inserted into the pBluescript (Stratagene) vector. Site-directed mutagenesis was performed (Kunkel *et al.*, 1987) using a complementary oligonucleotide that encoded a stop codon following the last residue of the extracellular domain (Asp236). Following transformation of the mutagenesis reaction into a wild-type bacterial strain (XL-1Blue, Stratagene), mutant molecules were identified by T-track analysis (Anderson, 1981) and subsequently confirmed by sequence analysis of putative mutants.

The altered fasciclin III cDNA was excised from pBluescript by digestion with *Eco*RV and *Bgl*II and inserted into a pVL1393 baculovirus transfer vector (a gift from M. D. Summers) that had been digested with *Sma*I and *Bgl*II. The correct orientation was confirmed by restriction mapping of the insert, and subsequently co-transfected into Sf9 cells with wild-type baculovirus as described (Summers & Smith, 1987). Recombinant viruses encoding truncated fasciclin III were initially enriched by plaque hybridization, and individual recombinants subsequently identified by visual inspection of plaque morphology (Summers & Smith, 1987). The identity of recombinant viral isolates was confirmed by restriction mapping and Southern-blot analysis of viral DNA isolated from infected Sf9 cells.

(b) *Expression of a soluble form of fasciclin III by recombinant baculovirus*

Sf9 cells were infected with recombinant virus at multiplicities of infection varying between 1 and 10, and levels of fasciclin III secreted into the media assessed by immunoaffinity purification (see below) of 1 ml aliquots at 24 hour intervals. Eluates from the affinity matrix were analyzed by SDS-PAGE and Coomassie blue staining. Protein levels were estimated by comparison with standards of known concentration. Expression levels reached a plateau of approximately 35 to 40 mg/liter at a multiplicity of infection of 5 (data not shown). Levels of fasciclin III expression were maximized at 120 hours post-infection, with longer times resulting in increased protein degradation, presumably due to the high levels of cell death and lysis observed at longer periods.

As seen in Figure 1A, secreted fasciclin III produced in Sf9 cells migrates on an SDS-PAGE gel as a broad band (which can be resolved into five discrete species; data not shown) ranging in molecular mass from 38 kDa to 42 kDa. This heterogeneity was shown to be due to variable glycosylation by treatment of the protein with peptide N-glycosidase F (New England Biolabs), which cleaves N-linked sugars (Plummer *et al.*, 1984). Such treatment results in a major species of molecular weight 36 kDa when analyzed by SDS-PAGE (Figure 1A). This result is consistent with the observation that fasciclin III possesses four potential sites for N-linked glycosylation (Marshall, 1972; Gavel & von Heijne, 1990), and suggests that Sf9 cells differentially glycosylate the protein backbone, with each of the species of increasing molecular mass corresponding to a form glycosylated at one additional site. We have observed similar glycosylation patterns with other, but not all, secreted proteins expressed in Sf9 cells (P.M.S., unpublished observations). It is interesting to note that the 80 kDa transmembrane form of fasciclin III, when expressed in Sf9 cells, does not show this heterogeneity of glycosylation (P.M.S., unpublished observations), suggesting alternative processing pathways for integral membrane proteins and at least some secreted proteins.

(c) *Purification of secreted fasciclin III for structural studies*

A monoclonal antibody directed against the extracellular domain of fasciclin III (2D5; Patel *et al.*, 1987) was coupled to a Protein-A-Sepharose matrix as described (Schneider *et al.*, 1982). Supernatants from recombinant baculovirus-infected Sf9 cells were passed over this affinity matrix, eluted with buffers ranging from pH 2·5 to pH 11·5, and neutralized immediately. Aliquots of each eluate were tested for their content of secreted fasciclin III by SDS-PAGE. Eluates which were determined to contain fasciclin III were then assayed for the structural integrity of the protein by native polyacrylamide gel electrophoresis. Eluted fasciclin III that had not been denatured by the elution conditions would be expected to yield a discrete band or series of bands when analyzed under non-denaturing conditions. The results indicated that either pH 2·5 or pH 11·5 were required for quantitative elution of fasciclin III from the matrix, and that neither of these conditions disrupted the structural integrity of the protein. As shown in Figure 1B, the purified protein migrates as a single band after elution at pH 11·5 and neutralization. The purified protein can be immunoprecipitated with the 2D5 monoclonal antibody (data not shown), offering further evidence of the structural integrity of the protein. Finally, when

purified fasciclin III was analyzed by isoelectric focusing under native conditions, a single species migrating with a pI between 4·0 and 5·0 was observed (data not shown), further assurance that the relatively harsh treatment at elevated pH required for removal from the affinity column did not denature the protein. This result also demonstrates that the extracellular domain of fasciclin III is acidic, and that the heterogeneous glycosylation noted above appears to contribute no charge heterogeneity to the protein.

Based upon these results, the following conditions were devised for purification of the secreted form of fasciclin III from baculovirus supernatants. After passage of the supernatant over the column matrix, the matrix was washed sequentially with 5 to 10 column volumes of 10 mM triethanolamine (pH 8·2), 0·5 M NaCl, 1 mM phenylmethylsulfonyl fluoride followed by 5 to 10 column volumes of 50 mM triethylamine (pH 10·0), 150 mM NaCl. Bound protein was eluted with 5 column volumes of 50 mM triethylamine (pH 11·5), 150 mM NaCl, and neutralized immediately with 0·1 volume 1 M sodium phosphate (pH 6·0). The eluate was subsequently dialyzed against 10 mM Hepes (pH 7·5), and concentrated by ultrafiltration.

(d) *Crystallization of the secreted form of fasciclin III*

Single crystals of the secreted extracellular domains of fasciclin III were grown as follows. Purified protein, concentrated to 20 mg/ml in 10 mM Hepes (pH 7·5), was mixed 1 : 1 with a precipitant solution: 5 to 10% (w/w) polyethylene glycol 8000 (Sigma), 2·5 to 5% saturated sodium citrate, 50 mM sodium acetate (pH 4·5) and with or without 1 mM dithiothreitol. Drops (2 to 4 μl) of this solution were suspended on siliconized cover slips over wells containing 1·0 ml of the precipitant solution in a vapor diffusion experiment (McPherson, 1982) at 22°C. Crystals appeared in one to six weeks; earlier in the highest precipitant concentrations, with larger, better formed crystals generally appearing later in the lower precipitant concentrations. These crystallization conditions were initially identified on the basis of results generated from the use of a crystallization factorial (Carter & Carter, 1979) using an "in-house" set of solutions. The crystals grow as smoothly curved, hexagonally faceted ellipsoids, with the long axis as long as 1·0 mm. Precession photographs show the space group to be $P6_122$ or its enantiomorph $P6_522$, with unit cell dimensions $a = b = 140$ Å, $c = 260$ Å as determined from data reduction (c is parallel to the long axis of the crystals). The solvent content of these crystals would range from 71 to 32%, assuming from two to four molecules per asymmetric unit; three molecules per asymmetric unit gives a solvent content of 46%, which is in the middle of the range observed for most protein crystals (Matthews, 1968). Experiments to enzymatically remove the N-linked oligosaccharides were conducted in an attempt to obtain improved crystals. This treatment, while significantly reducing the amount of oligosaccharide, has so far failed to yield any crystals (data not shown).

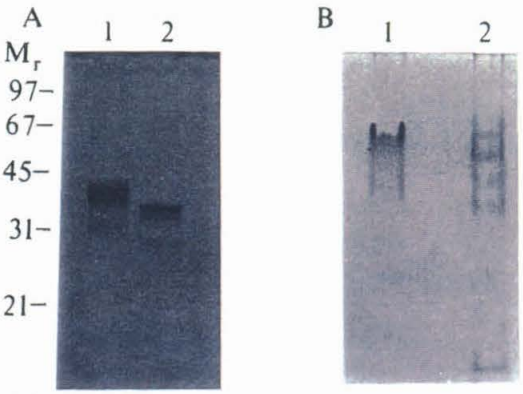

Figure 1. Purified secreted fasciclin III is heterogeneously glycosylated and maintains its native conformation after treatment with high pH. A, SDS/12·5% PAGE analysis of purified fasciclin III (1 μg) before (lane 1) and after (lane 2) treatment with N-glycosidase F (New England Biolabs). The positions of migration of molecular mass standards (M_r) are indicated in kilodaltons. B, Purified fasciclin III (2·5 μg) analyzed on a native 10% polyacrylamide gel (lane 1) with non-denatured protein markers (from top to bottom: human carbonic anhydrase, bovine carbonic anhydrase II (runs as 2 bands), β-lactalbumin, and soybean trypsin inhibitor; Sigma) for comparison (lane 2). The pH of the gel buffer was 8·8 and the gel was run from the negative to the positive electrode.

The crystals diffract to reciprocal lattice spacings of 3·25 Å at room temperature in experiments conducted at the Stanford Synchrotron Radiation Laboratory (beamline 7-1), but are particularly sensitive to radiation. The degree of the radiation damage is extreme enough to preclude data collection at room temperature. In an effort to overcome this difficulty, the crystals were flash-cooled (Hope, 1990) in a stream of nitrogen gas at −160°C (Molecular Structure Systems hardware). Effective cryo-preservation of a crystal could not be achieved in the mother liquor that the crystals grow in due to the formation of crystalline ice during cooling. Instead, crystals were first transferred to a holding solution of 10% (w/w) polyethylene glycol 8000, 2·5% saturated sodium citrate, 50 mM sodium acetate (pH 4·5) and 1 mM dithiothreitol. The crystals were then progressively transferred to solutions that incorporated higher and higher concentrations of polyethylene glycol 400, terminating at 30% (w/w) after a period of five hours. The crystals were then picked up in a rayon loop mounted on a magnetic pin (Teng, 1990) and flash-cooled in the gas-stream. This process reliably yields cryo-preserved crystals that diffract to reciprocal lattice spacings beyond 3·0 Å using synchrotron radiation.

Data collection is in progress on native crystals and one potential heavy-atom derivative (uranyl acetate).

This work was supported by a Basil O'Connor Starter Scholar Award (P.M.S.), the National Institute of Health (R29 NS28699 to P.M.S.) and the Howard Hughes Medical Institute (P.J.B.). P.J.B. was a Pew Scholar and held a Young Investigator award from the Cancer Research Institute during part of the work. R.K.S. was a post-doctoral fellow of the American Cancer Society; D.E.V. is supported by an NIH pre-doctoral training grant. We thank M. D. Summers for the gift of a baculovirus starter kit, Michael Blum and Leemor Joshua-Tor, who provided instruction on the cryo-preservation of macromolecular crystals, and Michael Soltis (SSRL), Leemor Joshua-Tor and Michael Stowell for assistance with data collection at SSRL.

References

Anderson, S. (1981). Shotgun DNA sequencing strategy using cloned DNase I-generated fragments. *Nucl. Acids Res.* **9**, 3015–3027.

Bastiani, M. J., Raper, J. A. & Goodman, C. S. (1984). Pathfinding by neuronal growth cones in grasshopper embryos. 3. Selective affinity of the G-growth cone for the P-cells within the A/P fascicle. *J. Neurosci.* **4**, 2311–2328.

Bastiani, M. J., Harrelson, A. L., Snow, P. M. & Goodman, C. S. (1987). Expression of fasciclin I and II glycoproteins on subsets of axon pathways during neuronal development in the grasshopper. *Cell*, **48**, 745–755.

Bieber, A. J., Snow, P. M., Hortsch, M., Patel, N. H., Jacobs, J. R., Traquina, Z. R., Schilling, J. & Goodman, C. S. (1989). *Drosophila* neuroglian: a member of immunoglobulin superfamily with extensive homology to the vertebrate neural adhesion molecule L1. *Cell* **59**, 447–460.

Bryant, S. H. & Lawrence, C. E. (1993). An empirical energy function for threading protein sequence through the folding motif. *Proteins: Struct. Funct. Genet.* **16**, 92–112.

Carter, C. W. J. & Carter, C. W. (1979). Protein crystallization using incomplete factorial experiments. *J. Biol. Chem.* **254**, 12219–12223.

Elkins, T., Hortsch, M., Bieber, A. J., Snow, P. M. & Goodman, C. S. (1990). *Drosophila* fasciclin I is a novel homophilic adhesion molecule that along with fasciclin III can mediate cell sorting. *J. Cell. Biol.* **110**, 1825–1832.

Gavel, Y. & von Heijne, G. (1990). Sequence differences between glycosylated and non-glycosylated Asn-X-Thr/Ser acceptor sites—implications for protein engineering. *Protein Eng.* **3**, 433–442.

Goodman, C. S., Bastiani, M. J., Doe, C. Q., du Lac, S., Helfand, S. L., Kuwada, J. Y. & Thomas, J. B. (1984). Cell recognition during neuronal development. *Science*, **225**, 1271–1279.

Grenningloh, G., Bieber, A. J., Rehm, E. J., Snow, P. M., Traquina, Z. R., Hortsch, M., Patel, N. H. & Goodman, C. S. (1990). Molecular genetics of neuronal recognition in *Drosophila*: evolution and function of the immunoglobulin superfamily cell adhesion molecules. *Cold Spring Harbor Symp. Quant. Biol.* **55**, 327–340.

Harrelson, A. L. & Goodman, C. S. (1988). Growth cone guidance in insects: fasciclin II is a member of the immunoglobulin superfamily. *Science*, **242**, 700–708.

Hope, H. (1990). Crystallography of biological macromolecules at ultra-low temperature. *Annu. Rev. Biophys. Biophys. Chem.* **19**, 107–126.

Jones, E. Y., Davis, S. J., Williams, A. F., Harlos, K. & Stuart, D. I. (1992). Crystal structure at 2·8 Å resolution of a soluble form of the cell adhesion molecule CD2. *Nature (London)*, **360**, 232–239.

Kolodkin, A. L., Matthes, D. J., O'Connor, T. P., Patel, N. P., Admon, A., Bentley, D. & Goodman, C. S. (1992). Fasciclin IV: sequence, expression, and function during growth cone guidance in the grasshopper embryo. *Neuron*, **9**, 831–845.

Kunkel, T. A., Roberts, J. D. & Zakour, R. A. (1987). Rapid and efficient site directed mutagenesis without phenotypic selection. *Methods Enzymol.* **154**, 367–382.

Marshall, R. (1972). Glycoproteins. *Annu. Rev. Biochem.* **41**, 673–702.

Matthews, B. W. (1968). Solvent content of protein crystals. *J. Mol. Biol.* **33**, 491–497.

McPherson, A. (1982). *Preparation and Analysis of Protein Crystals*. John Wiley & Sons, New York.

Patel, N. H., Snow, P. M. & Goodman, C. S. (1987). Characterization and cloning of fasciclin-III—a glycoprotein expressed on a subset of neurons and axon pathways in *Drosophila*. *Cell*, **48**, 975–988.

Plummer, T. H., Elder, J. H., Alexander, S., Phelan, A. W. & Tarentino, A. L. (1984). Demonstration of peptide N-glycosidase F activity in endo-β-N-acetylglucosaminidase F preparations. *J. Biol. Chem.* **259**, 10700–10704.

Raper, J. A., Bastiani, M. J. & Goodman, C. S. (1983*a*). Guidance of neuronal growth cones: selective fasciculation in the grasshopper embryo. *Cold Spring Harbor Symp. Quant. Biol.* **48**, 587–598.

Raper, J. A., Bastiani, M. J. & Goodman, C. S. (1983*b*). Pathfinding by neuronal growth cones in grasshopper embryos. 1. Divergent choices made by the growth cones of sibling neurons. *J. Neurosci.* **3**, 20–30.

Raper, J. A., Bastiani, M. J. & Goodman, C. S. (1983*c*). Pathfinding by neuronal growth cones in grasshopper embryos. 2. Selective fasciculation onto specific axonal pathways. *J. Neurosci.* **3**, 31–41.

Raper, J. A., Bastiani, M. J. & Goodman, C. S. (1984). Pathfinding by neuronal growth cones in grasshopper embryos. 4. The effects of ablating the A-axon and P-axon upon the behaviour of the G-growth cone. *J. Neurosci.* **4**, 2329–2345.

Ryu, S.-E., Kwong, P. D., Truneh, A., Porter, T. G., Arthos, J., Rosenberg, M., Dai, X., Xuong, N.-H., Axel, R., Sweet, R. W. & Hendrickson, W. A. (1990). Crystal structure of an HIV-binding recombinant fragment of human CD4. *Nature (London)*, **348**, 419–426.

Schneider, C., Newman, R. A., Sutherland, D. R., Asser, U. & Greaves, M. F. (1982). A one-step purification of membrane-proteins using a high-efficiency immunomatrix. *J. Biol. Chem.* **257**, 766–769.

Snow, P. M., Zinn, K., Harrelson, A. L., McAllister, L., Schilling, J., Bastiani, M. J., Makk, G. & Goodman, C. S. (1988). Characterization and cloning of fasciclin I and fasciclin II glycoproteins in the grasshopper. *Proc. Nat. Acad. Sci., U.S.A.* **85**, 5291–5295.

Snow, P. M., Bieber, A. J. & Goodman, C. S. (1989). Fasciclin III: A novel homophilic adhesion molecule in *Drosophila*. *Cell*, **59**, 313–323.

Summers, M. D. & Smith, G. E. (1987). A manual of methods for baculovirus vectors and insect cell culture procedures. *Texas Agricultural Experiment Station. Bulletin No. 1555.*

Teng, T.-Y. (1990). Mounting of crystals for macromolecular crystallography in a free-standing thin film. *J. Appl. Crystallogr.* **23**, 387–391.

Wang, J., Yan, Y., Garrett, T. P. J., Liu, J., Rodgers, D. W., Garlick, R. L., Tarr, G. E., Husain, Y. Reinherz, E. L. & Harrison, S. C. (1990). Atomic structure of a fragment of human CD4 containing two immunoglobulin-like domains. *Nature (London)*, **348**, 411–419.

Williams, A. F. & Barclay, A. N. (1988). The immunoglobulin superfamily-domains for cell surface recognition. *Annu. Rev. Immunol* **6**, 381–405.

Zinn, K., McAllister, L. & Goodman, C. S. (1988). Sequence analysis and neuronal expression of fasciclin I in grasshopper and *Drosophila*. *Cell*, **53**, 577–587.

Edited by A. Klug

(Received 29 April 1994; accepted 6 May 1994)